Novel Joining of Dissimilar Ceramics in the Si_3N_4-Al_2O_3 System Using Polytypoid Functional Gradients

by

Caroline Sunyong Lee

B.S. (Massachusetts Institute of Technology) 1993
M.S. (Massachusetts Institute of Technology) 1995

A dissertation submitted in partial satisfaction of the

requirements for the degree of

Doctor of Philosophy

in

Engineering: Materials Science and Mineral Engineering

in the

GRADUATE DIVISION

of the

UNIVERSITY OF CALIFORNIA, BERKELEY

Committee in charge:

Professor Gareth Thomas, Chair
Professor Lutgard C. De Jonghe
Professor Clayton Radke

Fall 2001

The dissertation of Caroline Sunyong Lee is approved:

Chair Date

Date

Date

University of California, Berkeley

Fall 2001

Abstract

Novel Joining of Dissimilar Ceramics in the Si_3N_4-Al_2O_3 System

Using Polytypoid Functional Gradients

by

Caroline Sunyong Lee

Doctor of Philosophy in Materials Science and Mineral Engineering

University of California, Berkeley

Professor Gareth Thomas, Chair

A unique approach to crack-free joining of heterogeneous ceramics is demonstrated by the use of sialon polytypoids as Functionally Graded Materials (FGM) as defined by the phase diagram in the system, Si_3N_4-Al_2O_3. Polytypoids in the Al_2O_3-Si_3N_4 system offer a path to compatibility for such heterogeneous ceramics. The first part of the dissertation describes successful hot press sintering of multilayered FGM's with 20 layers of thickness 500 μm each. Transmission Electron Microscopy was used to identify the polytypoids at the interfaces of different areas of the joint. It has been found that the 15R polytypoid was formed in the Al_2O_3-contained layers and the 12H polytypoid was formed in the Si_3N_4-contained layers.

The second part of the dissertation discusses the mechanical properties of these polytypoidally joined Si_3N_4-Al_2O_3. The thermal stresses of this FGM junction were analyzed using a finite element analysis program (FEAP) taking into account both

coefficient of thermal expansion (CTE) and modulus variations. From this analysis, the result showed a dramatic decrease in radial, axial and hoop stresses as the FGM changes from three layers to 20 graded layers. Scaling was considered, showing that the graded transition layer should constitute about 75% or more of the total sample thickness to reach a minimal residual stress. Oriented Vickers indentation testing was used to qualitatively characterize the strengths of the joint and the various interfaces. The indentation cracks were minimally or not deflected at the sialon layers, implying strong interfaces. Finally, flexural testing was conducted at room temperature and at high temperature. The average strength at room temperature was found to be 581 MPa and the average strength at high temperature (1200 ^{o}C) was found to be 262 MPa. Scanning electron microscope observation of fracture surfaces at a different loading rates indicated that the strength loss at higher temperatures was consistent with a softening of glassy materials present at grain junctions.

_____

Professor Gareth Thomas, Chair Date

TABLE OF CONTENTS

APPENDICES

LIST OF FIGURES

LIST OF TABLES

Acknowledgements

I am extremely grateful to Professor Gareth Thomas for initiating and supporting this project and for providing valuable discussions. Without his enthusiasm, encouragement and insight, this thesis would not have been possible to complete. I would also like to thank Professor Lutgard C. De Jonghe for providing facilities and resources for processing, and for many valuable discussions. I would like to thank Dr. Xiao Feng Zhang for his support in high-resolution electron microscope. Dr. Jim McNaney was instrumental in setting up and providing training on the creep furnace so that I could do the strength tests. Also, Dr. Terrance L. Berker, Jr. helped me to set up Finite Element Analysis Program (FEAP) to enable me to carry out the residual stresses calculations using that program.

I am especially grateful for many of my friends at LBL, UC Berkeley and at my church.

Special thanks to my husband, Sung hoon for supporting me and encouraging me all throughout my graduate school. I would like to thank my daughter, Heera, for growing healthy. I would also like to thank my in-laws for helping me in difficult times. I would like to thank my father and my sister Michelle, for their concern over the years. Also, I would like to thank my mother who is in heaven. Being able to study in America would have been impossible without the dedication and trust from my parents.

Most importantly, I want to thank God for being with me and keeping me strong in faith throughout the whole process.

CHAPTER 1: Introduction

1.1. Joining of dissimilar Materials

Ceramic joining has been the subject of much developmental research over the years. Engineering ceramics have been well known over the past decades for having superior properties in comparison with metals namely, refractoriness, high wear resistance, lower density, superior resistance to corrosion, high elastic modulus, low coefficient of thermal expansion. These 'superior materials, however, do suffer from drawbacks such as poor fracture toughness and high expense, which are at present limiting their industrial application. Metals in general are strong, ductile, and are good thermal and electrical conductors, but they are typically not well suited for high temperatures, are prone to corrosion and chemical attack, and shrink or expand significantly with temperature changes [1]. Therefore, metals and ceramics each have their advantages and disadvantages. The joining of metal to metal has been established for a long time using various techniques, such as welding and brazing [1].

Materials that have different properties at different regions are desirable in several structural areas of research and development, such as advanced engines, turbine blades and thermal barrier coatings. An example demonstrating the need for ceramic-to-metal joining is where a component may be required to withstand high temperature at one end (a ceramic) while being extremely tough at the other end (a metal). As this ceramic-to-metal joining has been developed over the years, various techniques such as brazing [2-12] and solid state diffusion bonding [13-21] were used. Not only has this ceramic-to-metal joining been developed over the years, but also

ceramic joining has been of current interest for various demanding structural applications. The reasons for the interest in joining ceramics are the same as those for joining metals to ceramics, however, the development of effective ceramic joining techniques could have a much greater impact on their use in mass-produced components. However, there are several challenges on component manufacturing by ceramic processing techniques and by the material themselves. First of all, deformation of densified ceramics to form complex shapes is practically impossible because most ceramic materials are brittle even at elevated temperatures. Moreover, ceramics are undesirable for mass production because of their high cost and machining difficulties. Effective ceramic joining techniques can play an important role in improving the reliability of ceramic structures as well. Ceramics are very sensitive to flaws, due to the quality of raw materials used in their production and to the characteristics of various processing techniques, such as machining. A single flaw can cause material rejection and lead to the failure of a ceramic part [3]. To overcome these difficulties, there are several joining techniques that have been developed to join ceramics for structural application as described in the next paragraph.

Brazing with filler metals is an attractive process for joining structural ceramics for many applications. Since wetting and adherence are the principal requirements for brazing, most ceramics have problem in wetting conventional brazing filler metals. This problem was overcome either by coating the ceramic surface with a suitable metal layer prior to brazing (indirect brazing) or through the use of specially formulated filler metals that wet and adhere directly to an untreated ceramic surface (direct brazing). For indirect brazing, the ceramic is first coated in the joint area with

a material that can be wetted by filler metal that does not wet the untreated surface. Coating techniques include sputtering, vapor plating, and thermal decomposition of a metal-containing compound such as TiH_4 [22,23,24]. Alumina ceramics can be joined with this technique with molybdenum-manganese (Mo-Mn) coating [25]. Direct brazing requires the enhancement of both wetting and adherence of active metals to ceramics without the need for coating the ceramic surface. Whether the ceramic is an oxide, carbide or nitride, the active metal reacts with the ceramic surface, forming an interfacial layer that can be wetted by the bulk of the filler metal. Titanium is the widely used active element addition to filler metals formulated to braze directly high melting oxide ceramics [26]. The critical interfacial reaction product in the case of oxide ceramics brazed with Ti-containing filler metals is either TiO or Ti_2O_3 with appreciably higher adhesion in systems that result in the formation of TiO [26]. Moreover, mullite and ZrO_2-toughened mullite (ZTM) were joined with Ag-Cu eutectic braze alloys that contain Ti or Zr as active elements with the resulting four-point bend strength of 108 Mpa [27]. Compared with the Ti-containing alloys, those with Zr were more refractory, they were less reactive with the mullite, and the Zr did not segregate as completely to the interface during heating [27].

Not only has active metal been used as the filler materials for brazing, but brazing with nonmetallic glasses as filler materials has been studied with structural ceramics, such as alumina, Partially Stabilized Zirconia (PSZ), Si_3N_4, and sialon [28, 29,30, 31]. The rationale for this approach is that many ceramics have amorphous phases remaining at the grain boundaries after the sintering process, so they would be expected to be wet by, and compatible with, similar glassy materials, introduced at the

joint. However, this joining technique has a problem where some of the glasses, even those formulated to match the grain-boundary composition of a specific ceramic, have Coefficients of Thermal Expansion (CTEs) significantly different from those of the ceramics, which can cause high residual stresses and cracking in the joint. The most extensive studies on brazing with glasses have been those on Si_3N_4. The glasses include those similar to that found at the grain boundaries of a hot pressed Si_3N_4 ($55SiO_2$, 35MgO, $10Al_2O_3$, wt%) [32].

Many nonoxide ceramics, such as Si_3N_4 and AlN, are densified with various sintering aids that leave oxide or oxynitride second phases on the grain boundaries of the ceramic. Because this idea is based on using glass or ceramic bonding agents with compositions that are similar to the ceramic grain boundary phase, chemical compatibility is guaranteed, and the joint can be made to resemble a single ceramic grain boundary. Strengths as high as 450 MPa have been obtained for end-sealed joints tested in four-point flexure at room temperature [33]. Also, bulk Si_3N_4 has been joined using rare-earth silicates, which were used as a sintering additive to sinter via a liquid phase, which could crystallize on cooling. Such rare-earth oxide joined parts are expected to exhibit improved high temperature performance [34,35].

Diffusion welding, also referred to as solid-state welding, or bonding, is the process to effect a joint without melting any of its component materials. Since the diffusion welding process requires joint surfaces to be in the most intimate contact possible, and enough diffusion between the material or materials being welded to produce a joint in a reasonable time, pressure across the joint needs to be applied at elevated temperatures. Diffusion welding of coarse-grained alumina to fine-grained

alumina was achieved when the fine-grained material was deformed enough to produce good contact at the joint surfaces. Moreover, dense SiC was diffusion welded when SiC surfaces were very fine and friction fitting was done by mating surfaces by hand [1]. Hot-pressed silicon nitride ceramics were joined using a diffusion welding technique in a nitrogen atmosphere. With optimized joining temperature, joining pressure, holding time and surface roughness of the joining couple, the joining strength was reported to be 567 MPa at room temperature and at high temperature [36].

Microwave joining is another method to join ceramic parts by using microwaves to heat ceramic materials to temperatures high enough to accomplish the joining. Microwave heating is fundamentally different from conventional heating techniques in that heat is generated within a material rather than from an external source. So the microwave-heated materials heat from the inside out, rather than the reverse as is common in conventionally heated materials. Advantage of this internal, volumetric heating is that both small and large parts can be heated rapidly and uniformly, a characteristic, which is especially attractive for ceramic materials [1]. Although microwave joining is still in a developmental stage, the application of microwave processing techniques to joining problems appears to be a viable and versatile approach, and several researchers have reported success with microwave joining. Studies done by Palaith and Silberglitt (1989) reported successful joining of Al_2O_3 joint and Si_3N_4 joint with microwaves, and the flexural strengths of these joints were quite similar to the bending strength for unjoined ceramics [37]. Moreover, microwave joining of alumina to magnesia was attempted, and the maximum bending

strength of the joint was about 60% of the strength of the raw MgO specimen and the reaction layer was formed at the joining interface [38]. Fukushima and coworkers have also reported on the application of microwave processing to the joining of ceramics, especially joints of 92%-96% pure Al_2O_3 and Si_3N_4 joints. These Al_2O_3 joints were obtained without the use of separate bonding materials, and the strengths of these joints were equal to the respective base material strengths. The joining was accomplished by the preferential melting of sintering additives that are located along Al_2O_3 grain boundaries without melting the Al_2O_3 [39]. Although interest in microwave processing has grown dramatically in the last decade, this technology is still largely in a developmental stage. The common problem in microwave sintering is "thermal runaway", when the temperature of the sample increases rapidly with time. This thermal runaway leads to the formation of local hot spots, with some regions having a much higher temperature than the rest of the sample, resulting differential densification and even to cracking of the sample [40].

Finally, although various conventional techniques have been used for joining Si_3N_4, sialon to itself or to metallic alloys, the range of approaches used reflects the severity of the problems in joining ceramics for high temperature structural application. Si_3N_4 reacts with many high melting point metals to form silicides and nitrides. Moreover, if the joining temperature is high, the properties of the metallic components degrade and Si_3N_4 decomposes. To overcome some of these difficulties that arise in ceramic-ceramic and ceramic-metal joining, joining methods with multilayer interlayers have been considered. These interlayers are designed to form a thin or partial layer of a transient liquid phase (TLP) at relatively low bonding

temperatures, and thereby, to permit low temperature joining. The components within the interlayer are selected to produce an alloy or compound that is useful for applications at elevated temperature, potentially, a temperature approaching or exceeding the joining temperature [41]. Using this TLP method, alumina has been joined using multilayer Cu/Pt/Cu interlayers because of the promising high-temperature properties of diffusion-bonded Al_2O_3/Pt/Al_2O_3. Interlayers of Cu/80Ni20Cr/Cu were also used to join Al_2O_3 to assess the benefits of reactive metal incorporation in the TLP layer. Also, a Si_3N_4 assembly was produced using a Cu-Au/Ni/Cu-Au based interlayer [41]. A joining process that combines a low joining temperature for use of the joined assembly at high temperature, the partial transient liquid phase (PTLP) bonding method, which is an extension of the TLP joining methods, was developed for the joining of Ni-based superalloys [42]. In both TLP bonding and in the PTLP method, the interlayer solidifies isothermally at the joining temperature. However, there is an important difference in the interlayer design. TLP bonding uses homogeneous interlayers that melt completely, and solidification occurs because the melting point depressant diffuses into the adjoining (metallic) material. In contrast, the PTLP method uses inhomogeneous, multilayer metallic interlayers within which only a thin or partial layer melts at the bonding temperature. For example, a thin cladding layer of a lower melting point metal such as Cu, Au, Ag or their alloys, can be paired with a thicker core layer of a higher melting point metal such as Ni, Pd, Nb and Pt, as shown schematically in Figure 1.1 [43]. By melting of the lower melting point component to initiate at temperatures well below the melting point of the core layer, joining can occur at a temperature well below the melting point of the more

refractory core material. This inhibits or prevents reactions between the core layer materials and the ceramic. Therefore, when compared to TLP bonding, PTLP bonding has greater flexibility in interlayer design and a much larger reduction in joining temperature is possible.

As described above, several methods have been developed to bond ceramics to ceramics and to bond ceramics to metals. However, the relief of the thermal stress generated across the joined interface due to the difference of thermal expansion coefficients of metals and ceramics is still not resolved using these methods. For this current research, Functionally Graded Material (FGM) concept is used to join dissimilar ceramics to resolve this thermal stress problem, and this concept is covered in the next section.

The joining of similar ceramics has been demonstrated using various techniques, such as brazing [22-35], diffusion welding [36], microwave joining [37-40] and Transient Liquid Phase methods [41-43]. However, the joining of dissimilar ceramics has been more difficult and problematic for several reasons. First, differences in the crystal structures and volumes of two dissimilar ceramics cause undesirable reactions at the interface. Second, the moduli of dissimilar ceramics are also different. Finally, the residual stress build up due to the different Coefficients of Thermal Expansion (CTE) is another problem since ceramics usually do not undergo plastic deformation to accommodate the shrinkage. This dissertation describes a new way of joining dissimilar ceramics in the Si_3N_4-Al_2O_3 system by following phase paths via the Si-Al-O-N quarternary (Figure 1.2) phase diagram and in this case by using sialon polytypoids.

The system of Si_3N_4-Al_2O_3 has been chosen as an example for the joining of dissimilar ceramics for several reasons. First, Silicon Nitride has been considered as one of the most promising structural materials for high temperature application because of its unique combination of properties, such as high strength, wear resistance, refractoriness, oxidation resistance, excellent thermal shock properties and resistance to corrosive environments [44]. Second, Al_2O_3 has been chosen because it is chemically compatible with Si_3N_4 and has a relatively large CTE value (8.8×10^{-6} /^{0}C) compared to that of Si_3N_4 (3.6×10^{-6} /^{0}C). This big CTE value can be very useful when Al_2O_3 is considered to be a buffer layer for joining high temperature ceramics to metals. Most of the high temperature ceramics have relatively low CTE values which are in the range of $3 - 4 \times 10^{-6}$ /^{0}C, and most of the metals used in the structural components are beyond 14×10^{-6} /^{0}C [3]. This difference in CTE causes large residual stress when silicon nitride and metal are joined directly and the joint can break easily, decreasing the strength. Therefore, Al_2O_3 can be used as a buffer layer for joining because of its intermediate CTE value. The successful joining of Al_2O_3 and metal has been developed via brazing [41] and solid state diffusion [19]. Therefore, my dissertation is focused on the joining of Si_3N_4 – Al_2O_3 system that has not been demonstrated before. Finally, another advantage of using the Si_3N_4 – Al_2O_3 system is the formation of stable sialons. Sialons are phases in the Si-Al-O-N and related systems. They are comparable in variety and diversity with the mineral silicates. Si_3N_4 is built up of Si_3N_4 tetrahedra joined in a three-dimensional network by sharing corners. Since the atomic arrangement of β-Si_3N_4 is the same as that of beryllium silicate, Be_2SiO_4, the simple principles of silicate crystal chemistry can be applied to

the nitrides. The following reversible replacement has shown that a wide variety of new oxynitride materials, vitreous as well as crystalline, can be built up with the (Si, Al)(O, N)$_4$ tetrahedron as a structural unit.

$$Si^{4+}N^{3-} \leftrightarrow Al^{3+}O^{2-} \quad (1.1)$$

Therefore, sialons are essentially solid solutions of Si, Al, O, and N in which oxygen is partly replaced by nitrogen and at the same time, the corresponding amount of silicon is partly replaced by aluminum, all without any change in structure. Because these sialons have fixed cation:anion ratio, it is possible to control the amount and composition of the intercrystalline phases. The relationships between Si-Al-O-N condensed phases are represented by the quaternary phase diagram shown in (Figure 1.2). Any point in the square diagram Si_3N_4-Al_4O_6-Al_4N_4-Si_3O_6 represents a combination of 12^+ and 12^- valences where the components adopt their usual valency states, (that is Si^{4+}, Al^{3+}, N^{3-} and O^{2-}) [44-46]. As shown in the phase diagram, there are various phases of sialons that can be used as an interlayer to join Si_3N_4 and Al_2O_3. For my research, polytypoid sialons, which are six phases from sialon composition between β' and AlN, are used to join Si_3N_4 and Al_2O_3 successfully. The structure and properties of these polytypoids are covered in Chapter 2 in more detail.

There are several potential applications for this Si_3N_4-Al_2O_3 system can be useful. One application would be to use that system in the oxidation/reduction environment. Since carbides/nitrides are resistant in reducing environment and oxides are more oxidation resistant, this Si_3N_4-Al_2O_3 system would be ideal in an environment where one side is more prone to the oxidation than the other.

1.2. Functionally Graded Material (FGM)

To overcome the thermal stress problems in the conventional joining methods, the concept of Functionally Graded Material (FGM) as the interlayers has been introduced. An FGM interlayer has a gradient in composition from one material to the other. For example, this FGM method can be applied to join Si_3N_4 and Al_2O_3 where this joint is Si_3N_4 rich at one end and changes to Al_2O_3 rich at the other end. The need for functionally gradient materials (FGMs) was initially proposed in Japan when vehicles require high-performance heat-resistant materials, which can withstand ultra high temperatures and extremely large temperature gradients [47]. FGM can minimize the stresses caused by the strains developed on differential shrinkage of the bulk material upon cooling by having a gradient in composition. Since there is a gradient in composition, there is also a corresponding gradient in the coefficient of thermal expansion (CTE) as it is proportional to the local composition. The gradient in CTE is proportional to a gradient in shrinkage, which can accommodate the volume difference between the two pieces during thermal cycling. A diagram showing how FGM works is shown in Figure 1.3.

The FGM concept is currently being adapted in various applications, such as thermal barrier coatings for gas turbines, ceramic engines, nuclear fusion, optical thin films, biomaterials, and electronic materials [48]. Because of these wide applications, there are several routes to fabricate these FGMs. They include chemical vapor deposition [49], plasma spraying [50], powder processing [51], combustion synthesis [52], electrophoretic deposition [53], multiple-step slip casting [54], and multiple-step

sedimentation [55]. While these processes are effective, and have been used for a variety of applications, they are usually system specific and are equipment intensive.

The control over the FGM is important to the joining of the ceramic, as the residual stresses are dependent on how well the FGM is controlled. There are several calculations that show a reduction in residual stress when FGMs are used for joining. The marked effect of the thermal stress reduction by varying the composition profile of the FGM was shown using calculations, which are based on linear elasticity models [56, 57] and on finite element methods [58]. Not only were some calculations shown to demonstrate that FGM does reduce the thermal stress to join two dissimilar materials, but there are some experimental results that demonstrate the validity of these calculations. Some of these fabrications were done using powder metallurgical process, and gave good compositional and microstructural control. These FGMs were mostly metal/ceramic graded composite, such as Partially Stabilized Zirconia (PSZ)/Stainless steel [59], Ni/AlN [60], Ni/Al_2O_3 [61], ZrO_2/Ni [62] and etc [63]. The successful fabrication of these FGMs showed that the thermal expansion coefficient changed smoothly with composition of the composite so that residual thermal stress in the FGM block was possibly reduced.

With this in mind, the powder metallurgical method was used to join two dissimilar ceramics for this research. A powder stacking method was used since this method offers good control of composition profile. The joining of Si_3N_4/Al_2O_3 using the FGM interlayer is discussed in the next chapter.

1.3. Overview of this work

This dissertation describes a new way of joining dissimilar ceramics using Si_3N_4-Al_2O_3 system as an example. To achieve this goal, the related phase diagram was used to identify the phase paths for compatibility, and the concept of FGM was employed to optimize the process. Chapter 2 describes the processing details on how this joint was obtained. To achieve this crack-free joint, the polytypoid sialons are used as functional gradient interlayers, and more details on these polytypoids are described in this chapter. Once this crack-free joint has been achieved, various aspects of this FGM are being studied. Chapter 3 reports microstructural characterization of this crack free joint using Transmission Electron Microscopy (TEM), X-ray diffractometer (XRD) and Electron Probe X-ray Microanalysis (EPMA), and the background information on how these tools work is explained in the Appendices. Chapter 4 develops the computational analysis of residual stress where the Finite Element Method (FEM) is used to calculate the residual stress build-up in the joints that have been processed. This analysis gives an estimate of residual stresses, calculated strictly from the properties and the volume fractions of the constituent. These values are indicative of why previous joints are cracked whereas the final sample is crack-free. The mechanical properties of this crack-free joint are investigated in Chapter 5. The interface strength along the joint is studied using the oriented indentation test, and 3-point bend tests were done at room and at high temperature to characterize the joint strength. Finally, Chapter 6 summarizes the results of my research.

1.4. References

1. N.D. Tinsley, J. Huddleston and M.R. Lacey, "The Reduction of Residual stress Generated in Metal-Ceramic Joining", *Materials and Manufacturing Processes*, **13** [4] 491-504 (1998)

2. M.M. Schwartz, Ceramic Joining, ASM International, Materials Park, Ohio (1990)

3. M. Stantella, "A review of Techniques for Joining Advanced Ceramics", *Ceram. Bull*., **71**[6], 947-954 (1992)

4. K. Suganuma, Y.Miyamoto and M. Koizumi, "Joining of Ceramics and metals", *Ann.Rev.Mater.Sci.*, **18**, 47-73 (1988)

5. J.E. McDonald and J.G. Eberhart, "Adhesion in aluminum oxide-metal systems", *Trans. AIME*, **233**, 512-517 (1965)

6. M.G. Nicholas, T.M. valentine and M.J. Waite, "The wetting of alumina by copper alloyed with titanium and other elements", *J. Mater.Sci*., **15** [9], 2197-2206 (1980)

7. X.S. Ning, K. Suganuma, M. Morita and T. Okamoto, "Interfacial reaction between silicon nitride and aluminum", *Philos. Mag*., **55** [3], 93-97 (1987)

8. A.F. Moodie and C.E. Warble, "Direct observation of Pd/MgO and Pd/SiO2 reactions in the transmission electron microscope", *Philos. Mag.*, **35** [1], 201-211 (1977)

9. Y. Ishida, H. Ichinose and S. Tanaka, (1985), "High resolution Electron microscopy of Silicon Nitride/Metal bonded interfaces", Ceramic Microstructures '86. Role of interfaces, Plenum Press, 379-386 (1987)

10. S.D. Peteves, G. Ceccone, M. Paulasto, V. Stamos and P. Yvon, "Overview: Joining Silicon Nitride to Itself and to Metals", *JOM*, 48-77 (January 1996)

11. J. Intrater, "The challenge of Bonding Metals to Ceramics", Machine Design, 95-100 (November, 1989)

12. G.J. Tennenhouse, A. Ezis and F.D. Runkle, "Interaction of Silicon nitride and metal surfaces", *J.Am.Ceram.Soc*. **68**[1], C30-31 (1985)

13. M.G. Nicholas, Joining of Ceramics, Chapman and Hall Publishing company (1990)

14. R.V. Allen and W.E. Borbidge, "Solid state bonding of noble metals to alumina. The effect of ambient atmosphere", *Science of Ceramics*, **12**, 383-389 (1983)

15. R.V. Allen and W.E. Borbidge, "Solid state metal-ceramic bonding of platinum to alumina", *J. Mater. Sci.,* **18**, 2835-43 (1983)

16. R.V. Allen, W.E. Borbidge and P.T. Whelan, "The reaction –bonded zirconia oxygen sensor: an application for solid-state metal-ceramic reaction-bonding", *Advanced Ceramics Science and Technology of Zirconia*, **12**, 537-43 (1984)

17. M.G. Nicholas and R.M. Crispin, "Diffusion bonding of stainless steel to alumina using aluminum interlayers", *J. Mater.Sci.*, **17**, 3347-60 (1982)

18. K. Suganuma, T. Okamoto, Y. Miyamoto, Y. Shimada and M. Koizumi, "Joining Si_3N_4 to type 405 steel with soft metal interlayers", *Mater.Sci. Technol*., **2**, 1156-61 (1986)

19. L. Esposito, A. Bellosi, S. Guicciardi and G. De Portu, "Solid state bonding of Al2O3 with Cu, Ni and Fe: Characteristics and Properties", *J. Mat. Sci*., **33**, 1827-1836 (1998)

20. M.G. Gee, "Surface Reaction between Alumina and Nickel at high temperatures", *Proceedings of the British Ceramic Society*, **34**, 261-72 (1984)

21. P. Lourdin, D. Juve and D. Treheux, "Nickel-Alumina bonds: Mechanical Properties Related to Interfacial Chemistry", *Journal of European Ceramic Society*, **16** [7], 745-52 (1996)

22. R.L. Bronnes, R.C.Hughes and R.C. Sweet, "Ceramic-to-metal bonding with sputtering as a metallization technique", *Philops tech. Rev.* **35**, 209-211 (1975)

23. S. Weiss and C.M. Adams, Jr., "The Promotion of Wetting and Brazing", *Weld. J.Suppl.*, **46**[2], 49s-57s (1967)

24. M.J. Ramsey and M.H. Lewis, "Interfacial Reaction Mechanisms in Syalon Ceramic Bonding", *Mater.Sci.Eng*., **71**, 113-122 (1985)

25. A.J. Moorhead and H. Kim, "Joining of Oxide Ceramics", Engineered Materials Handbook, Ceramics and Glasses, vol. 4, ASM international, Metals park, Ohio, 511-522 (1991)

26. M.G. Nicholas, "Active Metal brazing", *J. Br. Ceram. Trans*., **85**, 144-146 (1986)

27. R. E. Loehman, "Wetting and joining of Mullite Ceramics by Active-metal Braze alloys", *J. Am. Ceram. Soc.*, **77** [1], 271-74 (1994)

28. W.A.Zdaniewski, "Crystallization toughening of ceramic Adhesives for Joining Alumina", *Adv. Ceram. Mater*., **2**[3A], 204-208 (1987)

29. S.L. Swartz, "Joining of Zirconia Ceramics with a CaO-TiO2-SiO2 Interlayer", *Proc. Of the Twenty-Sixty Auto. Tech. Dev. Contractors' Coord. Mtg.*, 24-27 (1988)
30. M.E. Milberg, "The Nature of Sialon Joints between silicon nitride based bodies", *J. Mater. Sci.*, **22**[7], 2560-2568 (1987)

31. S. Baik and R. Raj, "Liquid-phase bonding of Silicon Nitride Ceramics", *J. Am. Ceram. Soc.*, **70**[5], C105-C107 (1987)

32. S.M. Johnson and D.J. Rowcliffe, "Mechanical properties of joined Silicon Nitride", *J. Am. Ceram. Soc.*, **68**[9], 468-472 (1985)

33. R.E. Loehman and A. P. Tomsia, "Joining of ceramics", *Ceram. Bull.*, **67** [2], 375-380 (1988)

34. M. Gopal, L.C. DeJonghe and G. Thomas, "Silicon Nitride: From sintering to joining", *Acta Mater*., **46**[7], 2401-2405 (1998)

35. M. Gopal, L.C. DeJonghe and G. Thomas, "Silicon Nitride joining using rare-earth reaction sintering", *Scripta Materialia*, **36**[4], 455-460 (1997)

36. M. Nakamura, K. Kubo and S. Kanzaki, "Joining of Silicon nitride ceramics by hot pressing", *J. Mater. Sci.*, **22**, 1259-1264 (1987)

37. D. Palaith and R. Silberglitt, "Microwave Joining of ceramics", *Ceram. Bull*., **68**[9], 1601-1606 (1989)

38. T. Sato, N.Takahashi and K. Shimakage, "Microwave joining of Alumina to Magnesia", *J. Ceram. Soc. Jap*., **104**[10], 905-907 (1996)

39. H. Fukushima, T. Yamanaka and M. Matsui, "Microwave heating of ceramics and its application to joining", *J. Mater. Res.*, **5**[2], 397-405 (1990)

40. M.N. Rahaman, Ceramic Processing and Sintering, Marcel Dekker, Inc., New York, 725-735 (1995)

41. B.J. Dalgleish, A.P. Tomsia, K. Nakashima, M.R. Locatelli and A.M. Glaeser, "Low temperature routes to joining ceramics for high-temperature application", *Scripta Metallurgica et Materialia*, **31**[8], 1043-1048 (1994)

42. D.S. Duvall, W.A. Owczarski and D.F. Paulonis, “TLP bonding: a new method for joining heat resistant alloys”, *Welding Journal*, **53**, 203 (1974)

43. A.M. Glaeser, “The use of transient FGM interlayers for joining advanced ceramics”, *Composites part B*, **28B**, 71-84 (1997)

44. K.H. Jack, “The Sialon”, *Mat.Res. Bull.,* **13**, 1327-1333 (1978)

45. M.H. Lewis, B.D. Powell and P. Drew, “The formation of single-phase Si-Al-O-N ceramics”, *J. Mat. Sci.,* **12**, 61-74 (1977)

46. K.H. Jack, “Sialon ceramics: Retrospect and prospect”, *Materials research Society Symposium proceeding*, **287**, 15-27 (1992)

47. M. Koizumi and M. Niino, “Overview of FGM research in Japan”, *MRS Bull*., **20**[1], 19-21 (1995)

48. B.H. Rabin and I. Shiota, “Funtionally Gradient Materials”, *MRS Bull*., **20**[1], 14-15 (1995)

49. M. Sassaki, Y. Wang, T.Hirano and T. Hirai, “Design of SiC/C functionally gradient material and its preparation by chemical vapor deposition”, *J. Ceram. Soc. Jpn.*, **97**[5], 539-543 (1989)

50. T. Hashida, H. Takahasi and K. Miyawaki, “Evaluation of thermal shock fracture of functionally gradient materials”, *J. Jpn.Soc.Powd.Metall.*, **37**[2], 307-312 (1990)

51. R.Watanabe, “Powder Processing of functionally graded materials”, *MRS Bull.*, **20**[1], 32-34 (1995)

52. A.Takahashi, K. Tanihata, Y.Miyamoto and M.Oyanagi, “Combustion synthesis of Nb-N graded material”, *J.Jpn.Soc. Powd. Metall.*, **37**[2], 263-266 (1990)

53. P. Sarkar, X.Huang and P.S. Nicholson, “Zirconia/alumina functionally gradient composites by electrophoretic deposition techniques”, *J. Am. Ceram. Soc.*, **76**[4], 1055-1056 (1993)

54. H. Takebe and K. Morinaga, “Fabrication of zirconia-nickel functionally gradient materials by slip casting and pressureless sintering”, *Materials and Manufacturing processes*, **9**[4], 721-733 (1994)

55. D.P. Miller, J.J. lannutti and R.D. Noebe, “Fabrication and properties of functionally graded NiAl/Al2O3 composites”, *J. Mater. Res.*, **8**[8], 2004-2013 (1993)

56. R.W. Messler, M. Jou and T.T. Orling, "A model for designing functionally gradient material joints", *Welding Journal*, **74**[5], S160-S167 (1995)

57. K.S. Ravichandran, "Thermal residual stresses in a functionally graded material system", *Mater. Sci. Eng. A*, **201**, 269-276 (1995)

58. R.L. Williamson and B.H. Rabin, "Numerical modeling of residual stress in Ni-Al2O3 gradient materials", Functionally gradient Materials, Eds. J.B. Holt, M. Koizumi, T. Hirai and Z.A. Munir, Ceram. Trans., **34**, 55-65, American Ceramic Society (1993)

59. A. Kawasaki and R. Watanabe, "Powder metallurgical fabrication of the thermal-stress relief type of functionally gradient materials", Sintering '87, Eds. S. Somiya, M. Shimada, M. Yoshimura and R. Watanabe, **2**, 1197-1201, Elsevier Applied Science (1987)

60. K. Atarashiya, Y. Ishida and T. Nagai, "Functionally gradient material of the system Ni-AlN by pressureless sintering", Functionally Gradient materials, Eds. J.B. Holt, M. Koizumi, T. Hirai and Z.A. Munir, Ceram. Trans., 141-148 (1993)

61. B.H. Rabin, R.L. Williamson, R.J. Heaps and Ad.W. Erickson, "Powder processing of Nickel-Aluminum Oxide gradient materials", *Adv. Powder Metall. Part. Mater.*, **9**, 1-9 (1992)

62. H. Takebe, T. Teshima, M. Nakashima and K. Morinaga, "Powder processing Technique for development of Zirconia-Nickel Functionally Gradient Materials", *J. Ceram. Soc. Jpn.*, **100**[4], 387-391 (1992)

63. M. Sasaki and T. Hirai, "Fabrication and Properties of functionally gradient materials", *The Centennial Memorial Issue of the Ceramic Society of Japan*, **99**[10], 1002-1013 (1991)

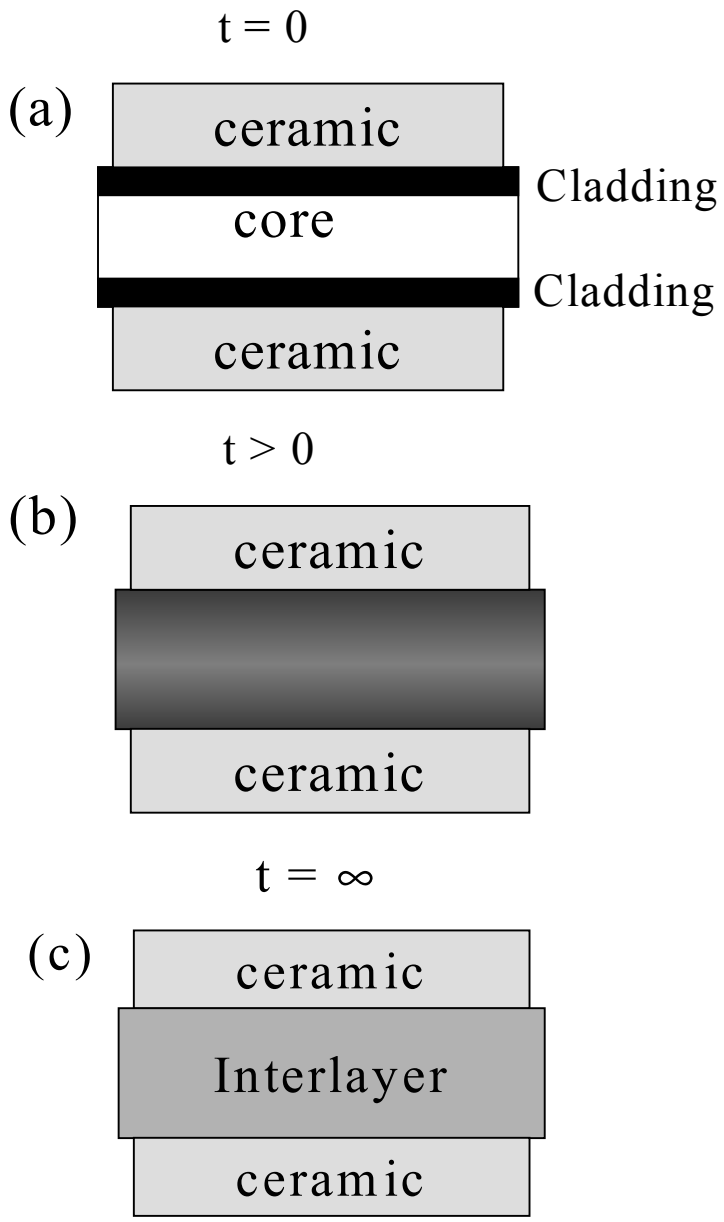

Figure 1.1. Schematic illustration of multilayer interlayer design and evolution. (a) Initially, a sharp discontinuity exists between the thicker core layer and the thinner cladding layers. (b) After some heat treatment and interdiffusion, the interlayer homogenizes, which increases the temperature. (c) After prolonged annealing of use at elevated temperature, a uniform interlayer results. (Ref. 43)

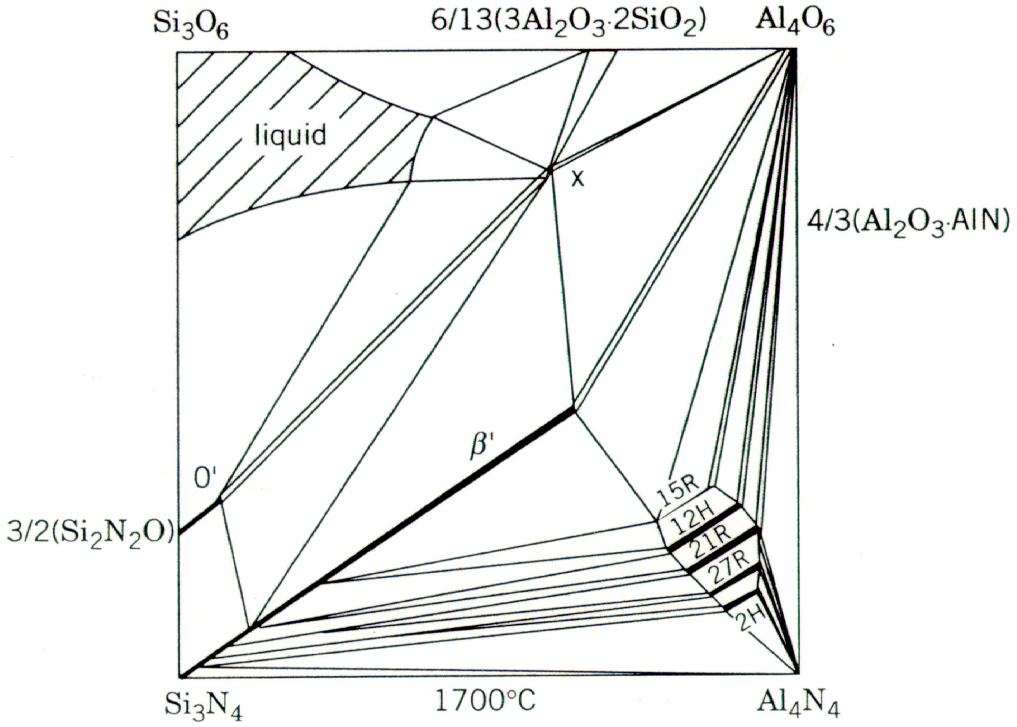

Figure 1.2. The Si-Al-O-N system (1700 ^{o}C) (Ref. K.H.Jack, Mat. Res. Soc. Sym. Proc., 1992, 287, p.16)

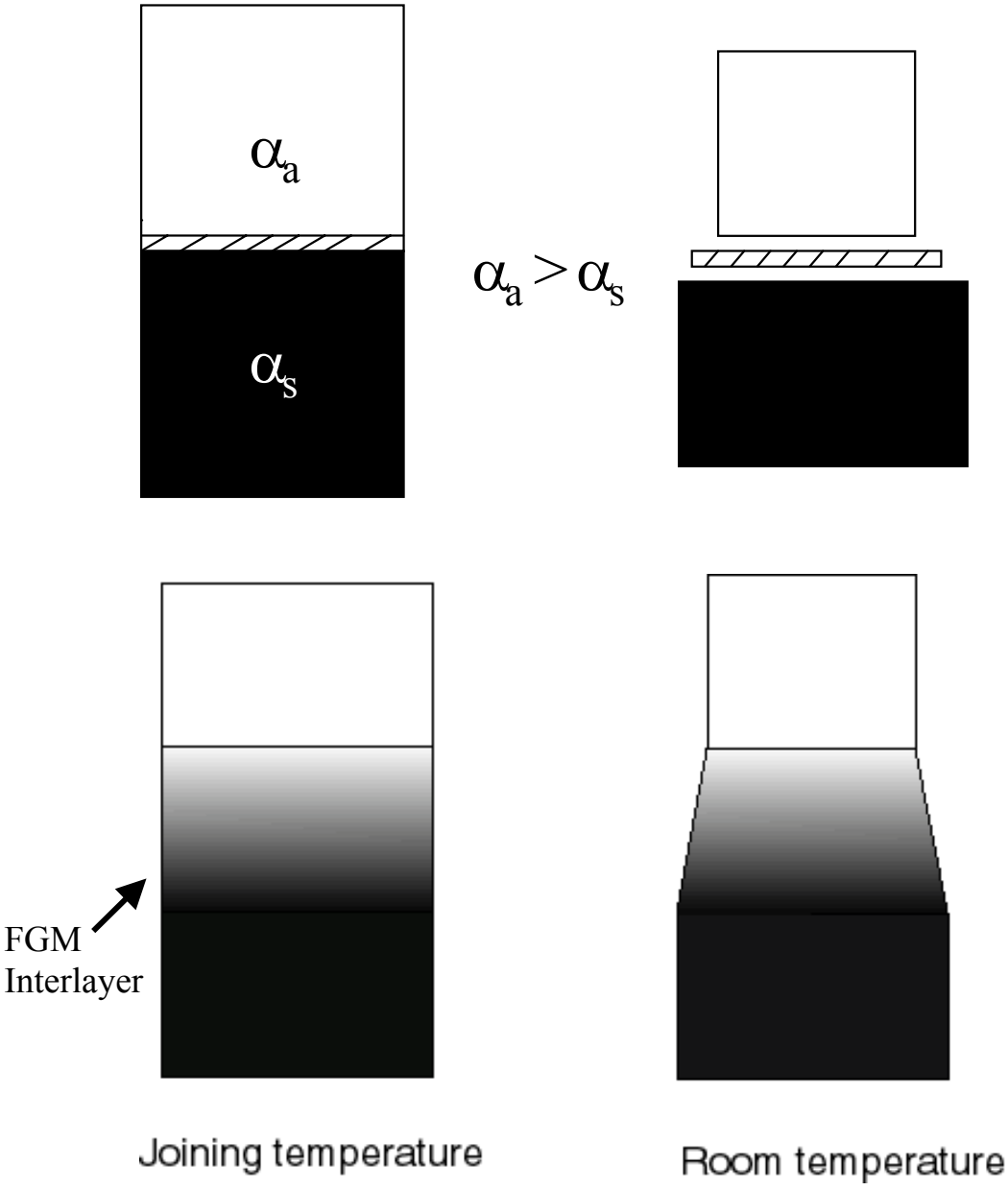

Figure 1.3. Rationale behind the approach to use FGMs to join different materials. When the interlayer has no gradient (top), the pieces do not join. However, when a graded interlayer is used (bottom), the two pieces can be joined.

CHAPTER 2: Joining of Dissimilar Ceramics in the Si_3N_4-Al_2O_3 System Using Polytypoid Functional Gradients

2.1. Introduction

As outlined in the previous chapter, the joining of materials is an important process commercially and technologically. Due to the existence of physical and economic limitations for the manufacture of large parts, joining is essential. Further, for fabrication of complex shapes, it is much easier to make regular geometrical shapes and then join them. Finally, having different materials at different regions of the same component is desirable for several applications [1]. Joining to form these components is often the only way for fabrication.

Gopal et al. [2,3], have performed experiments on the joining of Si_3N_4 to itself, using a rare-earth silicate glass which is a ceramic interlayer, following earlier work on sintering Si_3N_4 to produce glass free joints [4, 5]. However, these interlayers cannot be used to join dissimilar materials. This is because of the large difference in their coefficients of thermal expansion, which leads to the development of stresses, that cause failure. The joining of these different materials can be effected using Functionally Graded Materials (FGMs). In an FGM, there is a continuous change in composition from one region to another. When an FGM is used, the shrinkage depends on the concentration of the species present locally. The FGM can therefore accommodate the shrinkage strain and join with dissimilar materials. In this work, polytypoidal functional gradients are used to join the dissimilar ceramics, Si_3N_4 and Al_2O_3 as shown in Figure 2.1.

Silicon nitride has been considered as one of the most promising structural materials for high temperature applications for the following unique properties: high strength, oxidation and corrosion resistance, thermal stability and resistance to thermal shock [6]. However, because it is a covalent solid, its self-diffusivity is low, and so it is not easily densified by the high temperature firing used for conventional oxide ceramics. So the difficulty in the fabrication process of complex shaped and larger sized components requires the development of a joining technology for ceramics [7]. Alumina has been chosen for the joining material since it has an intermediate coefficient of thermal expansion between Si_3N_4 and metals, as shown in Figure 2.2. Alumina can be used as a buffer layer for joining Si_3N_4 and metal. Moreover, it has been widely used in high temperature structural components due to its chemical stability. As for the strength of alumina, it gradually decreases at high temperatures, probably due to its ionic bonding nature [8]. However, it has been found that hot pressed composites of alumina and sialon can improve the strengths at high temperature [9]. The composites fabricated by the dispersion of two phases, maintained a higher strength than single-phase alumina ceramics, up to 1400 ^oC. Therefore, the formation of two-phase structures is important in improving fracture toughness, by crack deflection to absorb the fracture energy [9].

To join Si_3N_4 to Al_2O_3, a sialon polytypoid has been used for several reasons: First, sialons are essentially silicates and alumino-silicates in which oxygen is partly or completely replaced by nitrogen, while silicon is partly replaced by aluminum [6]. Sialon polytypoids are physically and chemically compatible with both Si_3N_4 and Al_2O_3. Because metal-nitrogen bonding is in general more covalent than metal-

oxygen, there is freedom to vary the covalent: ionic contributions to the interatomic bonding in a variety of structures [10]. The relationships between Si-Al-O-N condensed phases are represented by the quaternary phase diagram in Figure 2.3. Any point in the square diagram Si_3N_4-Al_4O_6-Al_4N_4-Si_3O_6 represents a combination of 12^+ and 12^- valences where the components adopt their usual valency states (that is Si^{4+}, Al^{3+}, N^{3-} and O^{2-}). A polytypoid is defined as a faulted structure in which the fault periodicity depends on composition through the cation/anion ratio. These polytypoids are different from a polytype, which has a faulted structure with no change in composition, such as SiC. It was found that AlN polytypoids, such as 15R, 12H, 21R, 27R and 2H, have CTEs in the range of 5.1 to 5.9 x 10^{-6} /^{0}C [11]. Since the CTE of Si_3N_4 is 3.6x10^{-6}/^{0}C and that of Al_2O_3 is 8.8x10^{-6}/^{0}C, the use of sialon polytypoids for joining Si_3N_4 and Al_2O_3, is clearly attractive as shown in Figure 2.4.

In this Si_3N_4 - Al_2O_3 system, there are six polytypoid phases from the sialon compositions between β' and AlN as illustrated in Figure 2.3. They have structures based on the AlN wurtzite-type (Figure 2.5). These phases are members of a new series of polytypoids in which the structure is determined by the metal: nonmetal atom ratio M/X. The polytypoids have compositions M_mX_{m+1} where m is an integer 4 to 9, and the structures are described by the Ramsdell symbols 8H, 15R, 12H, 21R, 27R and 2H [6,10,12]. There are n double layers MX along the c-dimension of the hexagonal (H) or rhombohedral (R) unit cell where n is the Ramsdell numeral and nH = 2m, nR = 3m [6]. Hexagonal polytypoids thus contain two and rhombohedral polytypoids contain three symmetry-related blocks, each of m layers, per unit cell. From Figure 2.5, the metal atoms (Al) form a hexagonal close-packed arrangement

and the non-metal atoms (N) fill one-half of the available tetrahedral sites giving rise to the composition AlN. When the metal to non-metal ratio (M/X) decreases (reaching a minimum at ½ when all tetrahedra are occupied), the non-metal ions fill adjacent tetrahedra. The adjacent tetrahedra share common faces, which gives rise to impossibly short interatomic distances between non-metal atoms. This can be avoided if the metal atom configuration is locally changed from hexagonal (ABAB …) to cubic (ABC …), by introducing a stacking fault in the metal-ion configuration. So, for AlN-rich compositions of the sialon system, the excess non-metal atoms are taken up by creating periodic stacking faults in the metal configuration and filling up a double layer of tetrahedra at every fault [12 - 14]. It is clear that the further the M/X ratio deviates from 1, the smaller is the stacking fault spacing. The stacking sequence of 12H and 15R is shown in Figure 2.6 as an example. Therefore, polytypoid step functional joining can be obtained since the structure of this compound is determined by stacking-fault spacing (metal/non metal ratio).

In this chapter, the processing details on how this final FGM joint was obtained, will be discussed.

2.2. Experimental Procedure

2.2.1. Fabrication of FGMs

To create FGMs, a "mixture rule" was applied to make the gradient since it has been widely used in the modeling of FGMs [15,16]. A material having two components, denoted as A and B, is considered. Let P_A and P_B be the values of some particular property for pure A and pure B, respectively, and let their respective

volume fractions be f_A and f_B, where $f_B = 1- f_A$ assuming that the material is 100% dense. For an FGM, these values of f are dependent upon position along the graded direction. The well-known Voigt-type estimate for the effective value, P, of the property of FGM is

$$P = f_A P_A + f_B P_B \quad (2.1)$$

This "mixture rule" was applied to calculate Coefficient of Thermal Expansion (CTE) of each graded layer so that the final FGM with 18 graded layers would have a CTE difference of approximately 0.2 x 10^{-6} /^{0}C between each layer, to minimize residual stress (Figure 2.7).

FGMs can be fabricated by a number of methods, such as powder processing [17], thermal spraying [18], CVD[19] and combustion synthesis [20]. For the experiment, powder processing was used to provide a wide range of compositional and microstructural control. Powder blending was done by wet milling of powders using isopropanol as solvent. For powder processing, 6wt% Y_2O_3 and 2wt% Al_2O_3 were added as sintering additives to sinter Si_3N_4. Si_3N_4 powders from H.C. Starck with a particle size ranging from 0.4 - 1.2 μm were used, and Al_2O_3 powders from Sumitomo industries with the particle size ranging from 0.1 to 0.3 μm were used. 12H sialon polytypoid powders were obtained from Novel Technologies. 3 wt% Y_2O_3 was used as sintering additive for polytypoid powders.

Direct joining of Si_3N_4-polytypoid-Al_2O_3 was fabricated at first to study if residual stress build-up among layers can be minimized by using a thin polytypoid interlayer, which has an intermediate CTE between that of Si_3N_4 and Al_2O_3, as shown in Figure 2.9. Then, thicker polytypoid layer was used to directly join Si_3N_4 and

Al_2O_3 (Figure 2.10). After realizing that the direct joining is not enough to minimize the residual stress build-up, gradient layers were added between Si_3N_4 and Al_2O_3. At first, gradient layers were added by 25wt% increment in composition between two joining materials as shown in Figure 2.11. After observing certain areas had more cracks than the other areas, more gradient layers were added to remove those cracks (Figure 2.12). Finally, a FGM joint, which consists of 20 graded layers with 10 wt% increment in composition, was fabricated to obtain a crack-free joint (Figure 2.13).

2.2.2. Sintering of FGMs

All the FGMs were fabricated by the following method; first, powders of each composition were mixed in isopropanol solvent, and then powders were agitated using the Ultrasonicator to prevent agglomeration. These powders were dried, and sieved and were stacked layer by layer. The green body was pressed using a cold press to maintain a cylindrical shape. Finally, this green body was sintered using a Hot Press at 1700 ^oC for 2 hours in flowing N_2 gas to prevent decomposition of Si_3N_4, and the experimental setup is shown in Figure 2.8. A heating rate of 10^oC per minute was used to heat up to 1700 ^oC and hot pressing was used to achieve full density. Following densification, the sample was cooled with a cooling rate of 2 ^oC/min to minimize thermal stress build-up. Actual bulk densities were determined by the Archimedes method of weighing the sample in air and then in water, which was used as the immersion liquid.

2.3. Results and Discussion

2.3.1. Joint fabrication

Direct joining of Si_3N_4-polytypoid-Al_2O_3 was fabricated at first to study if residual stress build-up among layers can be minimized by using a thin polytypoid interlayer, which has an intermediate CTE between those of Si_3N_4 and Al_2O_3. Figures 2.9 through 2.13 are optical micrographes showing the cross section of the joints. As shown in Figure 2.9, cracks developed due to residual stress building up among the layers. Then, a thicker interlayer which has a similar thickness as the joining materials, was used in the middle as shown in Figure 2.10 since the thin interlayer did not resolve the problem. This thick interlayer was used possibly to relieve some of the strain energy that formed during the joining of these two materials. However, the result in Figure 2.10 shows that cracks still developed due to residual stress build up among the layers. For both Figures 2.9 and 2.10, cracks developed in the Al_2O_3 side rather than Si_3N_4 side. As the material cools, Al_2O_3, which has a higher CTE, shrinks in tension mode, whereas Si_3N_4, which has a lower CTE value, shrinks in compression. Since ceramics are weaker in tension than in compression, cracks develop in the Al_2O_3 side perpendicular to the direction of tension. Since adding a thicker layer did not resolve crack problems, grading layers were added between the joining materials to relieve residual stress, as shown in Figure 2.11. The gradient across the length of the joint was varied by 25 wt% increment in composition but some cracks were still observed, indicating that there is still some residual stress build-up. Large cracks seem to propagate from Al_2O_3 due to the large thermal mismatch between Si_3N_4 and Al_2O_3. Moreover, small cracks were observed in the 100%

polytypoid layer toward the Si_3N_4 side. It seems that more gradient layers are needed between 100% polytypoid and 75wt% 12H Polytypoid/25wt% Si_3N_4 so as to reduce residual stress. Figure 2.12 shows the joint, with more added gradient layers between 100% polytypoid layer and Si_3N_4 side to remove little cracks. Most of the small cracks were removed, but large cracks still exist across the FGM, indicating that a finer gradient is needed in the Al_2O_3 side as well. Therefore, from these series of joints that were processed, it is deduced that a more consistent gradient is needed to create a crack-free joint. Moreover, previous studies have indicated that a better result can be obtained by varying the number of layers and the incremental change in composition from layer to layer, than by increasing the overall graded joint thickness [21].

Finally, an FGM joint which consists of 20 graded layers, was introduced by a powder stacking method (Figure 2.13). The composition along the gradient was varied by 10 wt% to create a smooth gradient across the thickness. Thus, 20 layers were added to minimize the CTE mismatch stresses as much as possible (Figure 2.7). As can be seen from Figure 2.13, the composite Si_3N_4-polytypoids-Al_2O_3 is crack-free. The thermal residual stress that has been mentioned so far, can be calculated using the Finite Element Method, and this analysis will be discussed in Chapter 4. The density of this FGM sample using Archimedes method was measured to be 96-97 %.

2.3.2. Sintering Mechanism

The sintering mechanism of this FGM is mostly liquid-phase sintering as the process is essentially that of solution-reprecipitation within a eutectic liquid with accompanying particle rearrangement and phase transformation. Studies have shown that the alloying approach of Si_3N_4 and sialons to control the residual liquid content has been remarkably successful in producing an essentially single-phase ceramic with outstanding high-temperature mechanical properties. Although the sintering mechanism remains that of solution-reprecipitation, the liquid is transient, and its components are largely removed by the sialon solid solution such that grain boundaries contain only segregated ions within a width of the same order as the β' lattice spacing [22]. Nevertheless, glassy phases may still be retained especially at triple junctions, but these may be crystallized in the presence of certain rare-earth addition [2]. More detailed microstructural studies on the FGM joint are covered in Chapter 3.

2.4. Conclusions

The FGM of Si_3N_4-Al_2O_3 using polytypoid functional gradient was successfully fabricated by powder stacking method through a series of experiments. Crack-free joining of Si_3N_4 to Al_2O_3 (Figure 2.13) was produced by stacking 20 layers of polytypoids with thickness of 500 μm each, to minimize thermal residual stress. The result showed a smooth gradient across the thickness with varying the composition along the gradient by 10 wt%. This method can be applied to other dissimilar ceramics as long as there is no undesirable reaction between the systems. In

order to accomplish such processing effectively, accurate phase diagrams for each multicomponent system are needed.

2.5. References

1. M.M.Schwartz, Ceramic Joining, ASM International, Materials park, Ohio (1990)

2. M, Gopal, L.C. DeJonghe and G. Thomas, "Silicon Nitride joining using rare-earth reaction sintering", *Scripta Materialia,* **36** [4], 455-460 (1997)

3. M. Gopal, L.C. DeJonghe and G. Thomas, "Silicon Nitride:From Sintering to joining", *Acta Mater*., **46** [7], 2401-2405 (1998)

4. M.Cinbulk and G. Thomas, "Fabrication and secondary phase crystallization of Rare-earth disilicate-silicon nitride ceramics", *Journal of American Ceramic Society*, **75** [8], 2037 (1992)

5. Y.Goto and G.Thomas, "Microstructure of silicon nitride ceramics sintered with rare-earth oxides", *Acta metall. mater*., **43**[3], 923 (1995)

6. P.M. Johnson and A. Hendry, "The microstructure of hot-pressed sialon polytypes", *Journal of Materials science* **14**, 2439 (1979)

7. M. Nakamura, K.Kubo, S.Kanzaki and H.Tabata, "Joining of Silicon nitride ceramics by hot pressing", *Journal of Materials science*, **22**, 1259 (1987)

8. K. Takatori, "Pressureless sintering and mechanical properties of alumina-sialon composites", *Journal of materials science*, **26**, 4484 (1991)

9. K.Takatori and O. Kamigaito, "Mechanical properties of hot-pressed alumina-sialon composites", *Journal of materials science letters*, **7**, 1024 (1988)

10. K.H.Jack "The sialons", *Mat. Res. Bull*. **13**, 1327 (1978)

11. I. Yamai and T. Ota, "Thermal expansion of Sialon", *Advanced ceramic materials*, **2**[4], 784 (1987)

12. G. Van Tendeloo, K.T. Faber and G.Thomas, "Characterization of AlN ceramics containing long-period polytypes", *Journal of materials science*, **18**, 525 (1983)

13. K. H. Jack, "Review: Sialons and related nitrogen ceramics*", Journal of materials science* **11**, 1135 (1976)

14. K.M. Krishnan, R.S. Rai and G.Thomas, "Characterization of long period polytypoid structures in the Al2O3 – AlN system", *Mat.Res.Soc.Symp.Proc.*, **60**, 211-218 (1986)

15. A.J. Markworth, K.S. Ramesh and W. P. Parks Jr., "Review: Modeling studies applied to functionally graded materials", *Journal of Materials science*, **30**, 2183-2193 (1995)

16. Z. Fan, P. Tsakiropoulos and A. P. Miodownik, "A generalized law of mixtures", *Journal of materials science*, **29**, 141-150 (1994)

17. R.Watanabe, "Powder processing of functionally gradient materials", *MRS Bulletin*, **20**[1], 32-34 (1995)

18. S. Sampath, H. Herma, N.Shimoda and T. Saito, "Thermal spray processing of FGMs", *MRS Bull*. **20**[1], 27 (1995)

19. T. Hirai, "CVD Processing", *MRS Bull*., **20**[1], 45 (1995)

20. G.C. Stangle and Y. Miyamoto, "FGM fabrication by combustion synthesis", *MRS Bull.,* **20**[1], 52 (1995)

21. R.W. Messler, M. Jou and T.T.Orling, "A model for designing functionally gradient material joints", *Welding Journal*, **74**[5], S166 (1995)

22. M.H. Lewis and R.J. Lumby, "Nitrogen ceramics: liquid phase sintering", *Powder metallurgy*, **26**[2], 73-81 (1983)

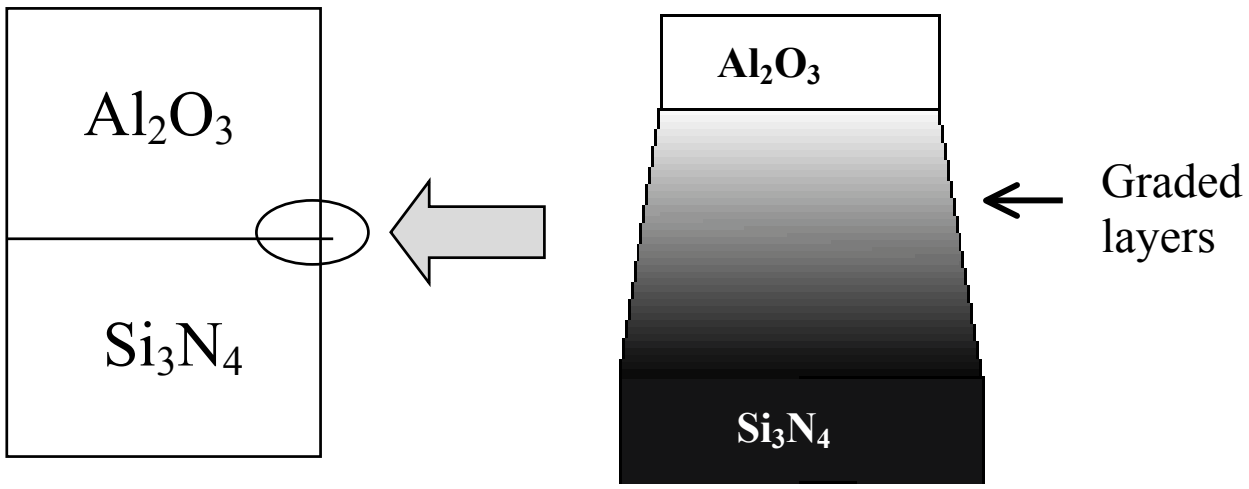

Figure 2.1. Schematic sketch showing the grading layers to join dissimilar ceramics in Si_3N_4-Al_2O_3 system.

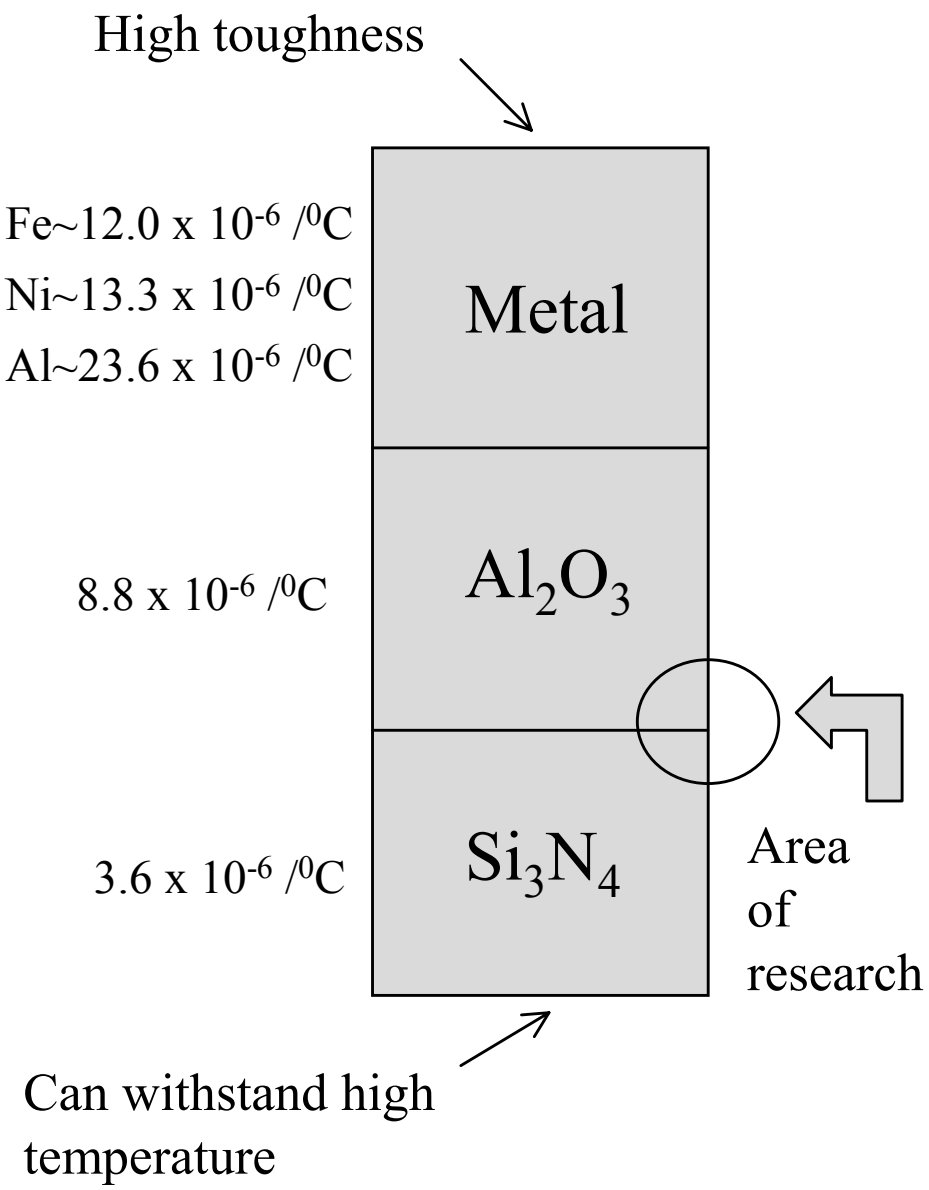

Figure 2.2. Schematic showing the choice of materials. Al_2O_3 has a coefficient of thermal expansion between that of Si_3N_4 and a metal. Therefore, it can act as a buffer layer between the two pieces. Further, Al_2O_3 is chemically compatible with both Si_3N_4 and the metal.

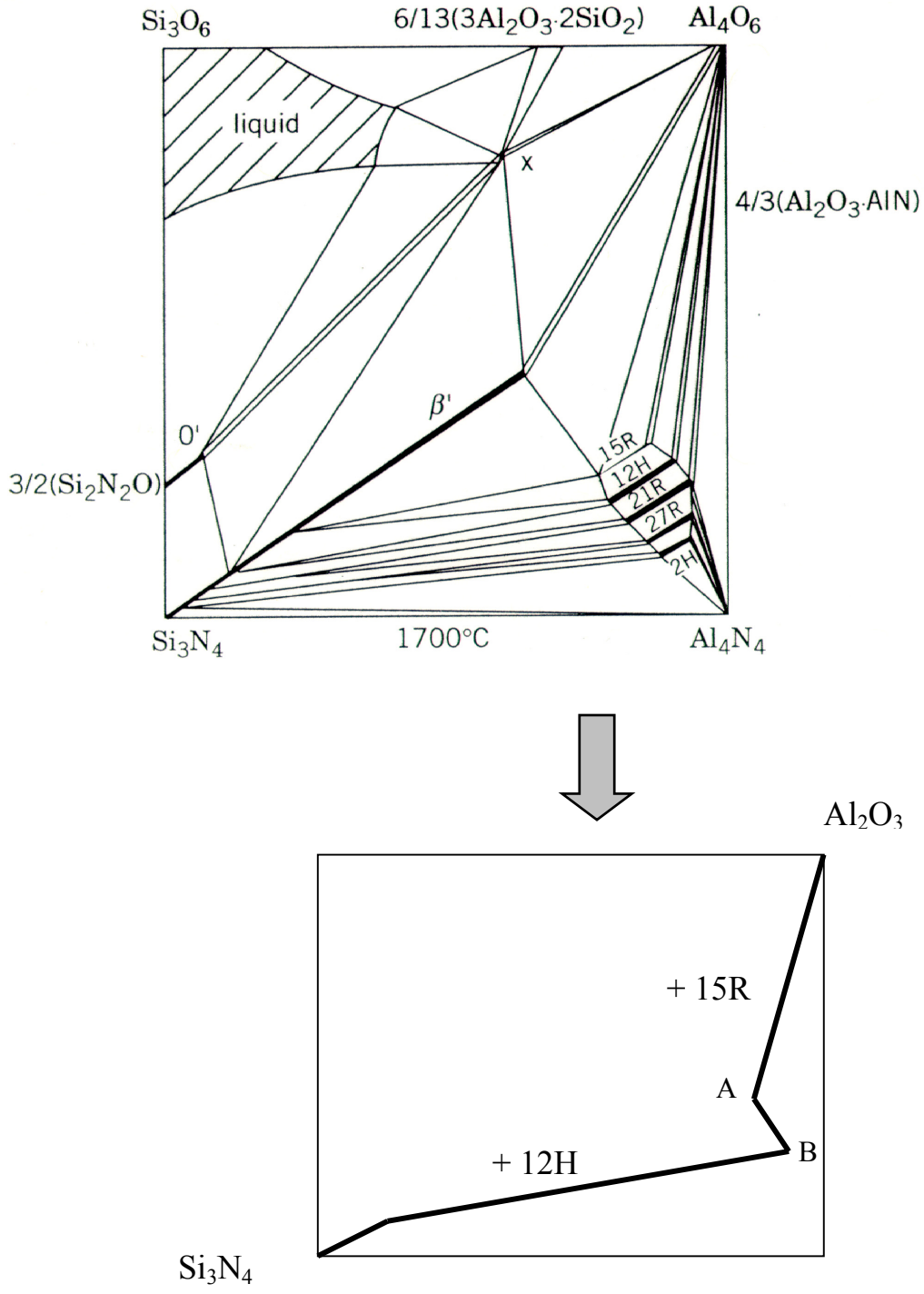

Figure 2.3. The Si-Al-O-N system (1700 ^{o}C) (Ref. K.H.Jack, Mat. Res. Soc. Sym. Proc., 1992, 287, p.16). The diagram below the quarternary phase diagram shows an equilibrium line path of Si_3N_4-12H-15R-Al_2O_3. A-B line refers to the 12H/15R "interface" at the center of the FGM.

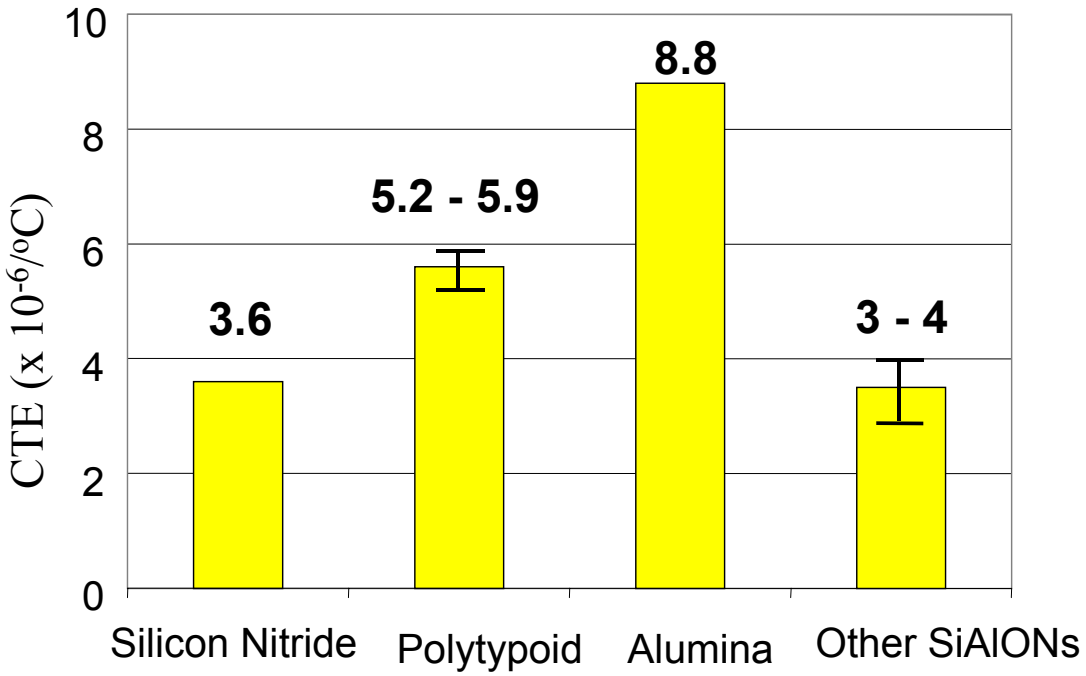

Figure 2.4. Coefficient of Thermal Expansion (CTE) of various ceramics. Other Sialons in the quaternary phase diagram were considered to be used as an interlayer, however, these sialons have their CTEs close to that of Silicon Nitride rather than being the intermediate value between that of Si_3N_4 and Al_2O_3 [11].

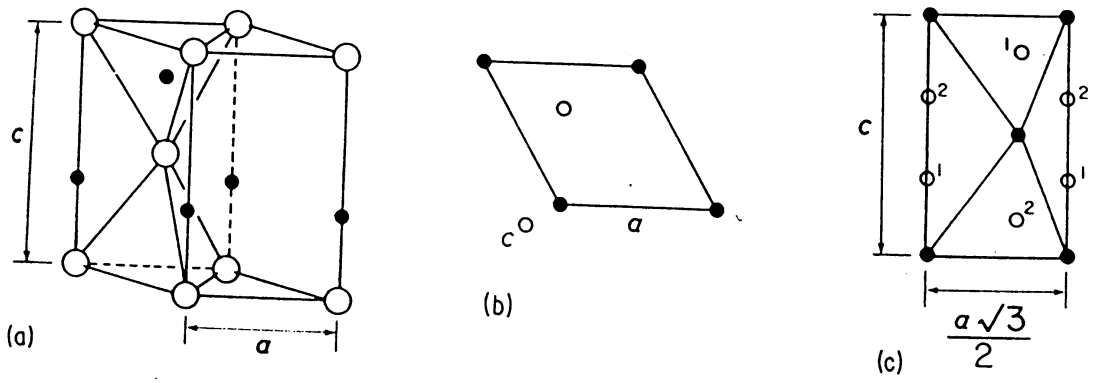

Figure 2.5. (a) Spatial view of the basic 2H wurzite structure. Metal atoms are represented by large open circles; anions are represented as small closed circles (b) Projection of the 2H structure along [0 0 1]; the non-metal atoms project along the metal atom configuration (c) Projection of 2H along [1 0 0]. The centers of two different tetrahedra are indicated as 1 and 2 (ref. 10)

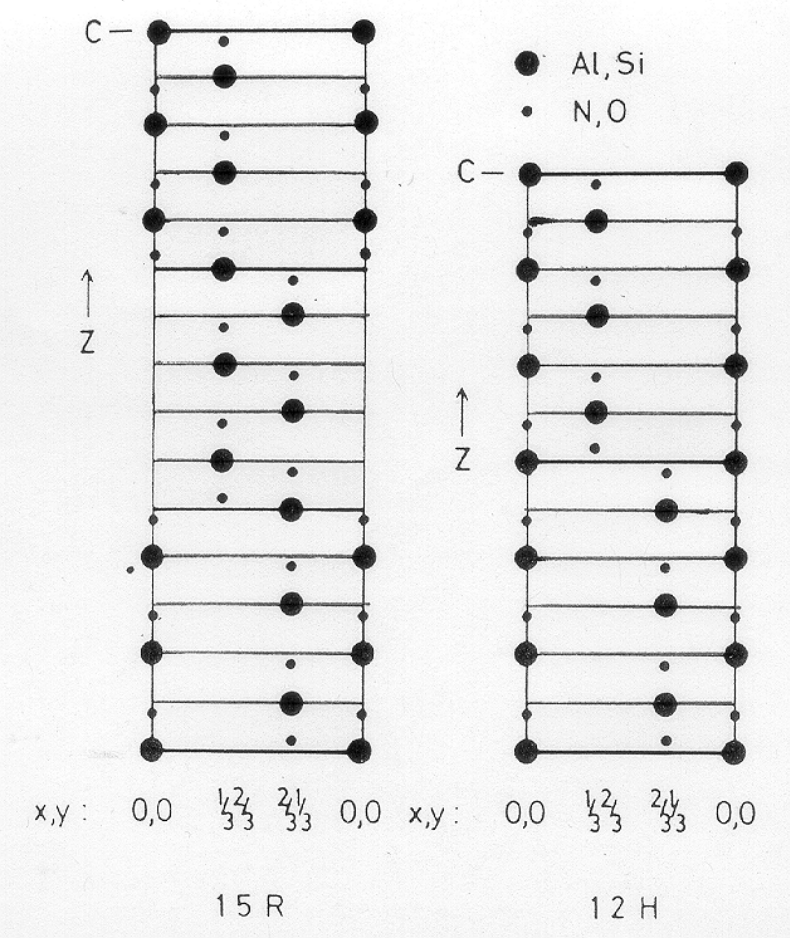

Figure 2.6. Stacking sequence of 15R and 12H along (110) section (ref. 13)

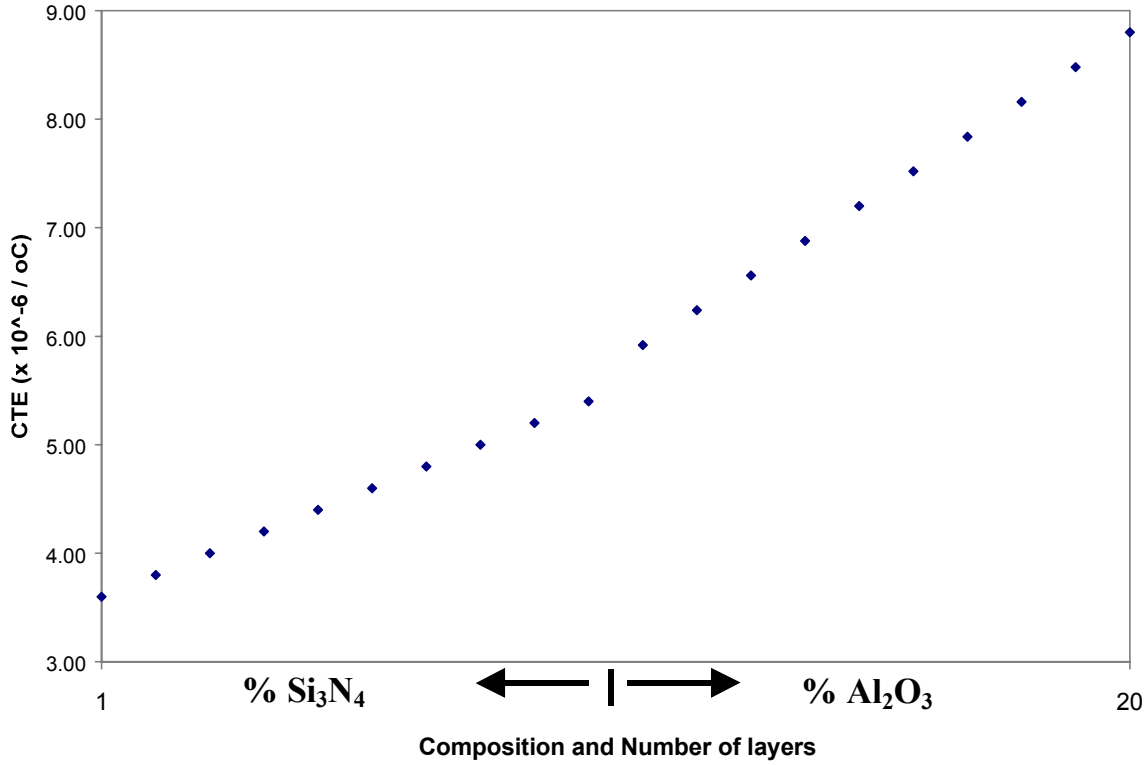

Figure 2.7. Calculated CTE gradient along the final FGM sample using the "Mixture rule".

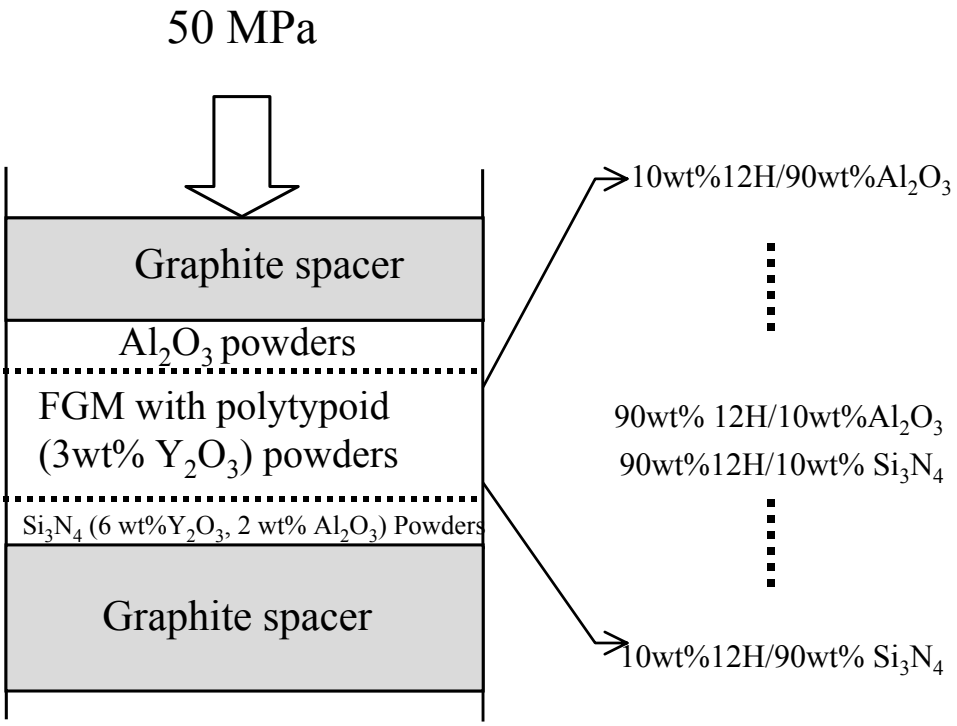

Figure 2.8. Experimental setup used for the fabrication of the Si_3N_4-Al_2O_3 joints using polytypoid functional gradient (Schematic of final FGM with total of 20 layers).

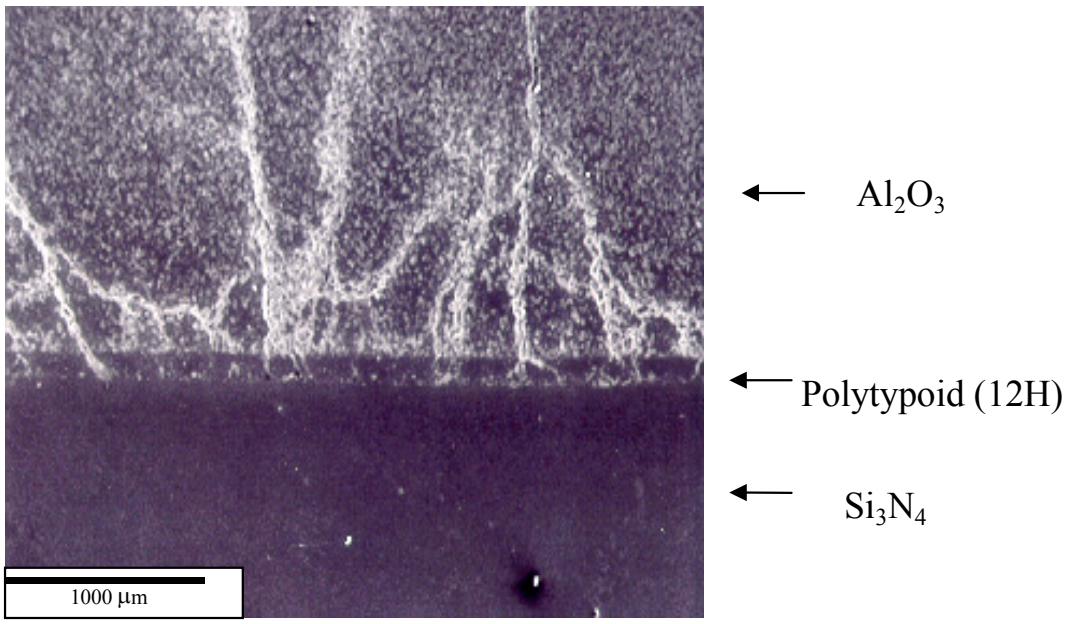

Figure 2.9. Direct joining using a thin polytypoid interlayer

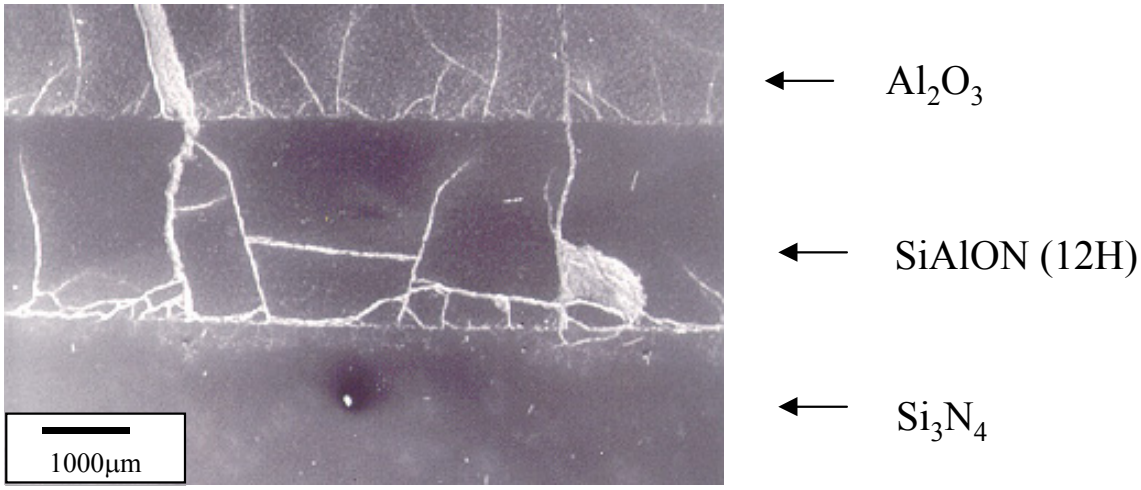

Figure 2.10. Direct Joining using a thick polytypoid interlayer

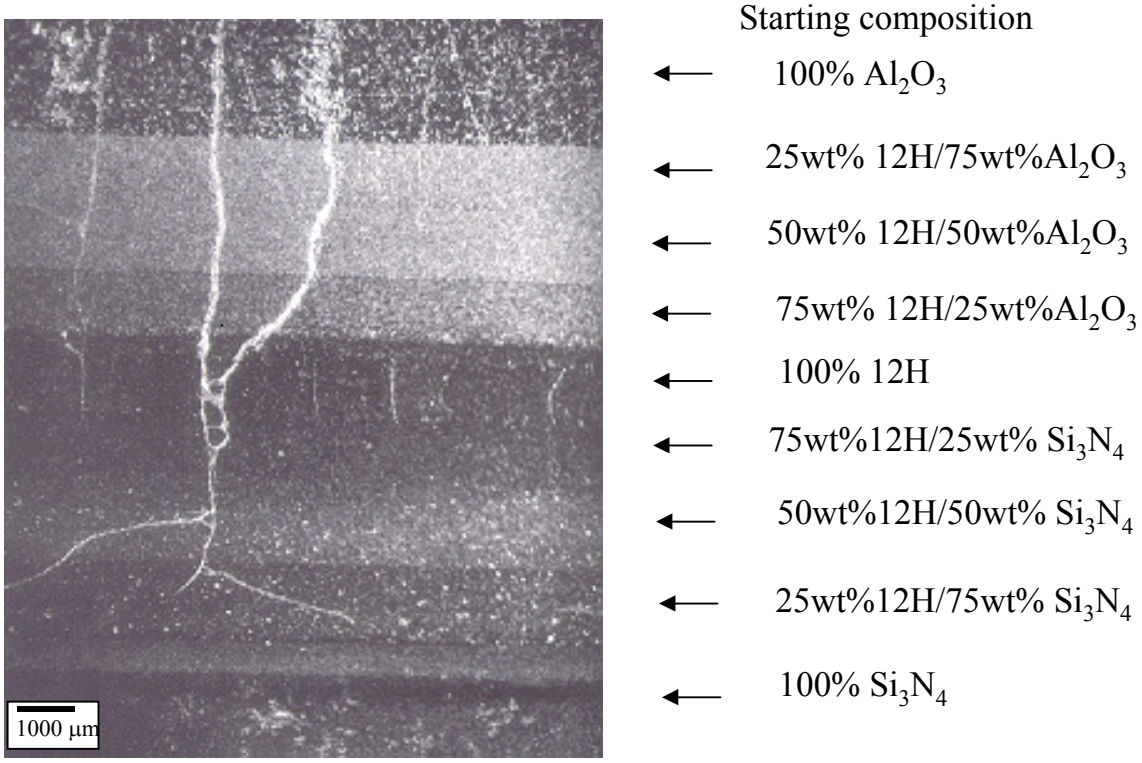

Figure 2.11. FGM joint between Al_2O_3 and Si_3N_4 with 25 wt% increment in composition

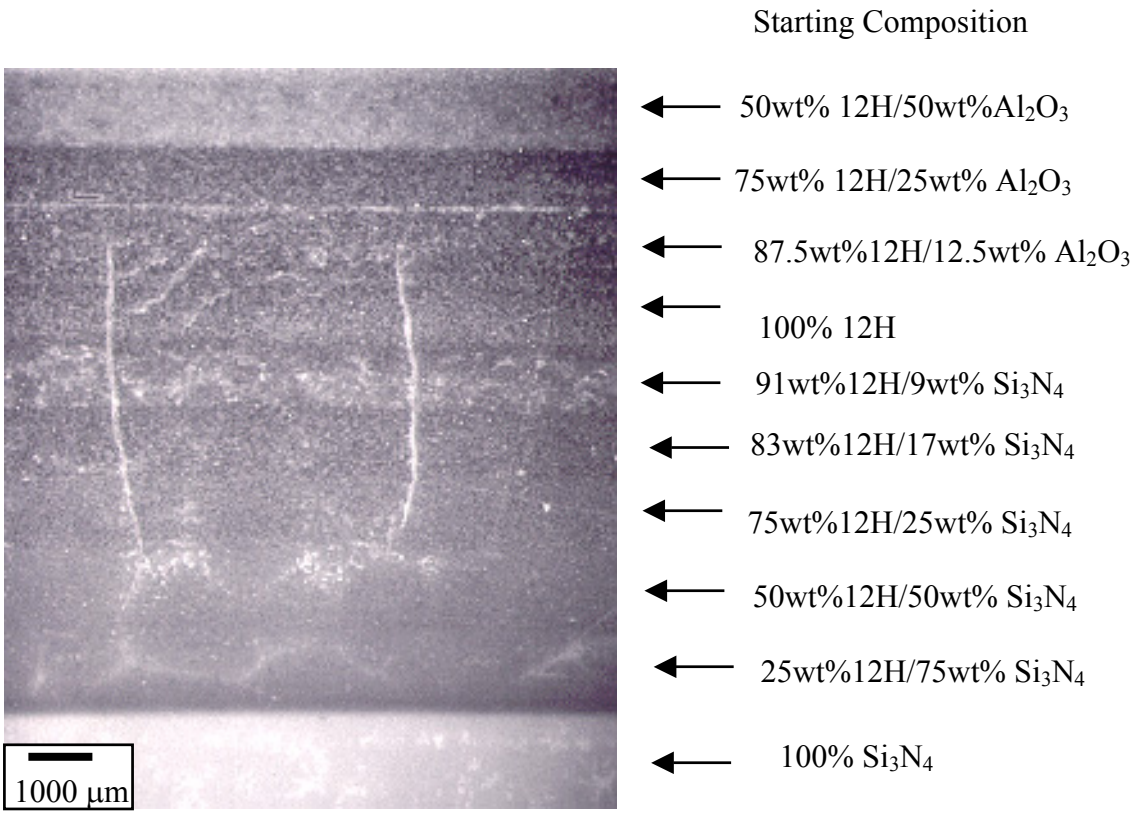

Figure 2.12. FGM joint between 50wt% 12H/50wt% Al_2O_3 and Si_3N_4 with more gradient layers

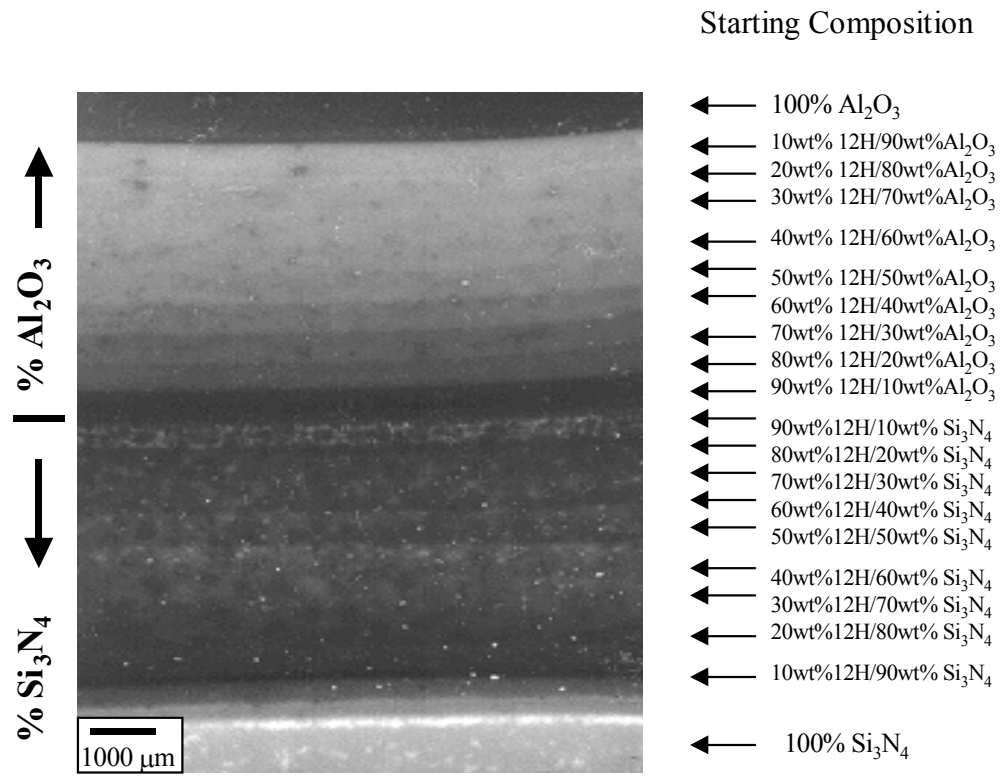

Figure 2.13. Final FGMs

CHAPTER 3: Characterization of Crack-Free Joint

3.1. Introduction

In Chapter 2, a unique approach to crack-free joining of heterogeneous ceramics is demonstrated by the use of sialon polytypoids as Functionally Graded Materials (FGM) as defined by the phase diagram in the system, Si_3N_4-Al_2O_3. In order to join Si_3N_4 to Al_2O_3, a sialon polytypoid has been used for several reasons: First, sialons are essentially silicates and alumino-silicates in which oxygen is partly or completely replaced by nitrogen, while silicon is partly replaced by aluminum [1]. Sialon polytypoids are physically and chemically compatible with both Si_3N_4 and Al_2O_3. Because metal-nitrogen bonding is in general more covalent than that in metal-oxygen bonding, there is freedom to vary the covalent: ionic contributions to the interatomic bonding in a variety of structures [2]. A polytypoid is defined as a faulted structure in which the fault periodicity depends on composition through the cation/anion ratio. It was found that AlN polytypoids, such as 15R, 12H, 21R, 27R and 2H, have Coefficients of Thermal Expansion (CTEs) in the range of 5.1 to 5.9 x 10^{-6} /^{0}C as defined in Chapter 2 [3]. Since the CTE of Si_3N_4 is $3.6x10^{-6}/^0C$ and that of Al_2O_3 is $8.8x10^{-6}/^0C$, the use of sialon polytypoids, which has an intermediate CTE value for joining Si_3N_4 and Al_2O_3, is clearly attractive.

Another advantage of using a polytypoid as a functional gradient is that polytypoid step functional joining can be obtained. The structure of polytypoid compounds is determined by the stacking-fault spacing along (001) basal plane (metal/non metal ratio) as explained in Chapter 2 and this step functional capability is

beneficial to the joint since the lattice mismatch can be accommodated by having this polytypoid transformation closest to the materials being joined. This trend in the polytypoid transformation is observed in the wide range of ceramic systems including the superconductors [4]. Studies done by Ramesh et. al. [4] have indicated that cation/anion ratio of Bi-Ca-Sr-Cu-O superconductor was varied without changing crystal structure. Therefore, structural periodicity is adjusted without change in crystal structure in order to accommodate compositional changes. The polytypoids in AlN-SiO_2 material have been investigated by means of electron microscopy [5]. Three new long-period polytypoids, close to the 2H hexagonal AlN structure, have been identified by high-resolution electron microscopy, namely 33R, 24H and 39R. These polytypoids are built on the same stacking principle as those in the previously observed shorter polytypoids in the AlN system. In order to detect the change in the structural periodicity for the crack-free FGM sample of this research, electron microscopy was used to determine the type of polytypoids.

Finally, another advantage of using a polytypoid as a functional gradient to join Si_3N_4 and Al_2O_3 is that polytypoids have mostly glass-free interface [5]. Studies done by G. Van Tendeloo et. al. (1993) have shown high-resolution images of a grain-boundary between two polytypoid grains having exactly perpendicular c-axes but a common a-axes, and they observed no glassy interface (Figure 3.1). However, glassy phases were sometimes seen at triple points in the FGM sample (see Figure 3.5). It is well known that elevated-temperature strength is decreased by the presence of glassy phases at interfaces, notably grain boundaries, and triple junctions. Therefore, a glass free interface gives thermal stability. In order to detect the presence of any glassy

phases at the interface for the crack-free FGM sample, High-Resolution Electron Microscopy (HREM) was used since it can easily detect any glassy phases thinner than 1 nm.

In this chapter, the microstructure of a processed crack-free FGM sample is reported in detail using various characterization tools, such as X-ray Diffractometer (XRD), Electron Probe X-ray Microanalysis (EPMA) and High-Resolution Electron Microscopy (HREM). In order to understand how these tools are used to analyze the sample, the principles of these tools are summarized in the Appedices I, II and III.

3.2. Experimental Procedure

3.2.1. Microstructural Characterization

After the crack-free FGM sample was successfully fabricated, as described in Chapter 2, X-ray Diffraction (XRD) was used to identify the phases present in the 100% polytypoid sample. The microstructure in the different areas of the joint was studied using Transmission Electron Microscope (TEM), and the TEM image of the microstructure in the alumna-rich side of the FGM joint is shown in Figure 3.3. Moreover, to identify different polytypoids at various interfaces, electron diffraction was used since polytypoid has a distinct interlunar spacing as shown in Table 3.1. Also, high-resolution images of grain boundaries were taken to identify grain boundary structure.

The specimens for Transmission Electron Microscopy (TEM) were prepared using conventional dimpling and ion-milling methods. The sample pieces with the interface were cut to a thickness of about 250 μm. From this, a 3-mm disc was cut out

using an ultrasonic drill. The discs were then ground to a thickness of 100 μm using a flattening tool. A dimple grinder was then used to form a dimple, with a 5-10 μm thin region in the middle. At this stage, the specimen is translucent to optical light. The specimens were then ion milled, coated with a thin layer of carbon, and analyzed in a Philips CM200 transmission electron microscope working at 200 kV.

3.2.2. EPMA of Crack-Free FGM sample

To study how the interface diffusion is taking place at each layer of FGM sample, EPMA was used for the compositional mapping across the length of the sample. Using a full transverse scan, data were taken every 20 μm, with a total of 486 points to make sure that the compositional mapping is done across each interface.

3.3. Results and Discussion

3.3.1. Microstructural Characterization

An X-ray diffractometer was used to identify the phases present in the 12H polytypoid powder before the FGM was fabricated (Figure 3.2). The polytypoid, $Si_3Al_7O_3N_9$ was identified. In addition, $Al_5Y_3O_{12}$ was found at the triple points (Figure 3.3). The 001 d-spacing for $Si_3Al_7O_3N_9$ was found to be 2.7350 Å, which matches the published d-spacing value for the 12H polytypoid which is 2.74 Å. $Al_5Y_3O_{12}$ was formed in addition to the polytypoid due to the Y_2O_3 used as a sintering additive. Thus in the initial stages of sintering, Y_2O_3 forms yttrium aluminates through a solid state reaction with the oxygen-containing phase on the AlN powder surface, which accelerates sintering [6].

A transmission electron micrograph of Al_2O_3-rich area of the FGM joint of a sample with 20 layers is shown in Figure 3.3. This micrograph shows that no undesirable reaction took place between the Si_3N_4, the Al_2O_3, or the polytypoids as predicted in the phase diagram (Figure 2.3). In this region, no phases other than Al_2O_3 and 15R were detected so that the rule of mixture could be used to design the gradient. The intergranular materials were found to be yttrium aluminates resulting from the use of Y_2O_3 as a sintering additive. Generally, the shape of Al_2O_3 grains was equiaxial with the size ranging from 3 to 10 μm. 12H and 15R polytypoids showed an elongated grain size, 0.5 to 0.9 μm in width and 3 to 6 μm in length. The grain shape of Si_3N_4 is mostly elongated with a grain size about 0.3 μm in width and 2.5 to 4 μm in length. The phase of these grains is mostly β-Si_3N_4, which grows into elongated needles.

High-resolution transmission electron microscopy was used to identify the polytypoid phases at various interfaces of the FGM, following earlier procedures [5,7]. For the areas in the Si_3N_4-polytypoid area, the 12H polytypoid was identified (c= 32.91 Å). So the polytypoid did not change in the Si_3N_4-polytypoid gradient area. However, in the Al_2O_3-polytypoid gradient area, the polytypoid changed to 15R, c= 41.81 Å (Figure 3.4). This agrees with the trend of the phase diagram in Figure 2.3 where the polytypoid was transformed close to the materials to be joined. 15R is the closest polytypoid to Al_2O_3 and the one closest to Si_3N_4 is 12H. Thus, the lattice mismatch is accommodated by having this polytypoid transformation closest to the materials being joined. Moreover, this trend in the polytypoid transformation from 12H to 15R as the ratio of cation to anion decreases, is exactly as predicted from the

phase diagram (Figure 2.3). Thus the present approach can be applied to a wide range of ceramic systems including the superconductors [8]. The center of the FGM sample where 12H/15R interface is located (A-B line from Figure 2.3), may in fact be mixtures of these polytypoids. Therefore, a sharp interface at the center of the FGM could not be resolved.

High-resolution images were used to detect any glassy phases presented in grain boundaries since thermal stability is crucial for high-temperature applications. Various grain boundaries, such as Si_3N_4/12H, 15R/15R, 12H/12H and 15R/Al_2O_3, were imaged but no intergranular glassy phases were detected (Figures 3.5 a, b, c and d). However, statistically, one cannot exclude the existence of intergranular glassy phases and indeed they were present (Figure 3.3). Also, mechanical tests at 1200 ^{0}C on these FGM samples implied the presence of some glassy phases in the triple junction, since there was strength degradation at high temperature [9].

3.3.2. Interface Diffusion Across the Graded Joint

Compositional mapping using EPMA was done on the crack-free graded joint to study the interface diffusion of each graded layer. Since this FGM was fabricated by the stacking method, each graded layer was visible using optical examination as shown in Figure 2.13. To make sure that interface diffusion did take place during sintering so as to have strong interfaces, EPMA was used to scan the sample across the length of the joint to plot each element as shown in Figure 3.6. The left side of the graph indicates the Si_3N_4-rich area of the joint, and the right side of the graph indicates the Al_2O_3-rich area of the joint. This figure shows a relatively smooth trend for each

element plot, indicating that interface diffusion did take place. If interface diffusion did not occur, the concentration profile would look more stepwise rather than being smooth. Therefore, this EPMA scan was useful in showing a smooth concentration profile to indicate good interface strength.

3.4. Conclusions

In this chapter, various characterization tools, such as XRD, HREM and EPMA, were used to study the FGM sample in more detail.

XRD was used to identify the phases present in the 12H polytypoid powder before the FGM was fabricated, and the polytypoid, $Si_3Al_7O_3N_9$ was identified. In addition, $Al_5Y_3O_{12}$ was found at triple points (Figure 3.3). Transmission electron micrograpy of the Al_2O_3-rich area of the FGM joint of a sample with 20 layers, shows that no undesirable reaction took place between the Si_3N_4, the Al_2O_3, or the polytypoids, as predicted in the phase diagram (Figure 2.3).

Microstructural characterization using HREM indicated that the 15R polytypoid was formed in the Al_2O_3-contained layers and the 12H polytypoid was formed in the Si_3N_4-contained layers. This transition in polytypoid from 12H to 15R is explained by the phase diagram in Figure 2.3 where the closest polytypoid type is matched to the materials to be joined, thus accommodating the lattice mismatch, by changing the polytypoid cation to anion ratios, without change in crystal structure.

No glassy phases were found at the interfaces of various phases, such as Si_3N_4/12H, 15R/15R, 12H/12H and 15R/Al_2O_3. A sharp 12H/15R interface in the

middle of the FGM sample could not be resolved since this interface may in fact be mixtures of these polytypoids as shown in the A-B line of Figure 2.3.

EPMA scans across the length of 20-layer FGM sample verified that the interface diffusion occurred during sintering at each graded layer by showing a smooth concentration profile.

3.5. References

1. P.M. Johnson and A. Hendry, "The microstructure of hot-pressed sialon polytypes", *Journal of Materials science* **14**, 2439 (1979)

2. K.H.Jack "The sialons", *Mat. Res. Bull*. **13**, 1327 (1978)

3. I. Yamai and T. Ota, "Thermal expansion of Sialon", *Advanced ceramic materials*, **2**[4], 784 (1987)

4. R.Ramesh, S. Green, C.Jiang, Y.Mei, M.Rudee, H.Luo and G. Thomas, "Polytypoid structure of Pb-modified Bi-Ca-Sr-Cu-O superconductor", *Physical Review B*, **38** [10], 7070-7073 (1988)

5. G.Van Tendeloo, K.T. Faber and G.Thomas, "Characterization of AlN ceramics containing long-period polytypes", *Journal of materials science*, **18**, 525 (1983)

6. N. Hashimoto and H. Yoden, "Sintering behavior of fine Aluminum Nitride powder synthesized from Aluminum polynuclear complexes" Journal *of American Ceramic Society*, **75** [8], 2098-106 (1992)

7. K. H. Jack, "Review: Sialons and related nitrogen ceramics*", Journal of materials science* **11**, 1135 (1976)

8. R.Ramesh, S. Green, C.Jiang, Y.Mei, M.Rudee, H.Luo and G. Thomas, "Polytypoid structure of Pb-modified Bi-Ca-Sr-Cu-O superconductor" *Physical Review B*, **38** [10], 7070-7073 (1988)

9. C. Lee, L.C. DeJonghe and G. Thomas, "Mechanical properties of Polytypoidally joined Si_3N_4-Al_2O_3 system", *Acta Mater*., accepted (2001)

Table 3.1. Si-Al-O-N "AlN" Polytypoid (Ref. 1)

M/X	Type	a (Å)	c (Å)	c/n (Å)
4/5	8H	2.988	23.02	2.88
5/6	15R	3.010	41.81	2.79
6/7	12H	3.029	32.91	2.74
7/8	21R	3.048	57.19	2.72
9/10	27R	3.059	71.98	2.67
1/1	2H	3.114	4.986	2.49

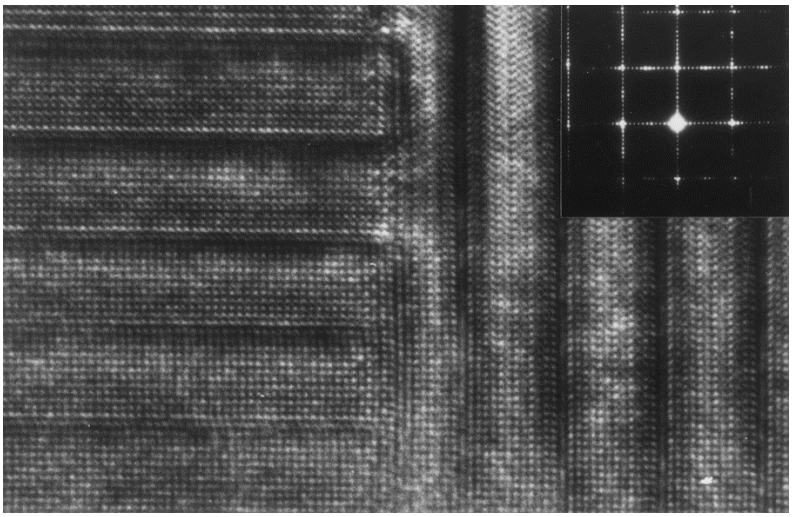

Figure 3.1. High-resolution image of a grain boundary between two polytypoid grains having exactly perpendicular c-axes but a common a-axes (parallel to the beam). There is no glassy phase detected at this boundary (Ref. 5).

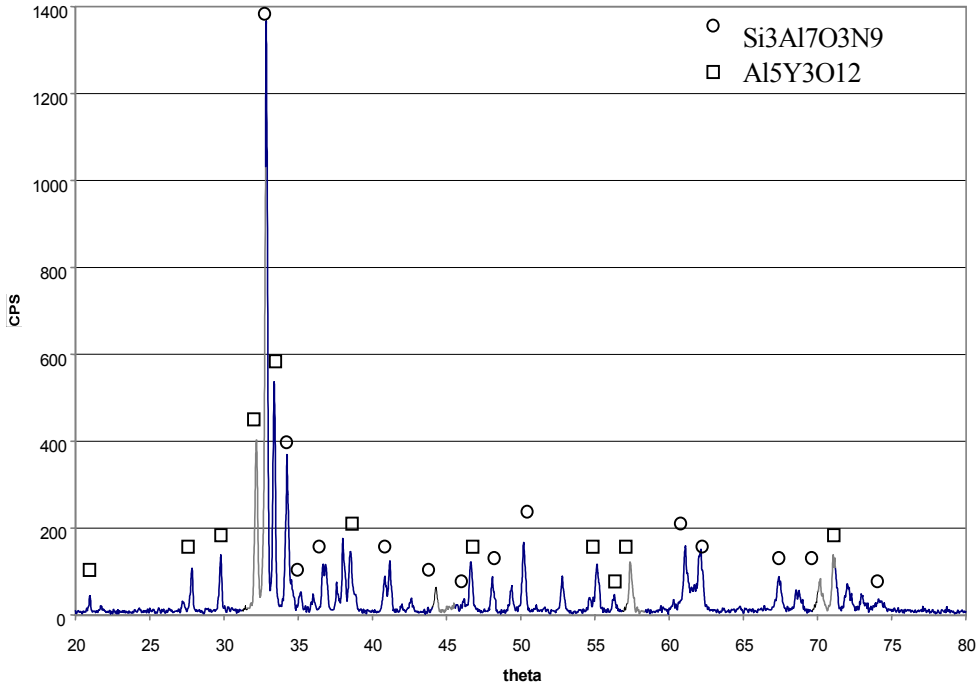

Figure 3.2. X-ray Diffraction pattern of polytypoid starting powder
Note the [001] d-spacing for $Si_3Al_7O_3N_9$ ~ 2.7350 Å (matches the d-spacing value for the 12H polytypoid ~2.74 Å)

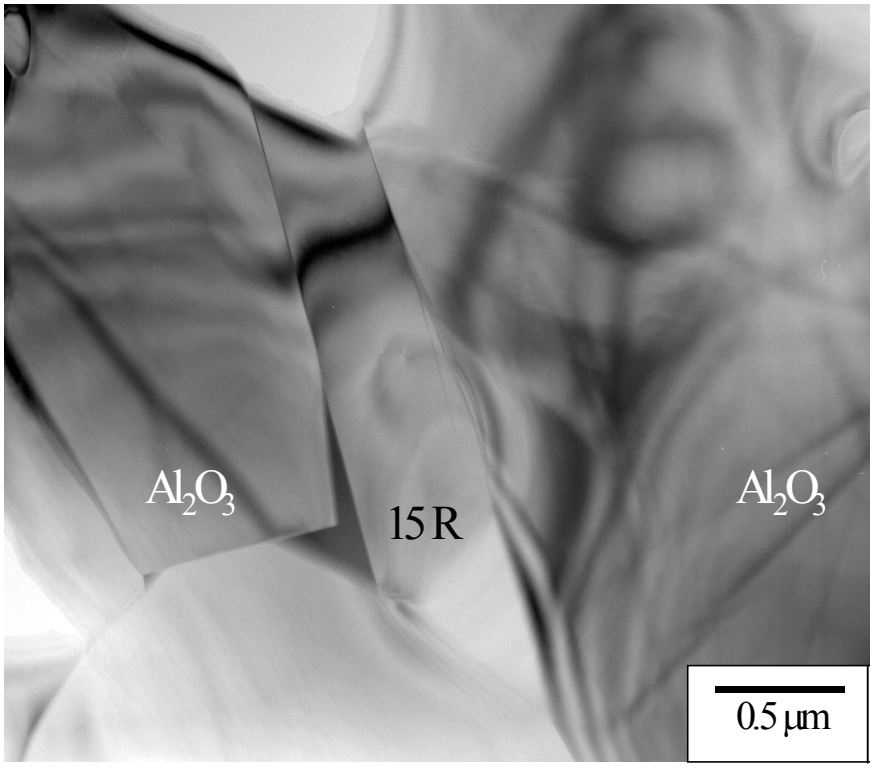

Figure 3.3. TEM image of the microstructure in the alumina-rich side of the FGM joint. Only alumina and 15R phases were detected, together with some glassy phase at triple junctions.

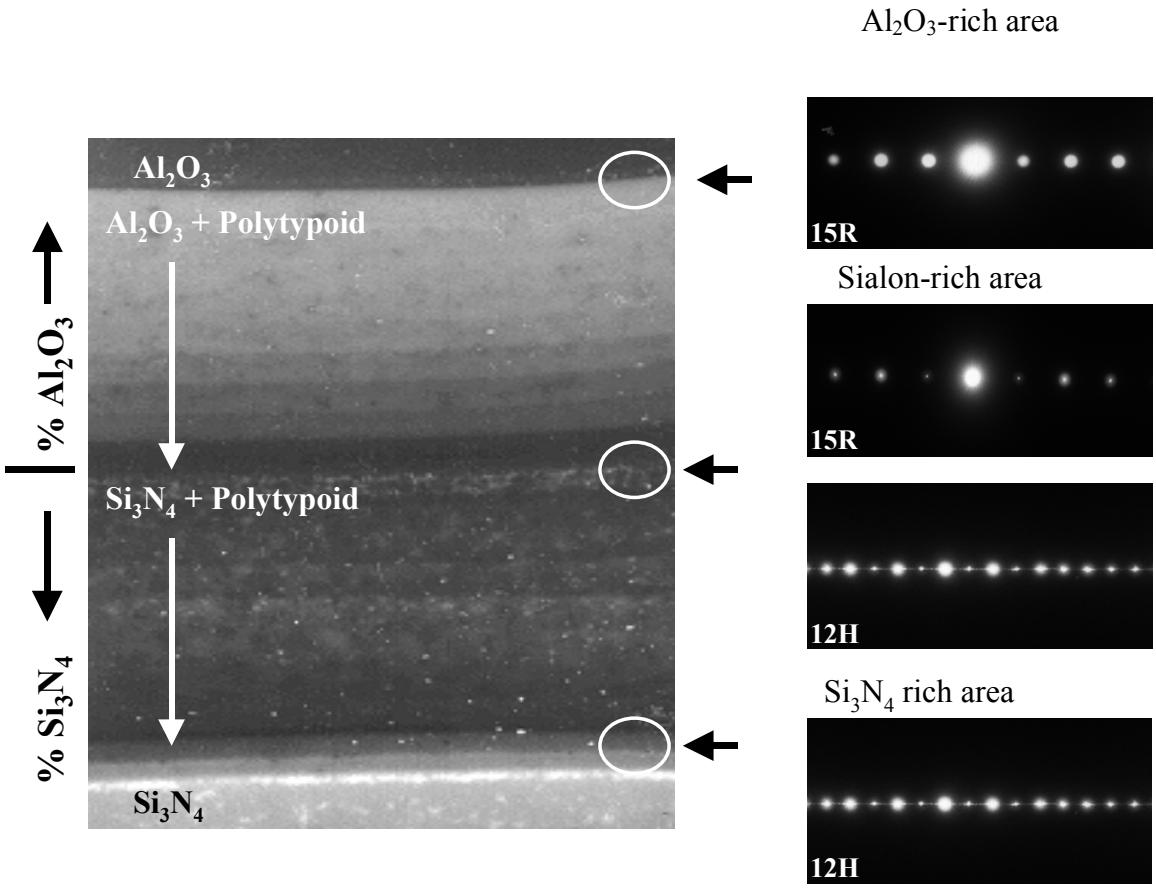

Figure 3.4. Diffraction patterns (RHS) of polytypoid near various interfaces (along c-axis), as shown in the light micrographs on the left side.

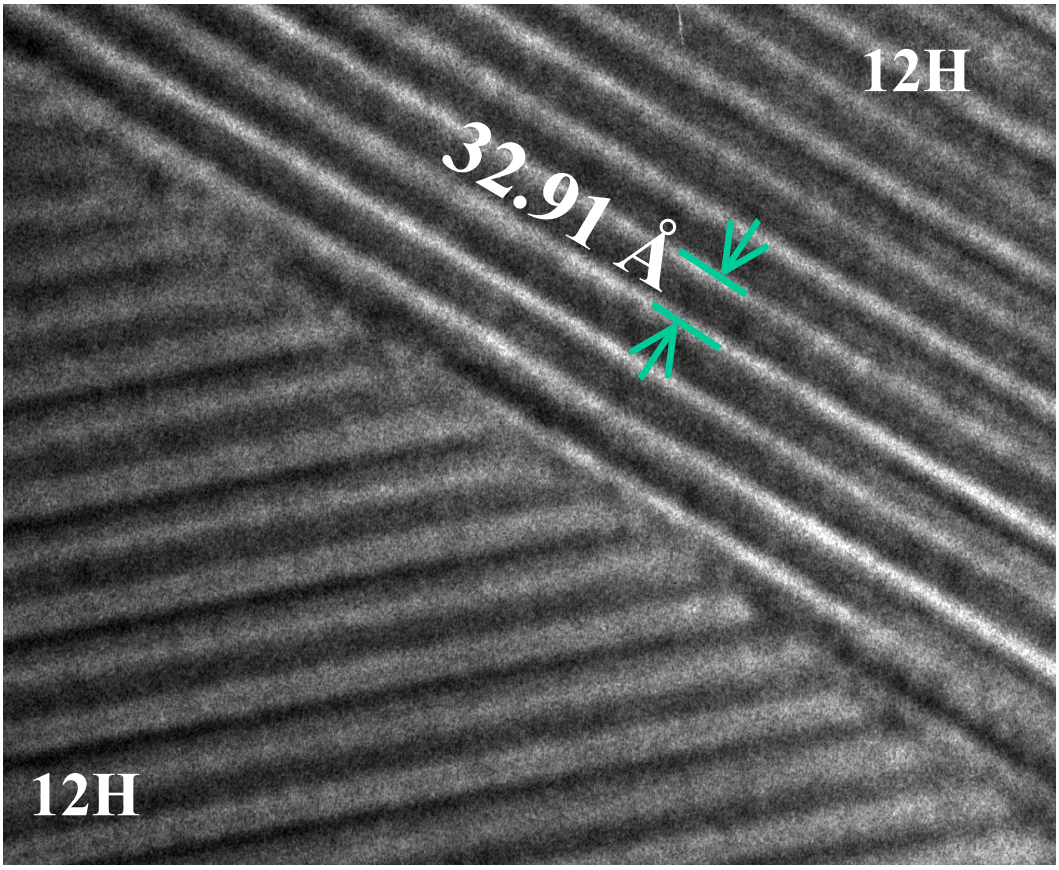

Figure 3.5 (a) 12H/12H. High-resolution electron microscopy images of grain boundary interfaces as indicated. (Courtesy of Dr. X.F. Zhang)

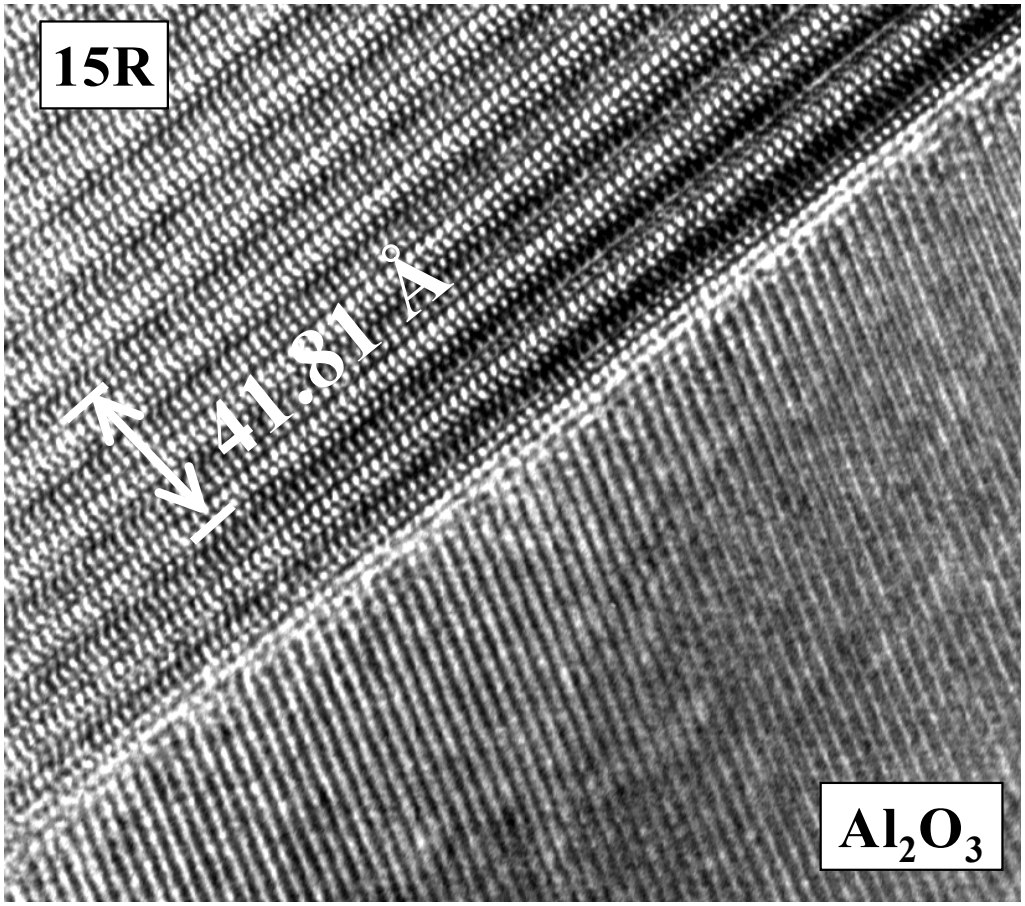

Figure 3.5 (b) 15R/Al_2O_3 High-resolution electron microscopy images of grain boundary interfaces as indicated. (Courtesy of Dr. X.F. Zhang)

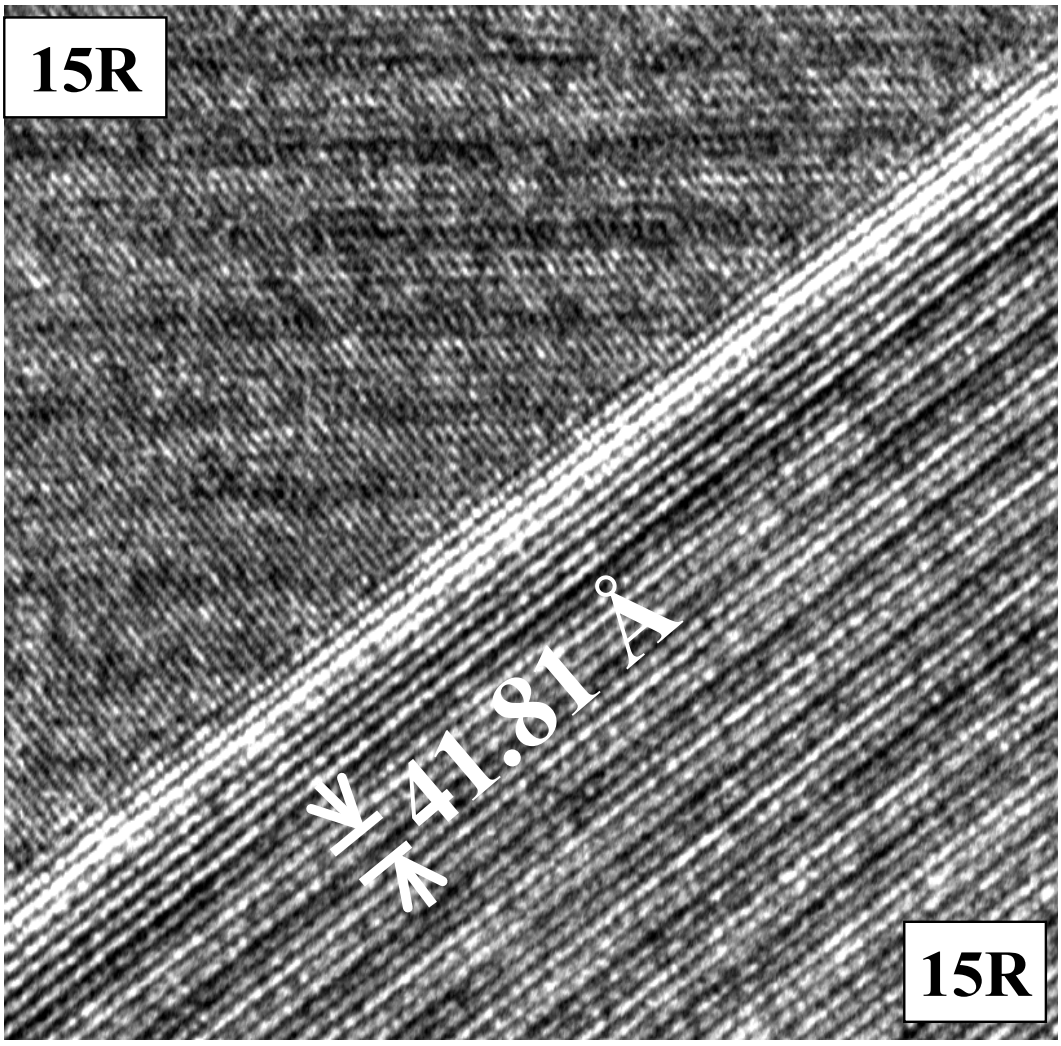

Figure 3.5 (c) 15R/15R. High-resolution electron microscopy images of grain boundary interfaces as indicated. (Courtesy of Dr. X.F. Zhang)

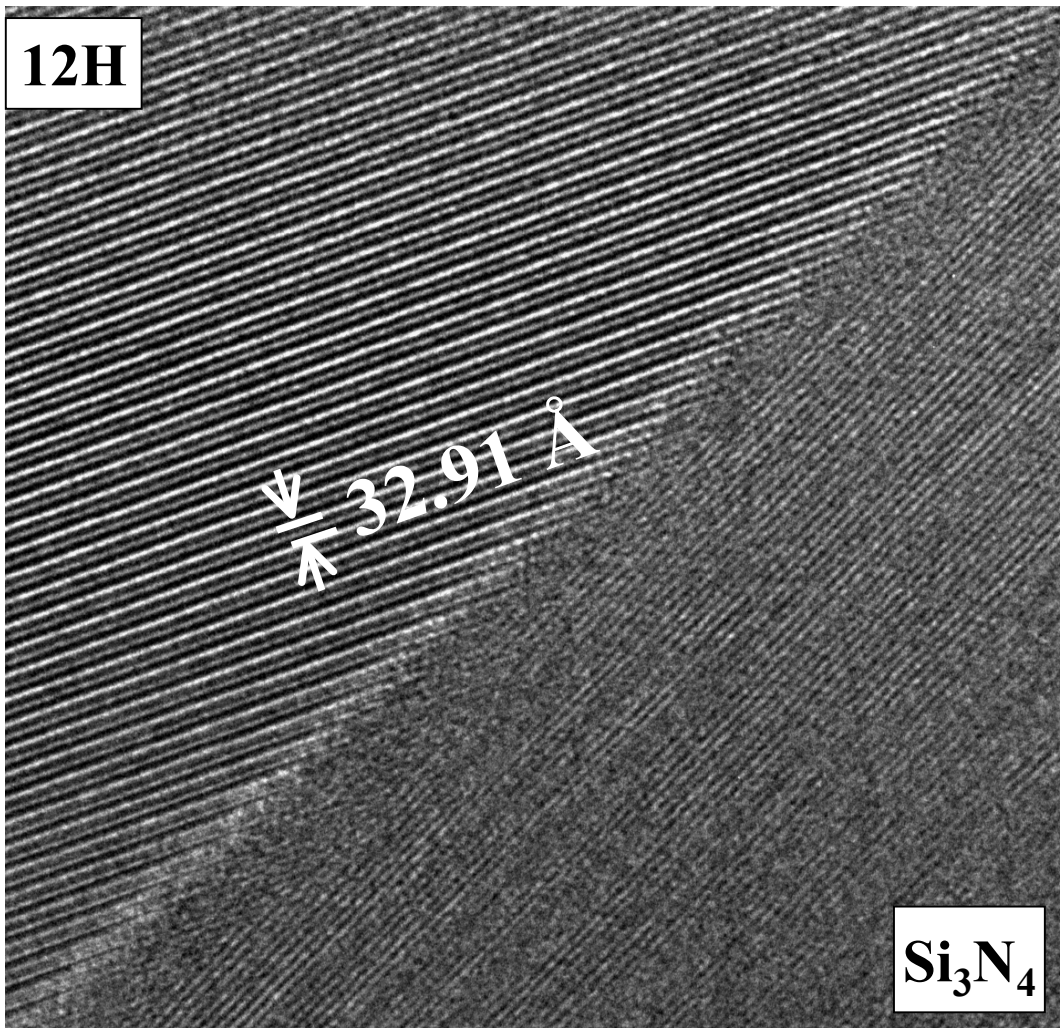

Figure 3.5 (d) 12H/Si_3N_4 High-resolution electron microscopy images of grain boundary interfaces as indicated. (Courtesy of Dr. X.F. Zhang)

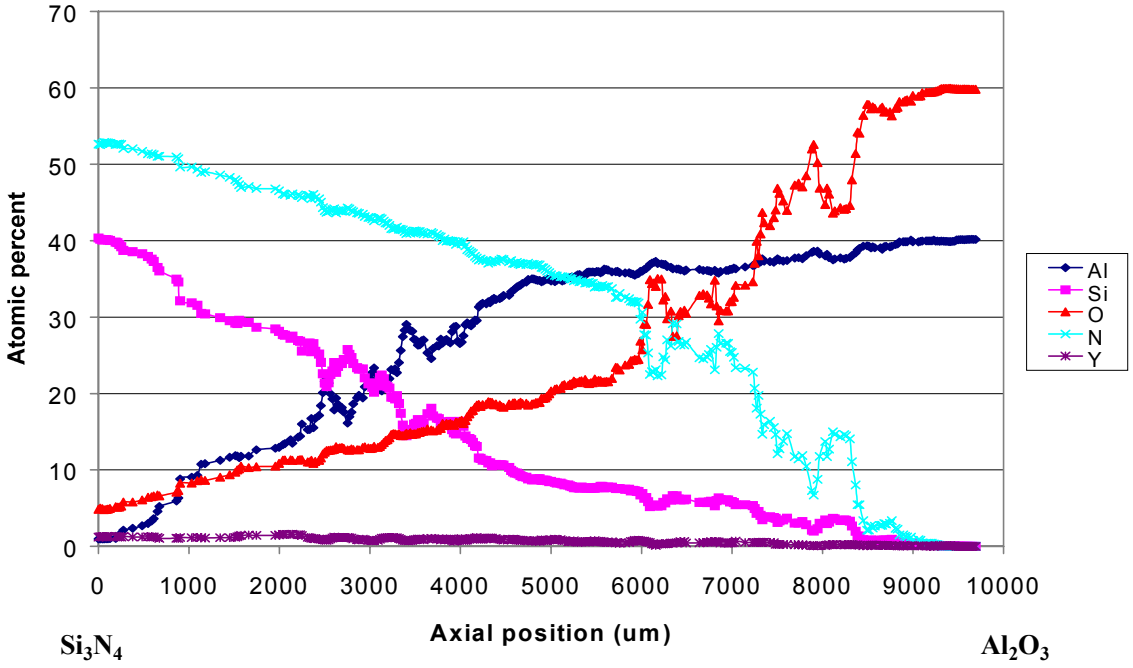

Figure 3.6. Electron Probe X-ray Microanalysis (EPMA) of crack-free FGM (20 layer) across the length of the sample to study the compositional gradient. Left hand side of the graph shows Si_3N_4-rich area and Al_2O_3-rich area of the joint is shown in the right hand side.

CHAPTER 4: Computational Analysis of Residual Stress

4.1. Introduction

The technological motivation for the development of functionally graded materials (FGMs) is the same as for any composite material: to obtain properties unavailable in any one homogeneous monolithic material. The design of FGMs is intended to take advantage of certain desirable features of each of the constituent phases. For example, if the FGM is to be used to separate regions of high and low temperature, it may consist of pure ceramic at the hotter end because of the better resistance to the higher temperatures. In contrast, the cooler end may be metallic because of its better mechanical and heat-transfer properties [1]. However, there are factors that mitigate the success of such a goal. Stress that arises due to the joining two dissimilar materials is one such factor. As in many joining and composites problems, the effect of residual stress, arising either from processing or from in-service temperature variations, takes on an important role. At a free surface of a joint, the sharp discontinuity in coefficients of thermal expansion (CTE) leads to a signularity, with the linear elastic stresses approaching infinity at the surface [2]. For a material without layers, where the properties vary continuously with position, these sigularities are eliminated [3]. Such a design allows a gradual change in thermal expansion mismatch, minimizing the thermal stresses arising from cooling or heating. Therefore, FGMs offer solution to the thermal stress problem and have created wide interest recently [4-9].

Not only a gradient in properties is designed to optimize the stresses, but also the functional aspect of spatial change in properties is beneficial to the application. For example, an FGM composed of a chemically resistant ceramic and a tough metal could be implemented to protect a structure in a chemically aggressive environment.

The FGM system consists of a gradual change in the volume fraction of constituents from one location to the other in a component. This concept was first evaluated in the development of graded thermal barrier coatings to increase the thermal shock resistance of blades in gas turbine engines. So FGMs can prevent the fracture of ceramics by minimizing thermal stresses and thermal shock [10]. Therefore, a major motivation for the FGM research is high-temperature service in transportation and power generation. The development of modern nickel-based superalloys allows for the increased operating temperature and efficiency of turbines in military and civilian aircraft and electric power turbines [11]. To allow higher combustor operating temperature, a high-melting-point ceramic, typically ZrO_2, has been coated on a high-toughness superalloy since monolithic ceramics and intermetallics have not yet achieved their promise as replacement materials, mainly because of their low fracture toughness [12]. FGMs are also used in coatings to improve tribological behavior by suppressing surface cracking [13], and the implantation of foreign objects into the human body (knee and hip implants, artificial teeth, etc.) is an example of the need for a bio-compatibility as well as the previously mentioned structure properties [14].

Since one critical design goal and motivation in FGM research is the minimization of thermal stresses, several studies have focused on the theoretical and

experimental assessment of these stresses in FGMs. A majority of this analytical work has been for FGM films or other simple structures, for which geometrical assumptions allow for much simplified 1-D linear elastic calculation [1]. For a more general 2-D or 3-D problem, numerical methods such as a finite element analysis (FEA) are required. In this chapter, the mechanics of functionally graded materials are reviewed and residual stresses are analyzed in the axisymmetric mode, using the computer program FEAP [15]. These formulations do not contain an explicit reference to the microstructure of the FGM, but assume that the behavior of the composite can be calculated solely from the properties and volume fractions of the constituents. By using the effective properties of the FGM and by tracking the changes in the composition through the effective properties, the residual stress calculations are obtainable without specific microstructural modeling.

The problem of determining the effective properties of a mixture of two materials has been long studied [16]. For simple elastic composites, modeling the structure as two springs provides wide bounds for the aggregate behavior of the composite. For two springs in parallel, the total stiffness is the sum of the stiffness of the two springs, $kt = k_1 + k_2$. Likewise, the linear rule of mixtures uses a volume-fraction-weighted sum of the Young's moduli to predict the Young's modulus of the composite

$$E_c = v_1 E_1 + v_2 E_2 \tag{4.1}$$

Where v_1 and v_2 are the volume fraction of phases 1 and 2, respectively, and $v_1 + v_2 = 1$. For two springs in series, the inverse of the total stiffness is the sum of the inverse stiffness, $1/k_t = 1/k_1 + 1/k_2$. The inverse rule of mixtures

$$E_c = (1/v_1E_1 + 1/v_2E_2)^{-1} \quad (4.2)$$

yields a nonlinear relation, which is dominated by the more compliant material. For the residual stress calculation using FEA in this chapter, the linear rule of mixtures was applied to calculate the effective modulus and the effective Coefficient of Thermal Expansion (CTE) of graded materials.

The accuracy of FEA method can be limited when microstructure is not taken into consideration, but only the properties of the constituents. So, many models are not accurate for mixtures of very dissimilar materials, and may result in substantial errors in the limit of rigid inclusions, voids, or very high volume fraction of inclusions. However, since the actual residual-stress measurement and stress analysis of this FGM sample is very difficult, the calculation using FEA will be beneficial to the majority of practical FGM material combinations.

4.2. Experimental Procedure

The thermal stresses of this FGM were analyzed taking into account both CTE and modulus variation of the multitude of joining layers. The residual stresses were computed with a finite element method: Finite Element Analysis Program (FEAP) [15]. A mesh of 600-4500 nine-node quadrilateral elements was constructed to analyze the problem in axisymmetric mode. For a 9-node quadrilateral element, a quadratic variation in each in-plane direction can be accomplished within a single element. A special finite element was formulated so that the Young's moduli and the CTEs varied in the z-direction within each element. Figure 4.1 shows the coordinate system, while Table 4.1 lists the materials properties used to calculate the stress. The material

composition is taken to be constant in both the radial and circumferential directions. The comparison in residual stress between abrupt joining, *i.e.* without a gradient, and the 20 layer FGM was evaluated. Moreover, other FGM samples, such as the 3-layer FGM sample with a thick sialon interlayer, as described in Chapter 2, were analyzed to show that the residual stresses were large enough to cause cracking in the sample. Additionally, the FEAP assessed the dependence of the stresses on the thickness of the graded region, x, relative to the overall sample thickness, T.

4.3. Results and Discussion

Figures 4.2 – 4.4 show the computed stress distribution of a 3 layer *vs.* a 20 layer FGM. In the three-layer sample, a 0.1 mm layer of 12H sialon was assumed to join the 19mm diameter cylindrical slabs of silicon nitride to alumina. The 20-layer FGM was assumed to consist of a sequence of 0.5 mm layers with the layer compositions evenly ranging from 100% silicon nitride to 100% alumina, with the intermediate compositions. This intermediate composition consisted of 18 graded layers with 12H polytypoid sialon mixed with either alumina or silicon nitride (see Chapter 2). The stresses were calculated in MPa/^{0}C, with the processing temperature of 1700 ^{0}C assumed to be the temperature of zero stress. Room temperature stress values (20 ^{0}C) are then obtained by multiplying these stresses by 1680 which is the difference between the processing temperature and room temperature. The results show a dramatic decrease in radial stresses as well as in the axial and hoop stresses, as expected, for the 20 layer FGM compared to the tri-layer (Si3N4/ 12H sialon/Al_2O_3). The maximum radial stress in Figure 4.3 shows that it is comparable to maximum

axial stresses. For the axial stress at r=R in the tri-layer joint, the range of stress was found to be from 9 x 10^5 Pa/^{o}C (compressive) to -1.2 x 10^6 Pa/^{o}C (tensile), whereas in the 20 layer FGM, the range of stress was found to be from 0 Pa/^{o}C to 1.8 x 10^5 Pa/^{o}C (compressive) near the center of the joint. These analyses can give an estimate of the expected residual stress in actual FGM joints and indicate the approximate number of layers necessary to achieve a crack-free juncture [17,18]. The variation of the stresses, σ_{rr}, with R at z=T/2 for the 20-layer sample is shown in Figure 4.11. σ_{rr} is zero at R=r, and is maximum at r=0, while σ_{zz} is maximum at r=R.

Figures 4.5-4.7 show the computed stress distribution of a 3-layer sample with the thick sialon interlayer. As described in Chapter 2, this thicker sialon interlayer was fabricated after using a thin sialon interlayer to join Si_3N_4 and Al_2O_3 and showed cracking in the sample. For the axial stress at r=R in the tri layer joint, the range of stress was found to be from 5 x 10^5 Pa/^{0}C to –7 x 10^5 Pa/^{0}C. These values are lower than the ones for the tri-layer joint with thin sialon interlayer, but not low enough to result in a crack-free joint, as shown in Figure 2.10. Therefore, using thicker sialon interlayers in the joint did reduce some residual stress but not cracking removal, as confirmed in the computational analysis. Figure 4.13 shows the importance of grading the layers to reduce the residual stress rather than using the same fixed thickness for the single sialon interlayer for abrupt joining between Si_3N_4 and Al_2O_3.

After realizing the importance of grading the layer, a series of computational analyses were done to study how the stress is reduced in the graded sample. Figures 4.8 – 4.10 show the computed stress distribution of a 5 layer FGM with 50 wt% increment in composition. So the sequence of the starting composition for this graded

layer is as follows: 100% Si_3N_4, 50% Si_3N_4/50% sialon (12H), 100% sialon (12H), 50% sialon (12H)/50% Al_2O_3 and finally 100% Al_2O_3. For this sample, the axial stress at r=R in this 5-layer FGM ranged from 3 x 10^5 Pa/^{o}C to –3 x 10^5 Pa/^{o}C. The stress was reduced significantly compared to that of the trilayer joint but more grading of the layer such as 20 layer FGM reduced the residual stress down to almost minimum as shown in Figure 4.2. Therefore, this computational analysis is a useful tool to estimate the stresses of various cases without actually processing the sample.

An important consideration for the potential applications of this 20 layer FGM sample is the range of geometries in which an FGM approach can be useful. Two situations were examined: the joining of equal thicker slabs of silicon nitride to alumina via a 20-layer graded joint of fixed thickness, with the relative thickness characterized by the ratio x/T (see Figure 4.13), and an asymmetrical joining of a thin alumina layer to a thick piece of silicon nitride, shown in Figure 4.12. The resultant calculations for the axial stress at r=R (the outer diameter) show that the stresses rise dramatically as the FGM joint becomes thin compared to total sample dimensions. The example for the symmetrical case shows that the maximum axial stress at r=R scales approximately linearly with the decreasing x/T ratio between x/T=0.75 and x/T=0. Also this figure compares using a fixed thickness for the graded joint *vs.* using the same fixed thickness for the single sialon interlayer (*i.e*. the tri-layer specimen) for abrupt joining between silicon nitride and alumina. There is an increasingly large difference in the maximum stress between graded layer and abrupt joining as x/T ratio increases, indicating the importance of grading the joint to minimize the stress. As x/T values become smaller, however, the graded approach

holds minimal or no practical advantage over single-layer joining. Large stresses also arise in the asymmetrical case as shown in the example in the Figure 4.12. It can thus be concluded that joining of dissimilar ceramics such as silicon nitride with alumina, can only be expected to be successful for situations where the FGM gradient make up 75% or more of the entire sample thickness, limiting severely the range of applications of the FGM approach to joining.

4.4. Conclusions

In this chapter, the computational analysis tool (FEAP) was used to calculate the residual stresses in the various FGM samples to compare stress distribution in the samples. The result showed a dramatic decrease in radial, axial and hoop stress as the FGM changes from three layers to 20 graded layers. This analysis explains why a 20 layer FGM was crack-free but a 3-layer FGM was cracked. Scaling computations for FGM samples indicate that at least 75% of the total sample thickness needs to be the graded thickness so as to minimize residual stresses. Such analyses are especially useful for graded FGM samples where the residual stresses are very difficult to measure experimentally.

4.5. References

1. K. Ravichandran, "Thermal Residual stresses in a functionally graded material system", *Mater. Sci. Eng.* **A201**, 269-276 (1995)

2. D. Munz and Y.Y. Yang, "Stress singularities at the interface in bonded dissimilar materials under mechanical and thermal loading", *J. Appl. Mech*., **59**, 856-61 (1992)

3. K. Tanaka, H. Watanabe and Y. Sugano, "A multicriterial material tailoring of a hollow cylinder in functionally gradient materials: scheme to global reduction of thermoelastic stresses", *Comput. Methods. Appl. Mech. Eng*., **135**, 369-80 (1996)

4. R. Watanabe, A. Kawakasi and H. Takahashi, "Design, Fabrication and evaluation of Functionally Gradient Material for high temperature use" in Mechanics and Mechanisms of Damage in composites and Multi-Materials, Mechanical Engineering publication, London, 285-299 (1991)

5. M. Koizumi, "Recent progress of Functionally Gradient Materials in Japan", *Ceramic Engineering and Science Proceedings*, July-August, 333-347 (1992)

6. B.H. Rabin and R.L. Williamson, "Graded ceramic-metal microcomposites for controlling interface stress" in Microcomposites and Nanophase Materials Eds. D.C. Van Aken, G.S. Was and A.K. Ghosh, TMS-AIME, Warrendale, PA, 103-113 (1991)

7. R. Watanabe and A. Kawasaki, "Recent development of Functionally Gradient materials for special application to space plane" in Composite Materials Eds. A.T. Di Benedetto, L. Nicolais and R. Watanabe, Elsevier Science, 197-208 (1992)

8. M.Koizumi and K. Urabe, "Fabrication and application of Functionally Gradient Materials", in Ceramics Today-Tomorrow's Ceramics Eds. P. Vincenzini, Elsevier Science, 1939-1945 (1991)

9. B.H. Rabin, R.L. Williamson, R.J. Heaps and A.W. Erickson, "Ni-Al2O3 Gradient Materials by powder metallurgy", *Proc. 1st Int. Conf. Advanced Synthesis of Engineered materials*, San Francisco, CA, 175-180 (1992)

10. J.R. Cavanagh, K.R. Cross, R.L. Newman and W.C. Spicer, "The graded thermal barrier – a new approach for turbine engine cooling", *AIAA/ASME/SAE 13th Structures*, Structural Dynamics and Materials Conference, ASME, 1-15 (1972)

11. C.T. Sims, N.S. Stoloff and W.C. Hagel, Superalloys II. New York: Wiley 1987

12. S. Suresh and A. Mortensen, Fundamentals of Functionally graded materials , The University Press, Cambridge (1998)

13. J. Jitcharoen, N.P. Padture, A.E. Giannakopoulos and S. Suresh, “Herzian-crack suppression in ceramics with elastic-modulus-graded surfaces”, *J. American Ceramic Soc*., **81**, 2301-8 (1998)

14. J.M. Gomez-Vega, E. Saiz, A.P. Tomsia, T.Oku, K.Suganuma and G.W. Marshall, “Novel bioactive functionally graded coatings on Ti_6Al_4V”, *Advanced Materials*, **12**[12], 894-8 (2000)

15. O.C. Zienkiewicz and R.L. Taylor, The finite element method, McGraw-Hill, New York, 1987

16. Z. Hashin, “Analysis of composite materials – A survey”, *J. Appl.Mech*., **105**,481-505 (1983)

17. T.L. Becker Jr., R.M. Cannon and R.O. Ritchie, "An approximate method for residual stress calculation in functionally graded materials", *Mechanics of Materials*, **32**, 85-97 (2000)

18. R.W. Messler, M. Jou and T.T.Orling, "A model for designing functionally gradient material joints", *Welding Journal*, **74**[5], S166(1995)

Table 4.1. Physical Constants for the materials used for FEAP calculation

Properties	Si_3N_4	Polytypoid	Al_2O_3
E (GPa)	330	290	390
ν (Poisson's ratio)	0.22	0.22	0.22
α ($*10^{-6}/^{0}C$)	3.6	5.6	8.8

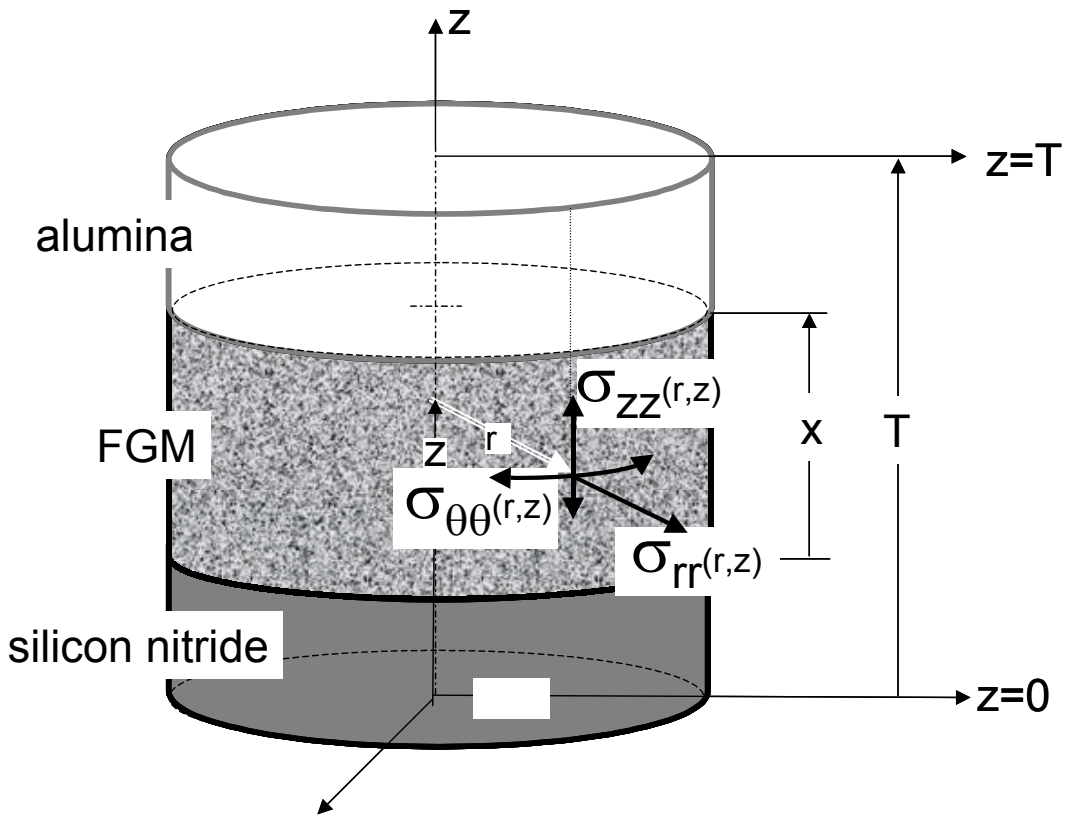

Figure 4.1. Sample geometry and coordinate systems

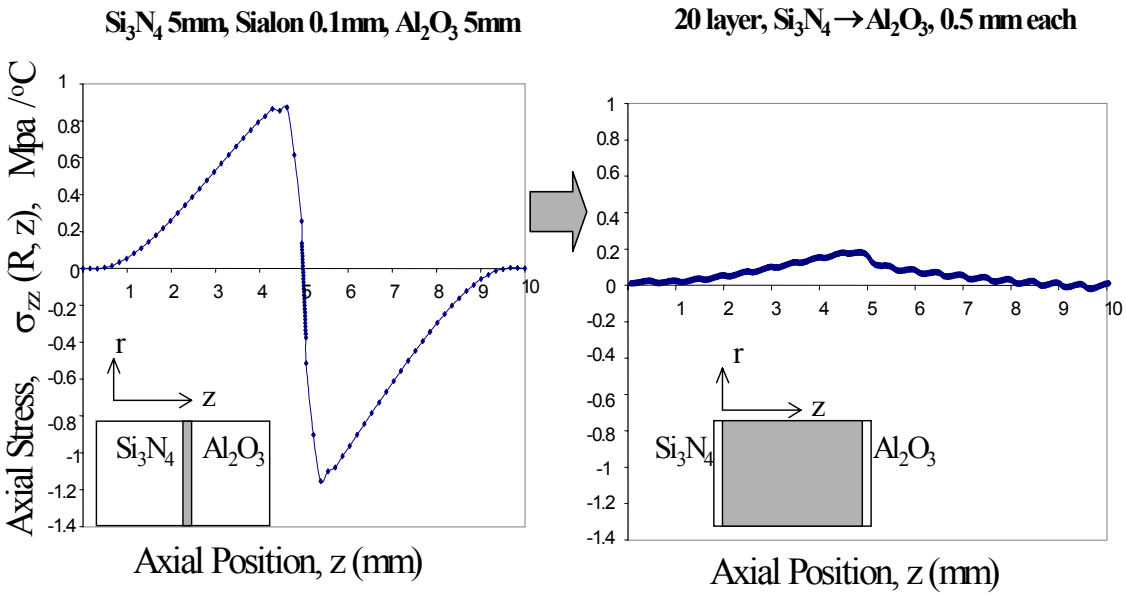

Figure 4.2. Comparison of the computed axial stress, σ_{zz} at r=R as a function of z, for a 3-layer sample versus a 20 layer FGM cylindrical sample with a 19 mm diameter.

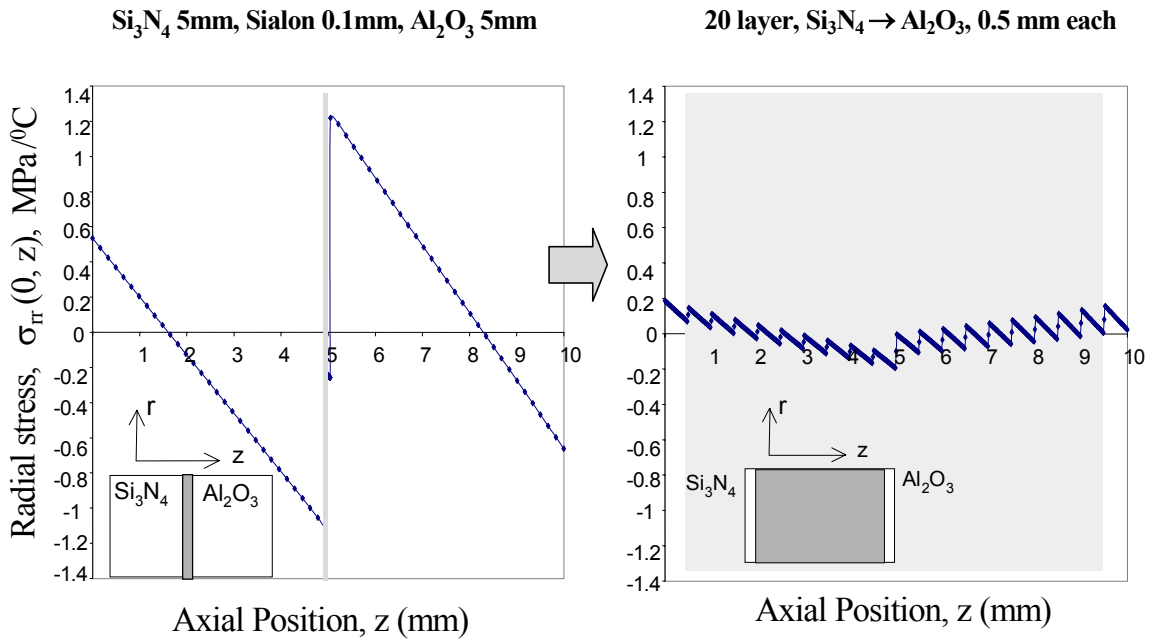

Figure 4.3. Computed radial stress, σ_{rr} at r=0 as a function of axial position, z, for the tri-layer and the 20 layer FGM samples.

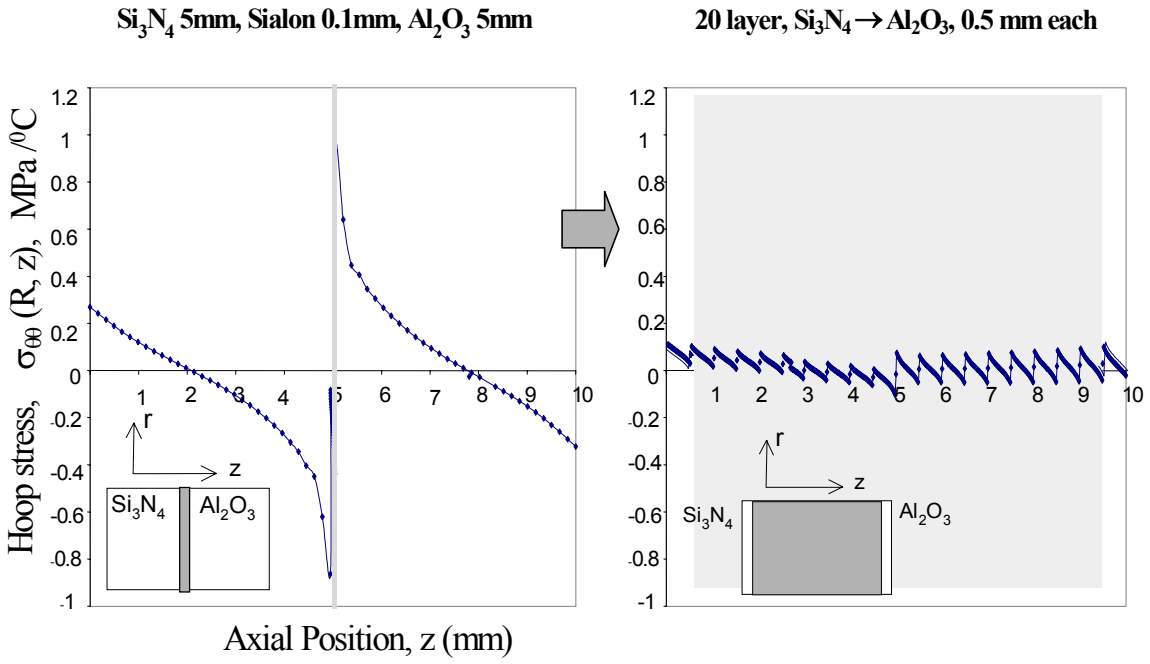

Figure 4.4. Computed hoop stresses as a function of axial position, z, at r=R.

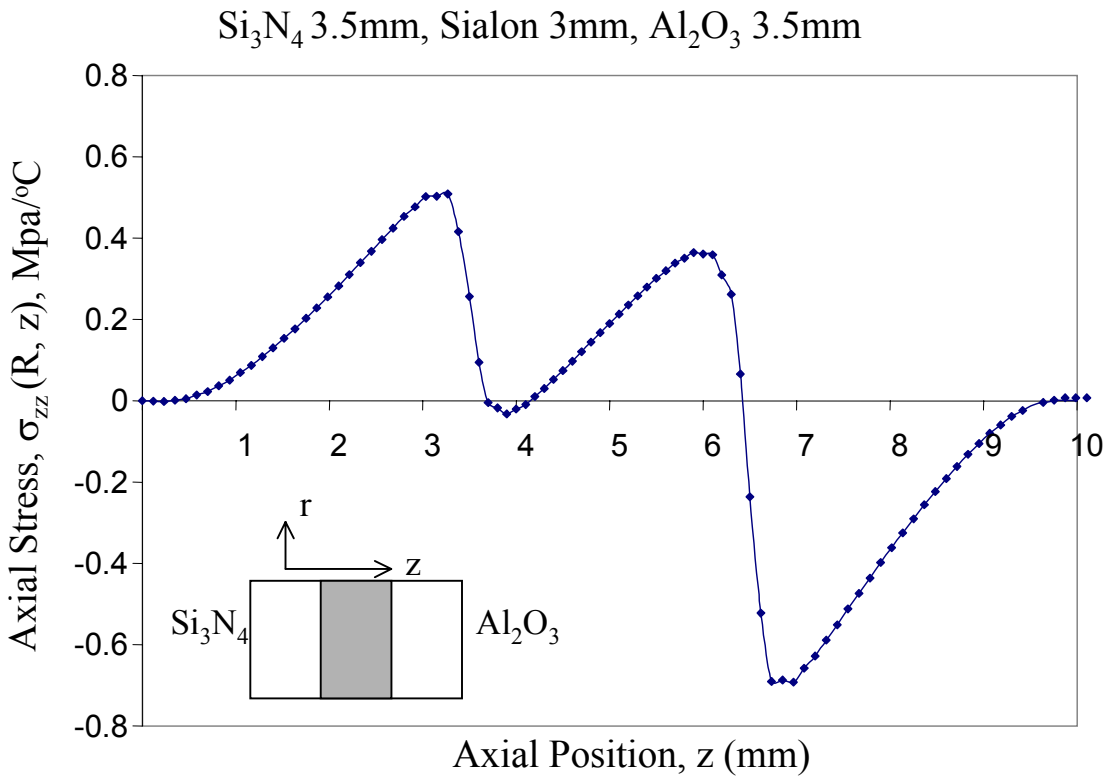

Figure 4.5. Computed axial stress, σ_{zz} at r=R as a function of z, for a 3-layer sample with thicker sialon interlayer.

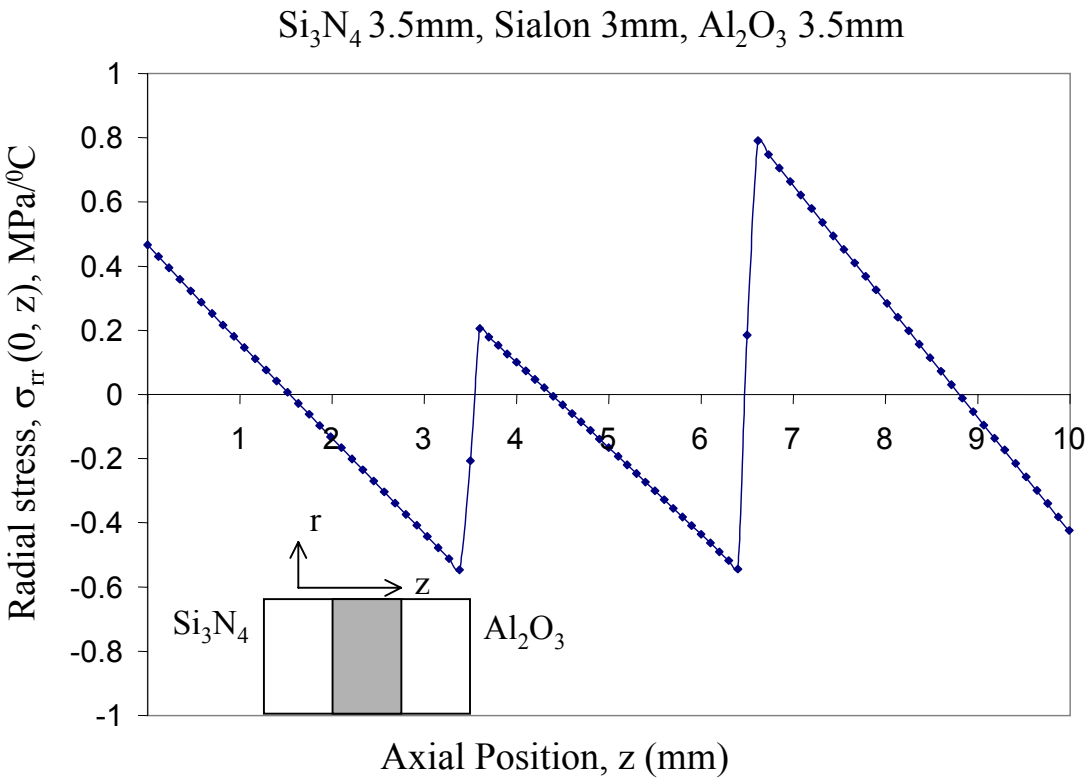

Figure 4.6. Computed radial stresses, σ_{rr} at r=0 as a function of axial position, z, for the tri-layer sample with thicker sialon interlayer.

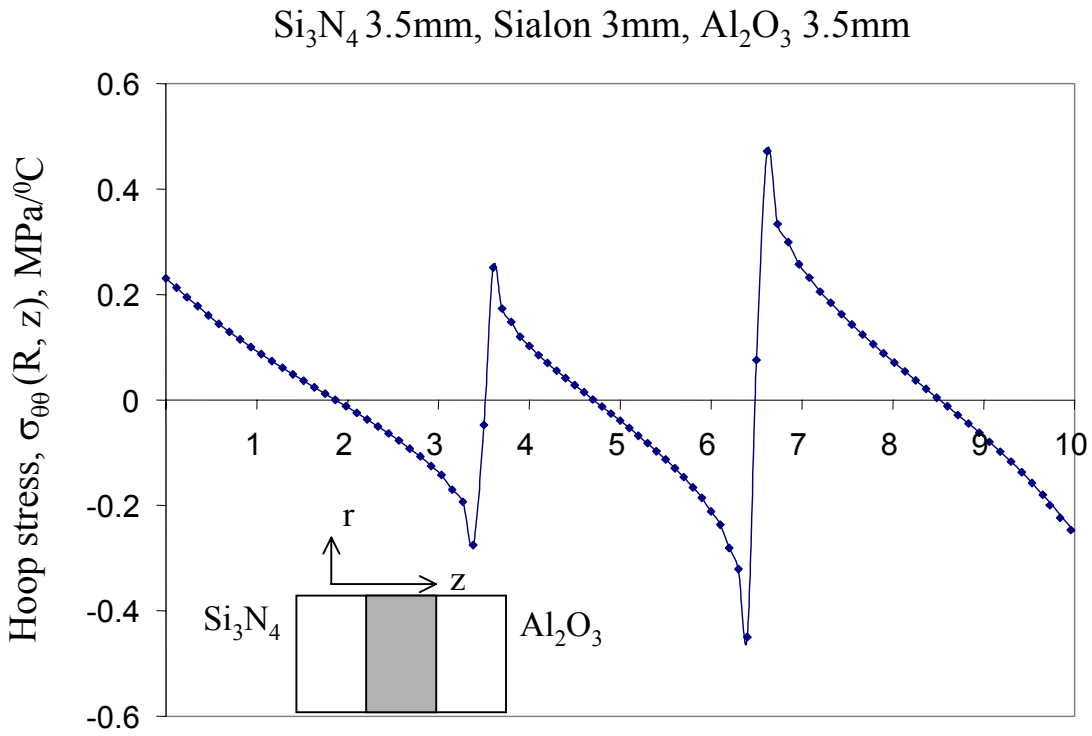

Figure 4.7. Computed hoop stresses as a function of axial position, z, at r=R for the trilayer sample with thicker sialon interlayer

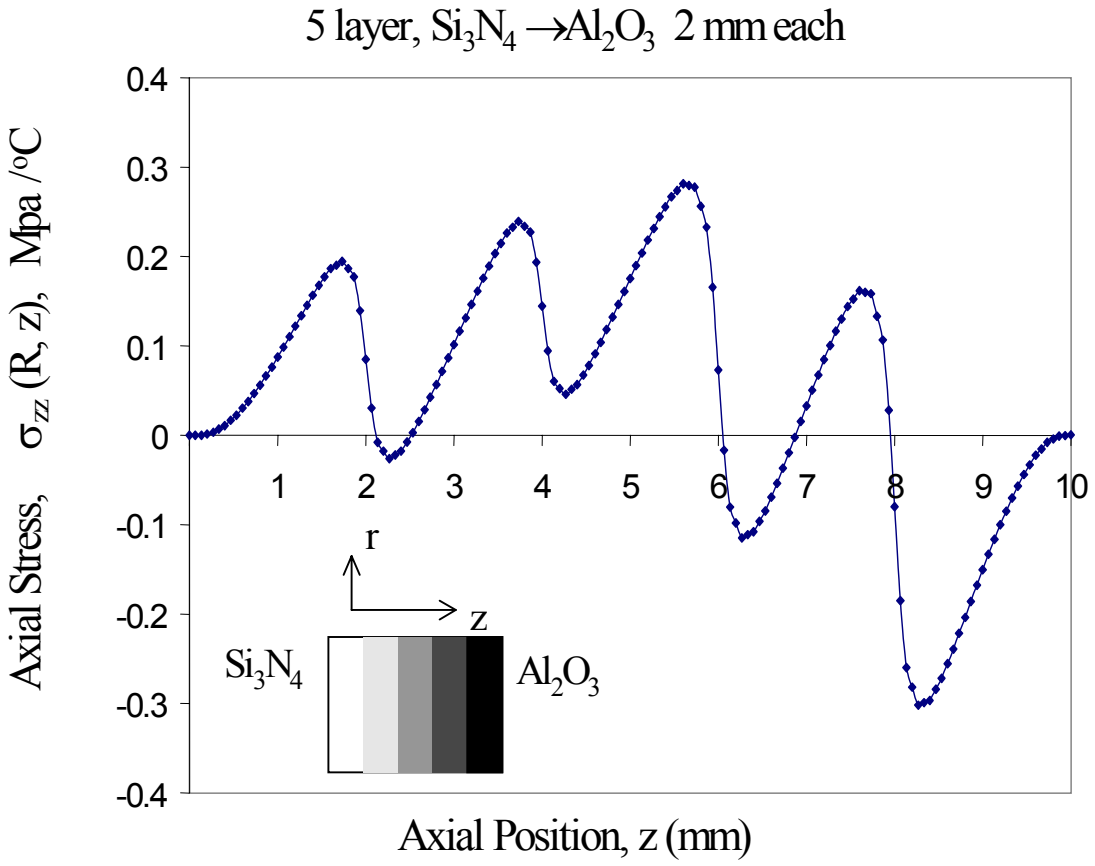

Figure 4.8. Computed axial stress, σ_{zz} at r=R as a function of z, for the 5-layer sample with sialon interlayer in the middle.

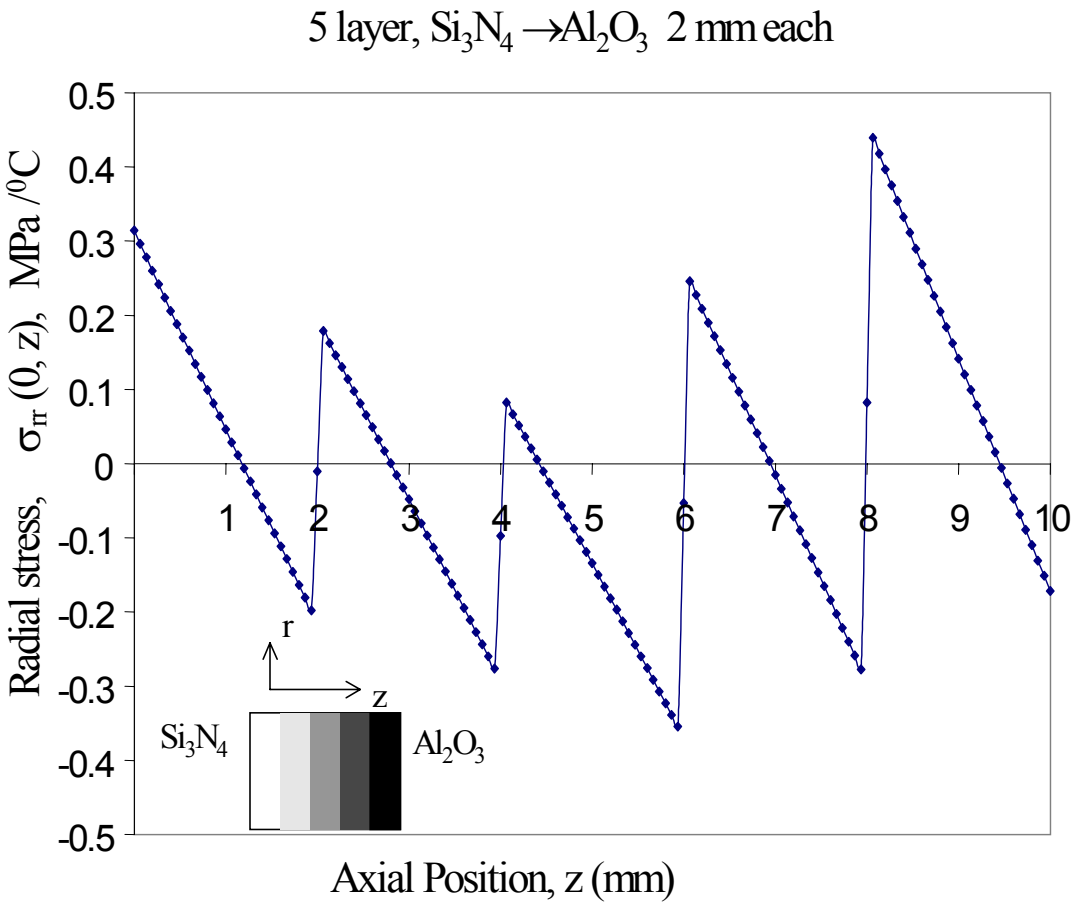

Figure 4.9. Computed radial stresses, σ_{rr} at r=0 as a function of axial position, z, for the 5-layer sample with sialon interlayer in the middle.

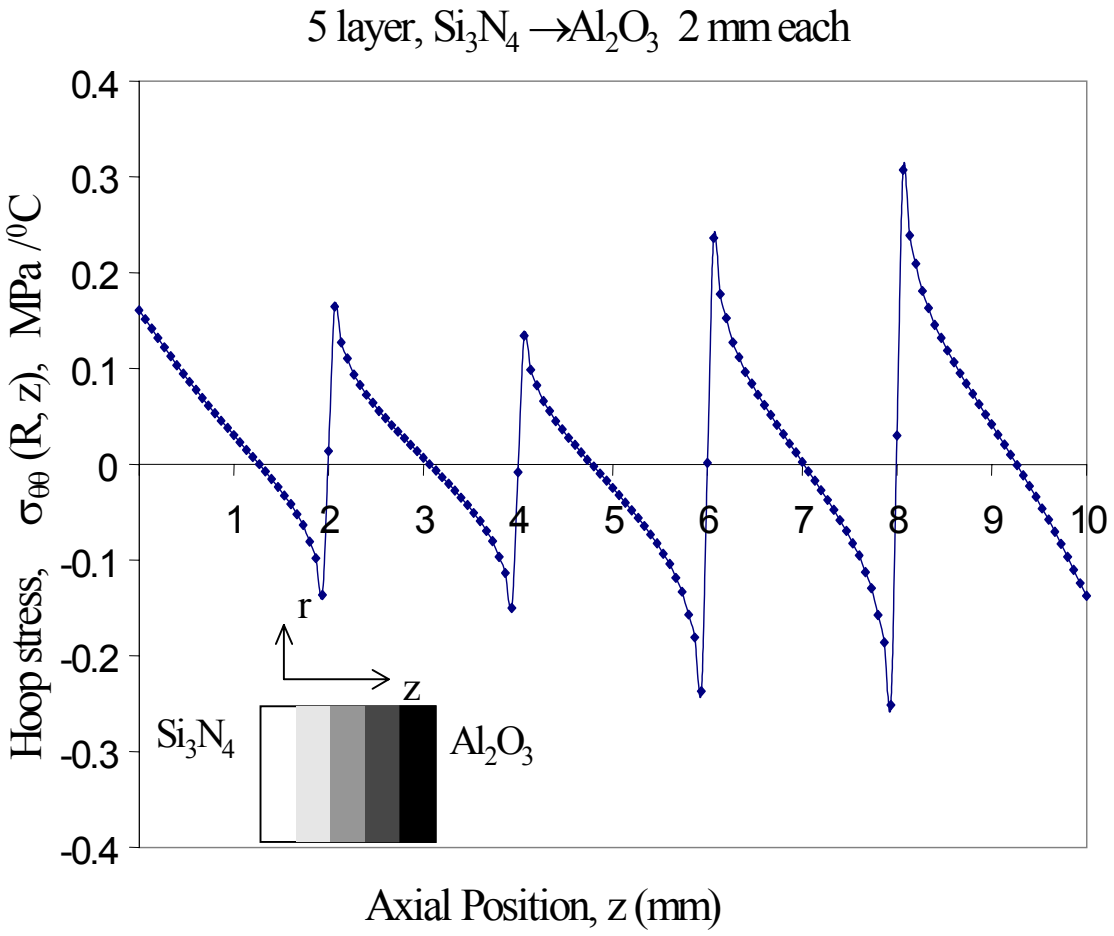

Figure 4.10. Computed hoop stresses as a function of axial position, z, at r=R for the 5-layer sample with sialon interlayer in the middle.

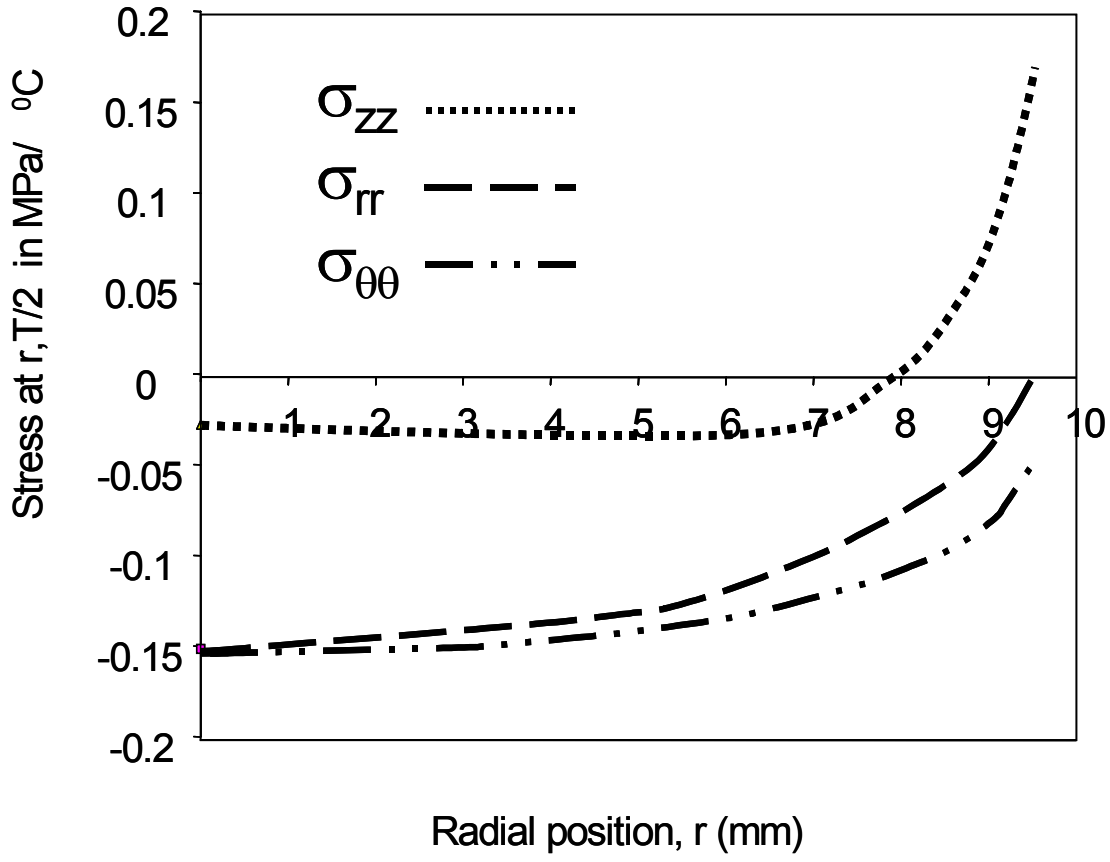

Figure 4.11. Computed stresses as a function of radial position, r, at z=T/2, for the symmetrical 20-layer FGM sample. The sample diameter is 19 mm; every layer has a thickness of 0.5 mm.

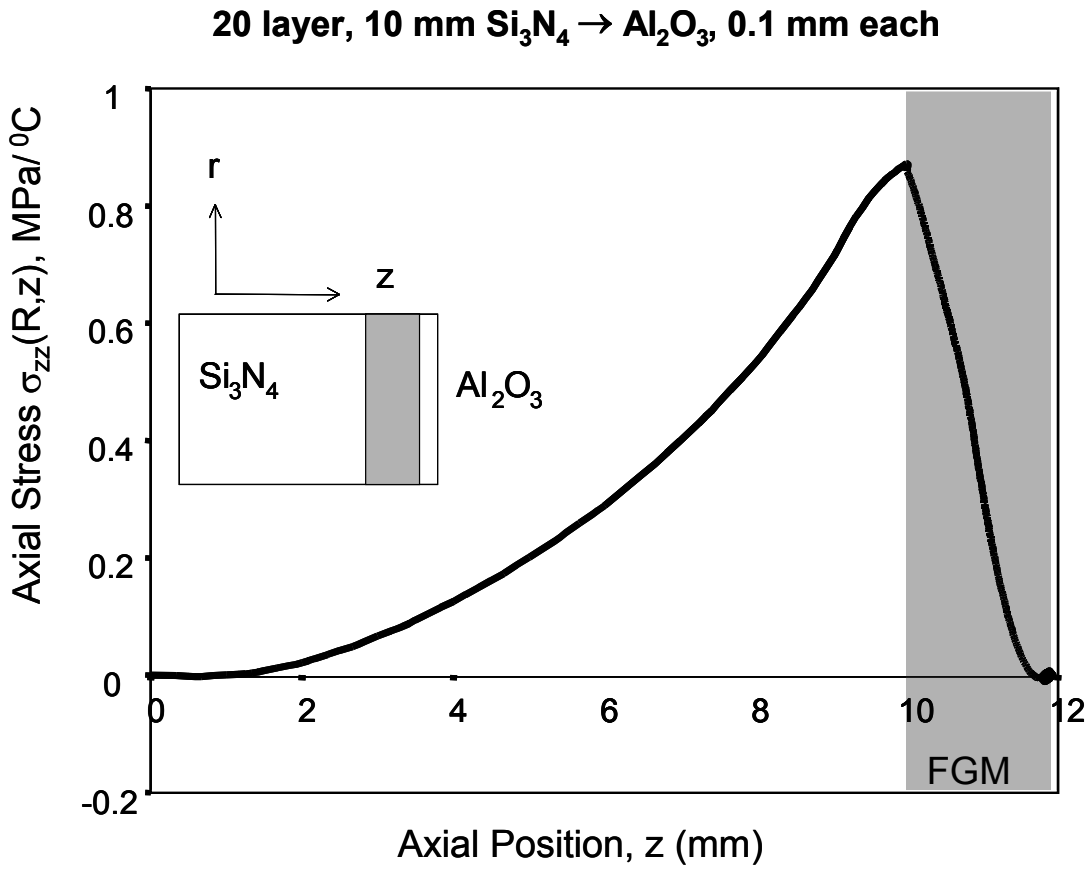

Figure 4.12. Computed axial stress, σ_{zz} at r=R of asymmetrical FGM sample. The shaded region indicates the position of the FGM.

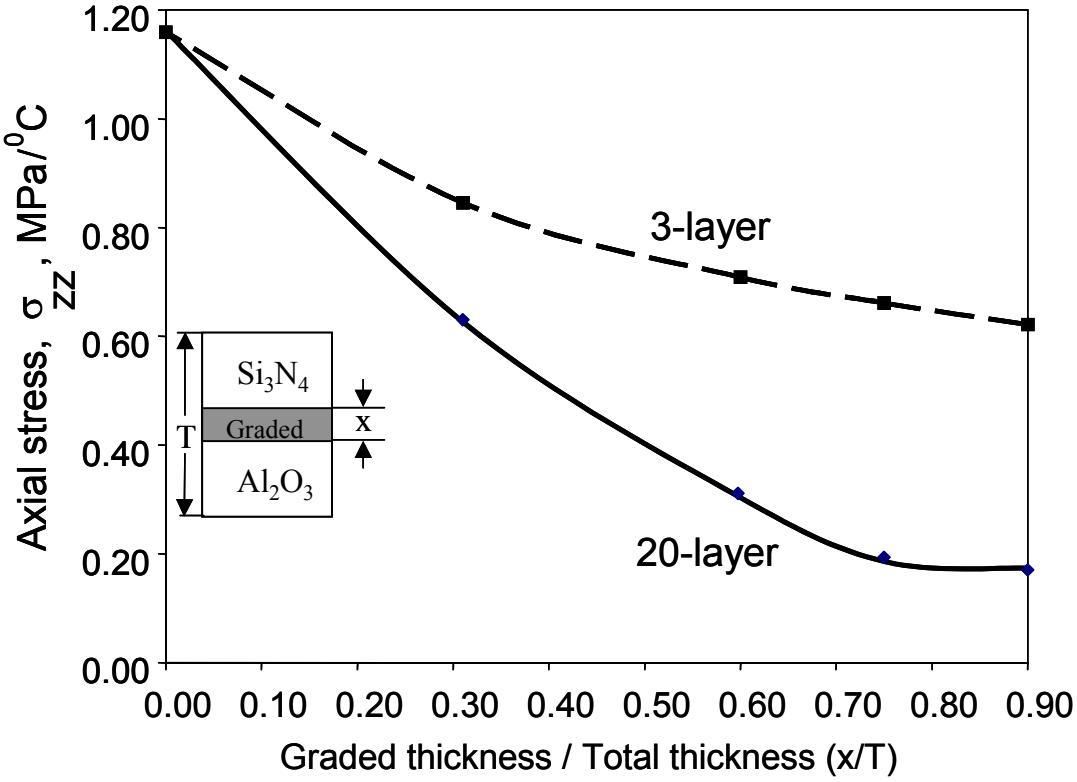

Figure 4.13. Computed maximum axial stress at r=R, for a fixed joint layer thickness, x, as a function of the total sample thickness T. The silicon nitride and the alumina slabs are assumed to be of equal thickness. As the slab thickness of the alumina and silicon nitride slabs increases, the value of x/T decreases. The actual stress is obtained by multiplying the stress per ^{0}C values by the temperature difference between the stress free temperature (here 1700 ^{0}C) and the evaluation temperature (e.g. 20 ^{0}C). This scaling computation sets the limits of sample geometry for which successful joining may be expected.

CHAPTER 5: Mechanical Properties of Polytypoidally Joined Si_3N_4-Al_2O_3

5.1. Introduction

Joining of high-temperature structural ceramics to other materials has often been a significant technological challenge. A commonly used joining technique for similar ceramics involves the introduction of some bonding interlayer. However, the simple bond-layer approach is ineffective for dissimilar materials when the thermal expansion coefficients (CTEs) of the materials to be joined are substantially different, since then large stresses arise that cause failure. The possibility of using a graded junction, rather than an abrupt bond layer allows for potentially effective joining of ceramics with widely differing CTEs. In such a graded bond layer, *i.e*. an FGM bond, there is a continuous change in composition from one side to the other, with an accompanying compatible gradient of thermal expansion properties. This concept has been used successfully in sialon polytypoidal functional gradient joining of dissimilar ceramics, Si_3N_4 and Al_2O_3, described in ref [1].

In this chapter, the various mechanical properties of the joined ceramics have been investigated by oriented Vickers indentation test, and strength testing at room and at high (1200 ^{0}C) temperatures.

Many of the present-day advanced materials are composites incorporating various types of dissimilar reinforcing elements such as fibers, whiskers, and particles, embedded in a matrix material, introducing a high density of interfaces. To study the mechanisms of how cracks behave along such interfaces, oriented indentation tests have been used [2]. He and Hutchinson [3] analyzed the energies for deflection and

penetration of a crack through the interfaces. They showed that the toughness of the interface may be determined from the critical angle at which the transition from crack penetration to deflection occurs, with a lower angle of transition implying a tougher interface [4]. When a crack impinges on the interface at a large angle, the penetration process is energetically favored. When the angle of incidence is shallow, the deflection process is favored. The angle, at which this transition occurs, from penetration to deflection, is a measure of the toughness of the interface [5].

Silicon nitride is a candidate ceramic for structural use because of its high strength and toughness. Sialon polytypoidal functional gradients have been used to join the dissimilar ceramics; Si_3N_4 and Al_2O_3 since sialon polytypoids are physically and chemically compatible with both Si_3N_4 and Al_2O_3. In this work, room temperature and high temperature (1200 ^oC) strength was evaluated on this ceramic joint [6].

5.2. Experimental Procedures

5.2.1. Material Fabrication

The samples were prepared by successively filling a graphite hot-press die with the appropriate layers of powder mixes. The sample was subsequently hot pressed at 50 MPa, at 1700 ^0C for two hours, and furnace-cooled to room temperature at 2^0C/min. Bend beams and microscopy samples were prepared from these hot-pressed specimens. Details of the processing and characterization methods are described in Chapters 2 and 3 [1]. After hot pressing, each layer had a thickness of 0.5 mm.

5.2.2. Oriented Indentation Test

Indentation techniques were used to characterize qualitatively the integrity of the joint. The results were used as guides to optimize the processing condition. Samples were prepared by cutting the FGMs, and polishing to a surface finish of 1μm. A Vickers indenter initiated cracks in the vicinity of the interfaces at shallow and high incident angles relative to the joining layer interfaces. The indenter loads ranged from 9 to 5 kilogram, with the lower loads applied on the softer, alumina-rich area side of the joint. Evidence of the possible interaction between the crack and the joining interfaces, and qualitative information about the strength of the joint were sought using optical microscopy.

5.2.3. Strength Characterization

Three-point bend tests were conducted at 25 ^{0}C and at 1200 ^{0}C to determine the effect of temperature on the strength of the joint. The sample location and test geometry are shown in Figure 5.1. The test jig was designed specifically for these bend specimens which were 2 mm x 4 mm x 10 mm. The test span form the center to the outer load point was 4 mm; the load displacement rate was 0.06 mm/min. Some tests were also done at a load displacement rate of 6 mm/min. The tensile surfaces of the bend bars were polished to a 1-μm surface finish, and the tensile edges were beveled on a 6-μm diamond wheel to reduce edge flaws. Tests at high temperature were carried out in Argon at 1 atm. The fracture surfaces were examined in the scanning electron microscope (SEM). The strength was determined from the following relation:

$$\sigma = M_b * y / I = (P*l*h)/(4*I) \quad (5.1)$$

Where 'σ' is the three-point bend strength, 'M_b' is the bending moment, 'h' is the beam height, 'y' is h/2, 'P' is the load at fracture, 'l' is the beam length and 'I' is the moment of inertia. I for the rectangular beam was calculated using the following formula:

$$I = b*h^3/12 \quad (5.2)$$

where 'b' is the width of the beam.

5.3. Results and Discussion

5.3.1. Indentation Test

Figure 5.2 shows some indentations in the Si_3N_4-rich part of the joint, at the juncture of the Si_3N_4 layer and the first polytypoid layer with composition 90 wt.% Si_3N_4/10 wt % 12H sialon ($Si_3Al_7O_3N_9$), at a high and a shallow incident angle to the layer interface. The interfaces generally could not be discerned in either the SEM or the optical microscope, so the indentations were made close to sporadic interface pores. The indent cracks ostensibly traversed the interfaces at all angles of incidence and were only minimally deflected, implying strong interfaces within the FGM joint [7, 8]. Figures 5.3 – 5.4 show some indentations in the sialon-rich part and in the Al_2O_3-rich part of the joint, and the indent cracks in both figures were also minimally deflected, implying strong interfaces within the FGM joint.

5.3.2. Strength Characterization

Flexural strengths at room temperature and at 1200 ^{o}C were obtained using a three-point bend test. The fracture for both temperatures occurred within the polytypoid, which is approximately in the middle of the sample. The average strength at room temperature was found to be 581 MPa, and the average strength at 1200 ^{o}C was found to be 262 MPa (Table 5.1). 4-5 samples were tested at each temperature. Fracture surfaces of the tested samples at room temperature and at high temperatures were examined by SEM. Figures 5.5 and 5.6 show that at both room temperature and at high temperature, the fracture modes are mixed intergranular and transgranular. The fracture surfaces of the materials tested at 1200 ^{o}C show evidence of viscous deformation of intergranular material, Figure 5.7. This observation agrees with the previous work of Cinibulk et. al. (1990) on Si_3N_4 sintered with Y_2O_3 + Al_2O_3 which reported grain-boundaries with poor resistance to softening at 1000 ^{o}C [9,10] and that done by Li et. al [6]. In these liquid-phase sintered ceramics, grain boundaries and triple-junctions often contain an amorphous phase, which can soften, resulting in ready grain-boundary sliding, cavitation, and cracking. To confirm the observation of softening of the glassy phases in the FGM joint, a loading rate of 6 mm/min was used at 1200 ^{o}C. The flexural test using 6 mm/min loading rate at 1200 ^{o}C resulted an average strength value of 356 MPa with a standard deviation of 36 MPa, compared to 262 MPa at the slow loading rate. This confirms that the strength degradation at high temperature is most likely due to the softening of intergranular glassy phases. Although high resolution images of various phase interface grain boundaries did not detect grain boundary glassy phases (see ref [1]), significant quantities of glass reside

at triple points (e.g. Figure 3.3). A combination of grain boundary sliding with triple point glass softening may thus be proposed as the origin of the loading-rate dependent modulus of rupture of the FGM joint. Further alloying to crystallize these grain boundary phases might be beneficial to improved high temperature performance [9-11].

5.4. Conclusions

In this chapter, mechanical properties of this crack-free FGM sample were studied. Based on the mechanical characterization obtained by indentation testing and strength testing, the following conclusions can be made:

(1) The indentation test at high and shallow incident angles shows that cracks pass through the interface without being deflected, which is evidence that the interface is strong.

(2) The average strength was found to be 581 MPa and 262 MPa at room and 1200 ^{o}C, respectively. The fracture for both temperatures occurred in the middle of the sample which is in the polytypoid phase. This strength loss at high temperature was consistent with a softening of glassy phases at triple junctions

5.5. References

1. C. Lee, X. Zhang and G. Thomas, "Polytypoid Functional Gradients; Novel joining of dissimilar Ceramics in the Si_3N_4-Al_2O_3 system", *Acta Mater.,* accepted (2001)

2. A.K. Bhattacharya, J. J. Petrovic and S.C. Danforth, "Indentation method for determining macroscopic fracture energy of brittle bimaterial interfaces", *Journal of American Ceramic Society*, **75**[2], 413-417 (1992)

3. M. He and J. Hutchinson, "Crack deflection at an interface between dissimilar elastic materials", *Int. J. Solids Structures,* **25**[9], 1053-1067 (1989)

4. A.G. Evans, B.J. Dalgleish, M.Y. He and J.W. Hutchinson, "On crack path selection and the interface fracture energy in bimaterial systems", *Acta metall. Mater*., **37**[12], 3249-3254 (1989)

5. P. Becher, S. Hwang and C. Hsueh, "Using Microstructure to attack the brittle nature of Silicon Nitride Ceramics", *MRS Bull.*, **20**[2], 23-27 (Feb. 1995)

6. H. Li, W. Sun and D. Yan, "Mechanical properties of Hot-pressed 12H ceramics", *J. European Ceramics Society*, **15**[7], 697-701(1995)

7. P.F. Becher, S.L. Hwang and C.H. Hsueh, *MRS Bull.*, **20**[2], 22 (1995)

8. M. Gopal, L.C. DeJonghe and G. Thomas, "Silicon Nitride joining using rare-earth reaction sintering", *Scripta Materialia,* **36** (4), 455-460 (1997)

9. M. Cinbulk and G. Thomas, "Grain-boundary-phase crystallization and strength of Silicon nitride sintered with a YSiALON glass", *J. Am.Ceram. Soc.*, **73** [6] 1606-12 (1990)

10. G. Thomas, "Designing for improved high temperature strength, Creep, Oxidation and Fatigue resistance in Si3N4", Critical issues in the development of high temperature structural materials : proceedings from the Conference on Critical Issues in the Development of High Temperature Structural Materials, 349-364 (1993)

11. Y.Goto and G.Thomas, "Microstructure of silicon nitride ceramics sintered with rare-earth oxides", *Acta metall. mater*., **43**[3], 923 (1995)

Table 5.1. Strength test results

Temp/Strength	Strength (MPa)
At Room temperature (25 ^{o}C)	581 $\pm$ 60
At High temperature (1200 ^{o}C) (loading rate 0.06 mm/min)	262 $\pm$ 20
At High temperature (1200 ^{o}C) (loading rate 6 mm/min)	356 $\pm$ 36

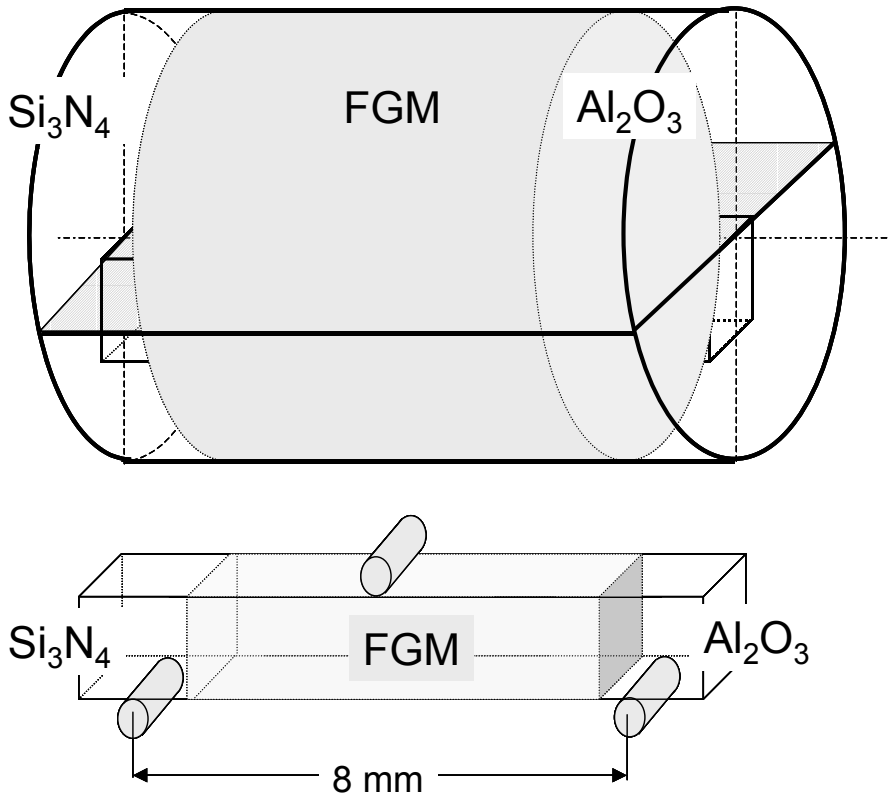

Figure 5.1. Sample Position and test jig geometry.

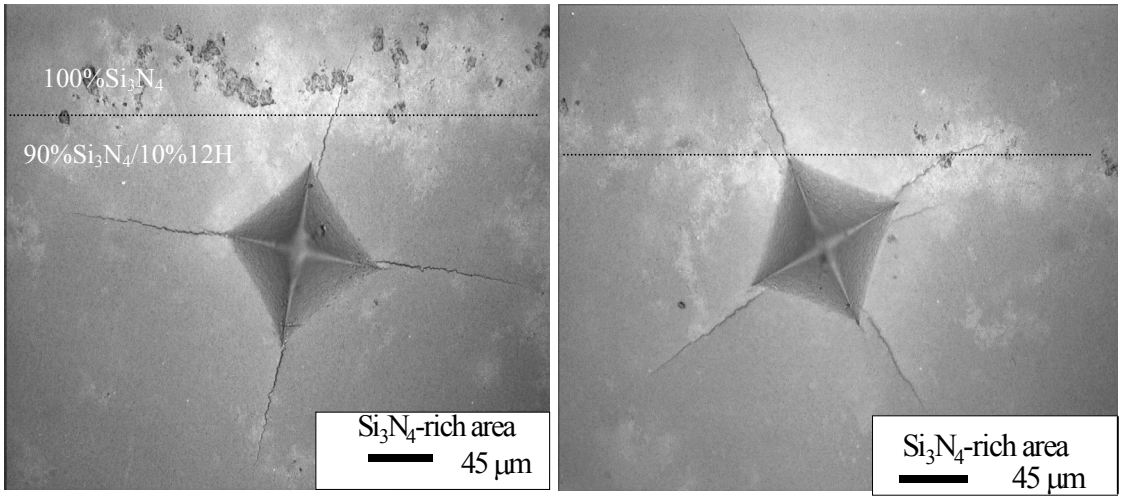

Figure 5.2. Optical micrographs of the joints showing Vickers indents at high (right) and shallow (left) incident angles in the Si_3N_4-rich area. The cracks pass through the joint without being deflected. The dotted lines indicate the approximate position of the interfaces.

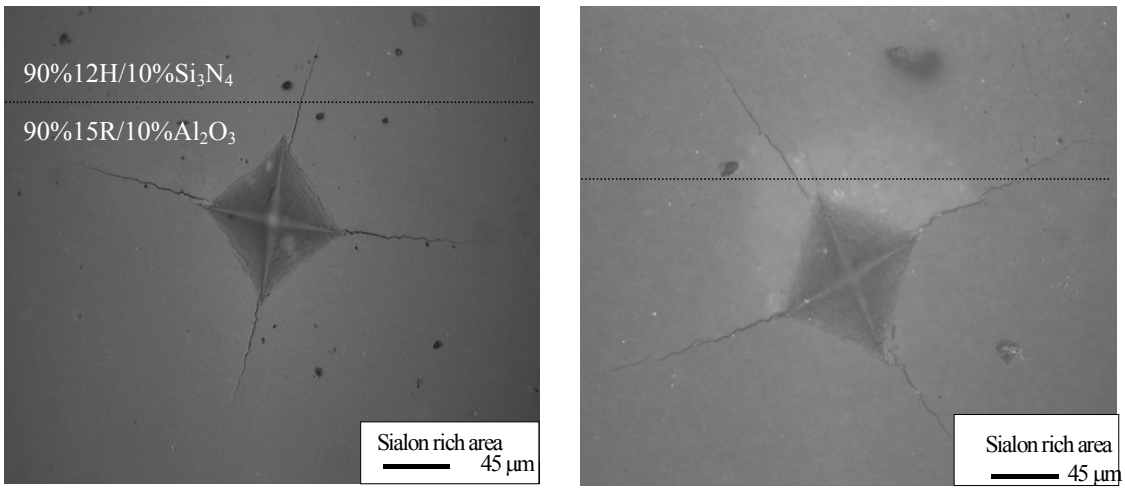

Figure 5.3. Optical micrographs of the joints showing Vickers indents at high(right) and shallow (left) incident angles in the sialon-rich area. The cracks pass through the joint without being deflected. The dotted lines indicate the approximate position of the interfaces.

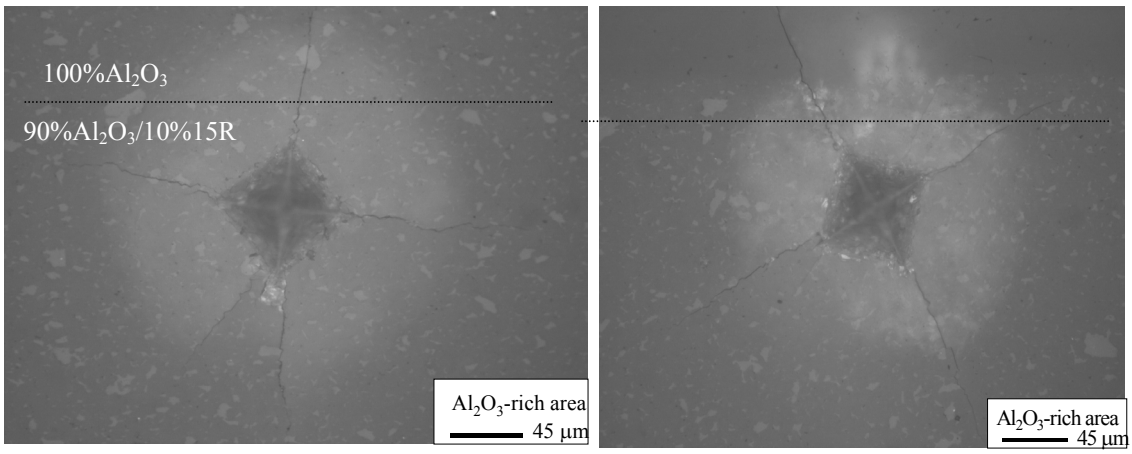

Figure 5.4. Optical micrographs of the joints showing Vickers indents at high (right) and shallow (left) incident angles in the Al_2O_3-rich area. The cracks pass through the joint without being deflected. The dotted lines indicate the approximate position of the interfaces.

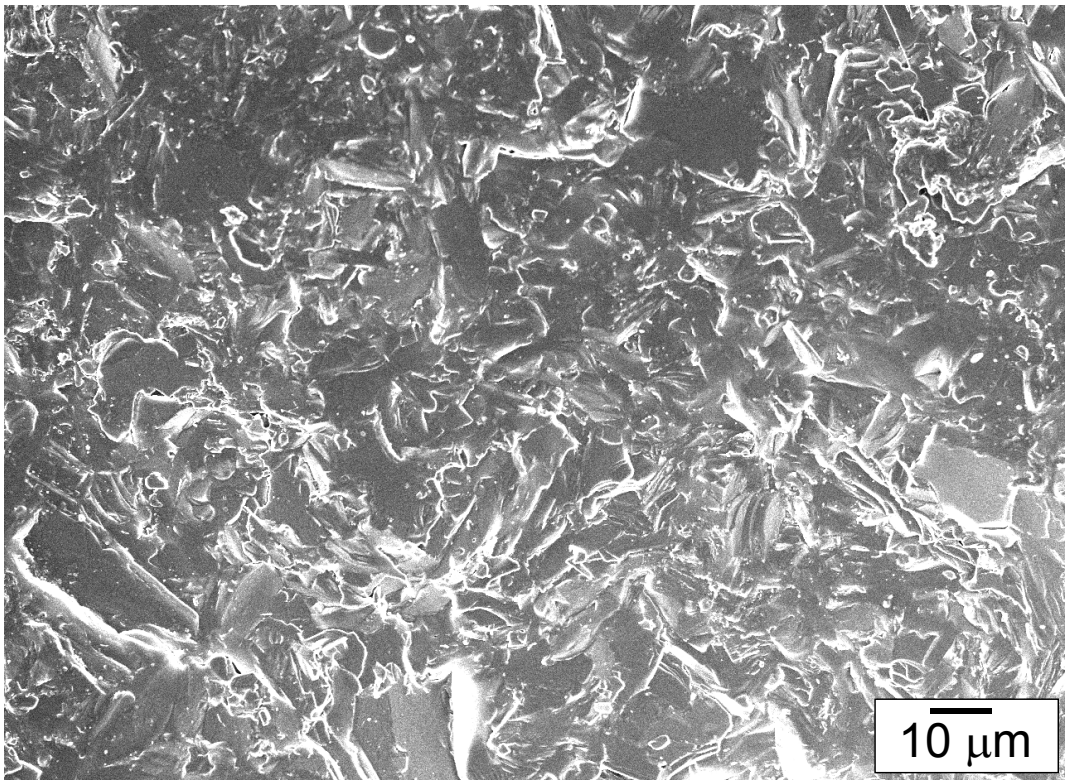

Figure 5.5. SEM image of room temperature fracture surface at z~ T/2 of a 20-layer FGM sample. The fracture modes are mixed intergranular and transgranular.

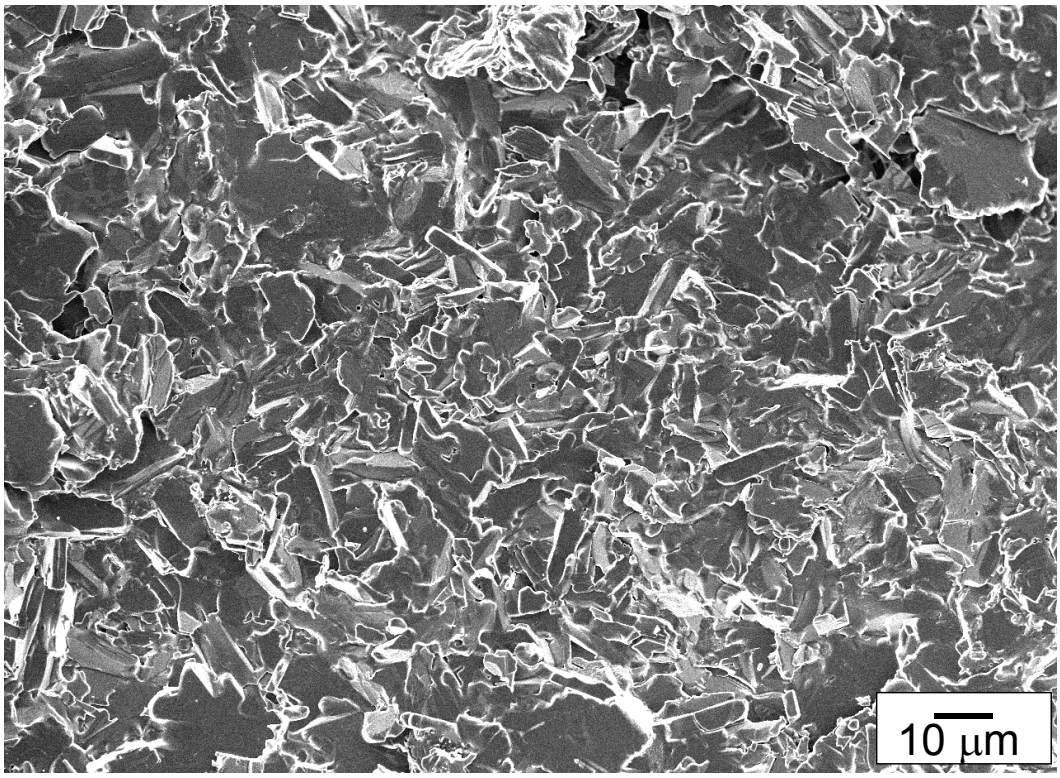

Figure 5.6. SEM image of 1200 ^{0}C temperature fracture surface at z~ T/2 of a 20-layer FGM sample. The fracture modes are mixed intergranular and transgranular.

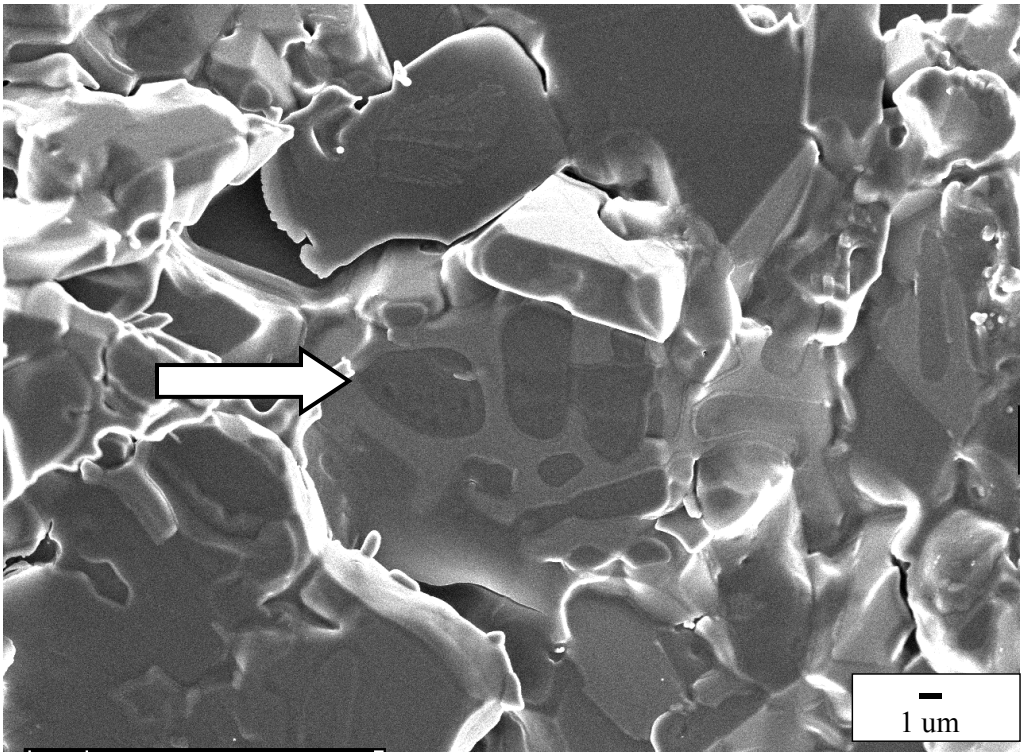

Figure 5.7. SEM image of 1200 ^{0}C fracture surface with presence of viscously deformed intergranular phase indicated.

CHAPTER 6: Conclusions

Crack-free joining of heterogeneous ceramics is demonstrated by the use of sialon polytypoids as Functionally Graded Materials (FGM) as defined by the phase diagram in the system $Si_3N_4 – Al_2O_3$. Silicon nitride has been considered to be one of the most promising structural materials for high temperature applications for the following unique properties; high strength, oxidation and corrosion resistance, thermal stability and resistance to thermal shock [6]. Also, alumina has been widely used in high temperature structural components due to its chemical stability. Alumina has been chosen for the joining material since it has an intermediate coefficient of thermal expansion between Si_3N_4 and metals for the application of ceramic-metal joining. Moreover, alumina is chemically and physically compatible with both Si_3N_4 and metal. Therefore, alumina can be used as a buffer layer for joining Si_3N_4 and metal. In order to join Si_3N_4 to Al_2O_3, a sialon polytypoid has been used for several reasons: First, sialons are essentially silicates and alumino-silicates in which oxygen is partly or completely replaced by nitrogen, while silicon is partly replaced by aluminum. Sialon polytypoids are physically and chemically compatible with both Si_3N_4 and Al_2O_3. A polytypoid is defined as a faulted structure in which the fault periodicity depends on composition through the cation/anion ratio. It was found that AlN polytypoids, such as 15R, 12H, 21R, 27R and 2H, have CTEs in the range of 5.1 to 5.9 x 10^{-6} $/^0$C [8]. Since the CTE of Si_3N_4 is 3.6x$10^{-6}/^0$C and that of Al_2O_3 is 8.8x$10^{-6}/^0$C, the use of sialon polytypoids for joining Si_3N_4 and Al_2O_3 is clearly attractive. Finally,

polytypoid step-functional joining can be obtained since the structure of this compound is determined by stacking-fault spacing (metal/non metal ratio).

Based on the fabrication method, microstructural characterization, and mechanical characterization, the following conclusions can be made:

(1) Crack-free joining of Si_3N_4 to Al_2O_3 was produced by stacking 20 layers of polytypoids with thickness of 500 μm each, to minimize thermal residual stress. The result showed a smooth gradient across the thickness with varying the composition along the gradient by 10 wt%. This method can be applied to other dissimilar ceramics as long as there is no undesirable reaction between the systems. In order to accomplish such processing effectively, accurate phase diagrams for each multicomponent system are needed.

(2) Microstructural characterization indicated that the 15R polytypoid was formed in the Al_2O_3-contained layers and the 12H polytypoid was formed in the Si_3N_4-contained layers. This transition in polytypoid from 12H to 15R is explained by phase diagram in Figure 2.3 where the closest polytypoid type is matched to the materials to be joined to accommodate the lattice mismatch, by changing the polytypoid cation to anion ratios.

(3) XRD was used to identify the phases present in the polytypoid powders before the FGM was fabricated, and the 12H polytypoid, $Si_3Al_7O_3N_9$ was identified. In addition, $Al_5Y_3O_{12}$ was found at triple points. The transmission electron micrographs of FGM joint show that no undesirable reaction took place between the Si_3N_4, the Al_2O_3, or the polytypoids, as predicted in the phase diagram, Figure 2.3.

(4) EPMA scan across the length of 20-layer FGM sample showed a smooth concentration profile, verifying that interface diffusion occurred during sintering at each graded layer.

(5) No glassy phases were found across the various phases, Si_3N_4/12H, 15R/15R, 12H/12H and 15R/Al_2O_3, using High Resolution Electron Microscopy. A sharp 12H/15R interface in the middle of the FGM sample could not be resolved since this interface may in fact be mixtures of these polytypoids as shown in Figure 2.3.

(6) The indentation test at high and shallow incident angles shows that cracks pass through the interface without being deflected, which is evidence that the interface is strong.

(7) FEAP indicates the stress distribution in the FGM sample. The result showed a dramatic decrease in radial, axial and hoop stress as the FGM changes from three layers to 20 graded layers. This analysis explains why a 20 layer FGM was crack-free but a 3-layer FGM was cracked. Scaling computations for FGM samples indicate that at least 75% of the total sample thickness needs to be the graded thickness so as to minimize residual stresses. Such analyses are especially useful for graded FGM samples where the residual stresses are very difficult to measure experimentally.

(8) The average strength was found to be 581 MPa and 262 MPa at room and high temperatures, respectively. The fracture for both temperatures occurred in the middle of the sample. This strength loss at high temperature was consistent with a softening of glassy phases at triple junctions.

APPENDICES

APPENDIX I. Transmission Electron Microscopy

The transmission electron microscope (TEM) is used to obtain structural information from specimens that are thin enough to transmit electrons. TEM's strong capabilities are its high lateral spatial resolution (better than 0.2 nm, "point-to-point" on some instruments) and its capability to provide image and diffraction information from a single sample. In addition, the highly energetic beam of electrons used in TEM interacts with sample matter to produce characteristic radiation and particles; these signals often are measured to provide materials characterization using Energy Dispersive Spectrometers (EDS), Electron Energy Loss Spectroscopy (EELS), Extended Energy Loss Fine Structure (EXELFS), backscattered and secondary electron imaging [1, 2].

The basic principle of TEM is as follows; a focused electron beam is incident on a thin (less than 200 nm) sample. The signal in TEM is obtained from both undeflected and deflected electrons that penetrate the sample thickness. A series of magnetic lenses at and below the sample position are responsible for delivering the signal to a detector, usually a fluorescent screen, a film plate, or a video camera. A schematic of a TEM instrument, showing the location of a thin sample and the principal lenses within a TEM instrument, is illustrated in Figure A1, and Figure A2 shows a schematic for the ray paths of both scattered and unscattered electrons beneath the sample. Accompanying this signal transmission is a magnification of the spatial information in the signal by as little as 50 times to as much as a factor of 10^6.

The high magnification of all TEM methods is a result of the small effective wavelengths (λ) employed. According to the de Broglie relationship,

$$\lambda = h / \sqrt{(2*m*q*V)} \quad \text{(A1)}$$

Where m and q are the electron mass and charge, respectively, and h, the Planck's constant, and V is the potential difference through which electrons are accelerated. Electrons of 100 KeV energy have wavelengths of 0.037 Å and are capable of effectively transmitting through about 0.6 μm of Si [3]. Since electrons in a TEM probe are in phase as they enter the specimen, their phase relationships upon exiting are correlated with spatial associations between scattering centers (atoms) within the material. High lateral spatial resolution is maintained through the use of extremely thin samples, which are usually less than 200 nm. This ensures relatively few scattering events as each electron traverses the sample. Moreover, the higher the operating voltage of a TEM instrument (lower λ), its lateral spatial resolution is greater. The theoretical instrumental point-to-point resolution is proportional to $\lambda^{3/4}$ [4]. So some commercially available 300 kV and 400 kV instruments, classified as high-voltage TEM instruments, have point-to-point resolution better than 0.2 nm. One shortcoming of TEM is its limited depth of resolution since electron scattering information in a TEM image originates from a three-dimensional sample, but is projected onto a two-dimensional detector (a fluorescent screen or a film plate). The collapse of the depth scale onto the plane of the detector necessarily implies that structural information along the beam direction is superimposed at the image plane. However, in some cases, it is possible to obtain limited depth information using TEM

by tilting the specimen to obtain a stereo image pair, using extinction contours in image mode, using convergent beam diffraction patterns and etc [1].

TEM offers two methods of specimen observation, diffraction mode and image mode. The Diffraction pattern is obtained in diffraction mode where the post specimen lenses are set to examine the information in the transmitted signal at the back focal plane of the objective lens. The diffraction pattern is entirely equivalent to an X-ray diffraction pattern but is obtained in specific rather than averaged as in X-rays: a single crystal will produce a spot pattern on the screen, a polycrystal will produce a powder or ring pattern (assuming the illuminated area includes a sufficient quantity of crystallites), and a glassy or amorphous material will produce a series of diffuse halos. Using this diffraction mode, the polytypoid grain in the crack-free FGM joint was observed along the c-axes to identify the different types of polytypoids at various regions of the joint. The image mode produces an image of the illuminated sample area. The post-specimen lenses are set to examine the information in the transmitted signal at the image plane of the objective lens. Here, the scattered electron waves finally recombine, forming an image with recognizable details related to the sample microstructure. There are three primary modes that are used in conventional TEM work: bright-field microscopy, dark-field microscopy, and high-resolution electron microscopy [5]. The bright-field image is obtained by intentionally excluding all diffracted beams and only allowing the central beam through. This is done by placing suitably sized apertures in the back focal plane of the objective lens. Intermediate and projection lenses then magnify this central beam. Dark-field images are also formed by magnifying a single beam; this time one of the diffracted beams is

chosen by means of an aperture that blocks the central beam and the other diffracted beams [3]. The last example of imaging techniques in TEM is high-resolution transmission electron microscopy. High-resolution TEM (HREM) is made possible by using a large-diameter objective diaphragm that admits not only the transmitted beam, but at least one diffracted beam as well. All of the beams passed by the objective aperture are then made to recombine in the image-forming process, in such a way that the amplitudes and phases are preserved. This is the technique employed in high-resolution lattice imaging, enabling diffracting planes and arrays of individual atoms to be distinguished. The HREM technique has become popular in recent years due to the more common availability of high-voltage TEMs with spatial resolutions in excess of 0.2 nm [1]. In this research, using such HREM, various grain boundaries of a crack-free FGM sample were studied to detect glassy phases present.

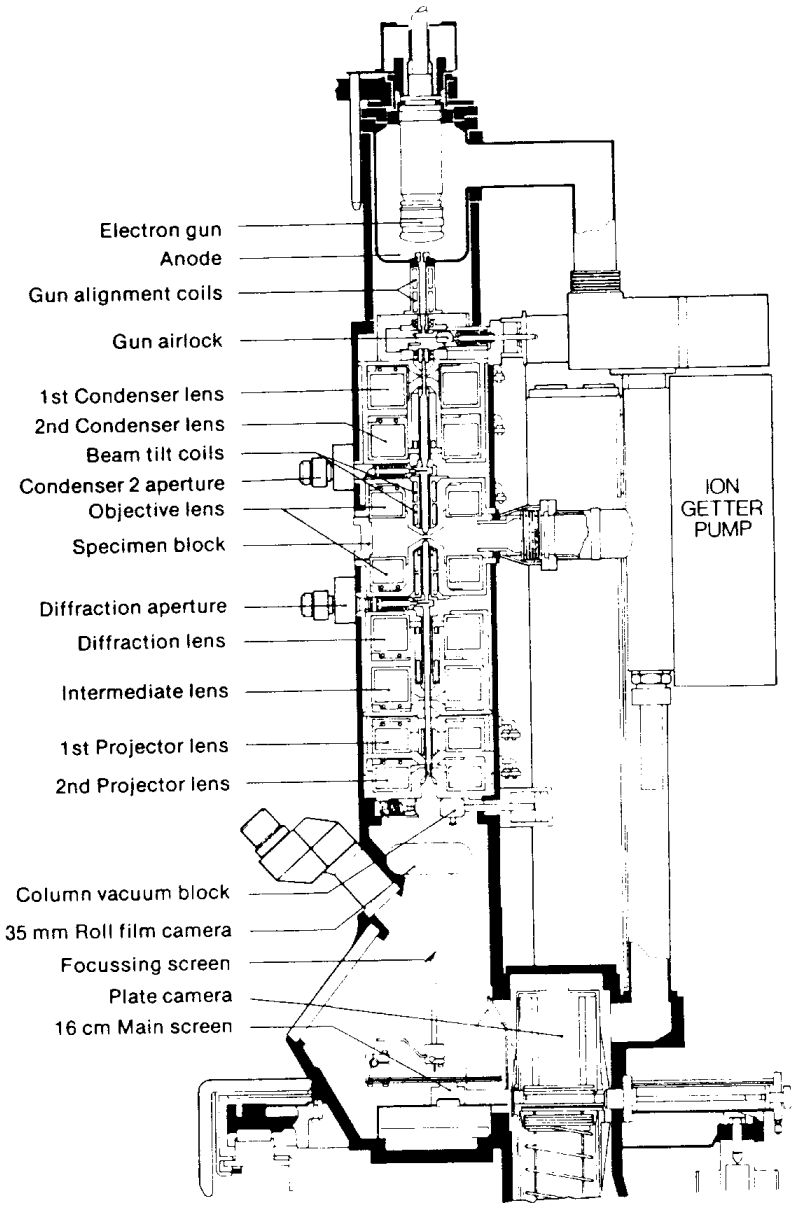

Figure A1. Schematic diagram of a TEM instrument, showing the location of a thin sample and the principal lenses within a TEM column (Ref. 1).

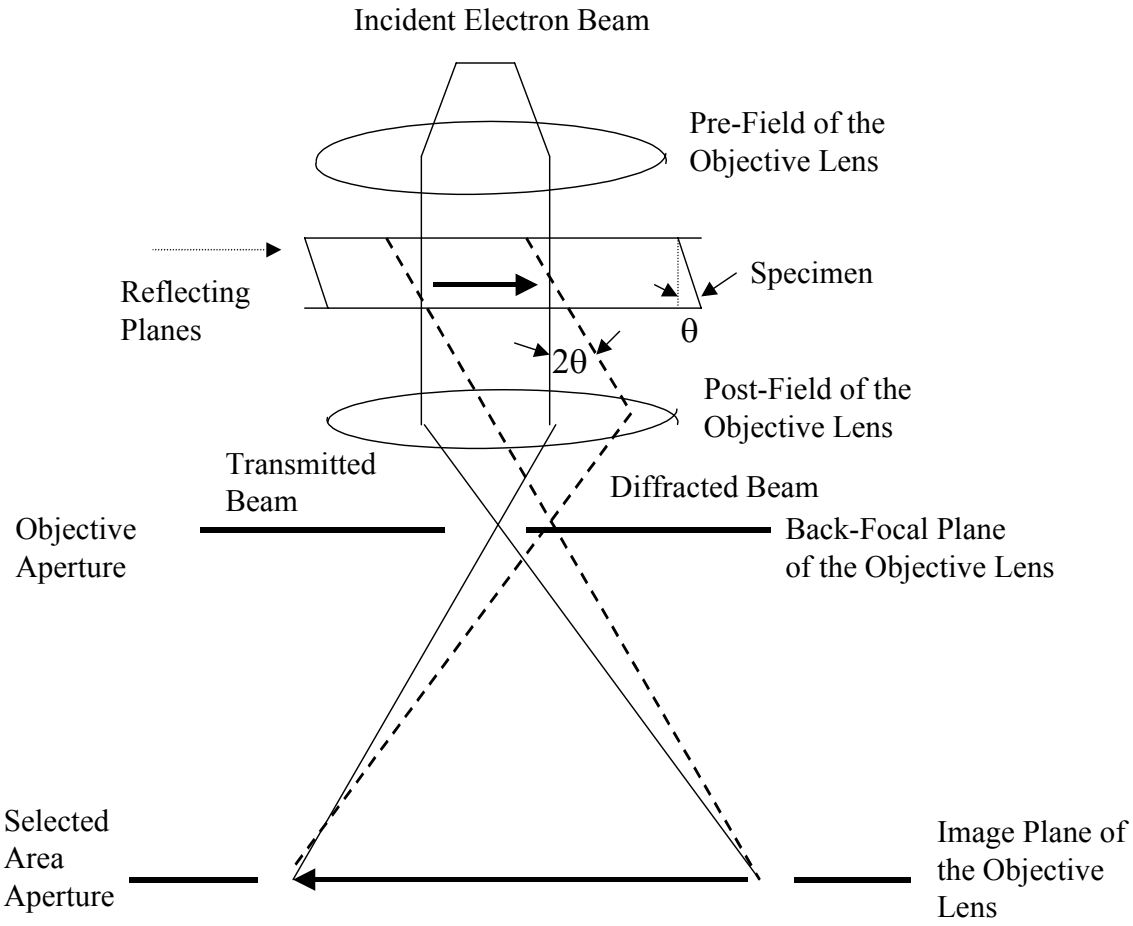

Figure A2. Schematic representation for the ray paths of both unscattered and scattered electrons beneath the sample (Ref. 1).

APPENDIX II. X-ray Diffractometer (XRD)

X-ray Diffraction (XRD) is a powerful technique used to uniquely identify the crystalline phases present in materials and to measure the structural properties (strain state, grain size, epitaxy, phase composition, preferred orientation, and defect structure) of these phases. XRD is noncontact and nondestructive, which makes it ideal for in situ studies. So this capability is advantageous compared to TEM and electron diffraction where their specimen preparation methods make these techniques destructive. However, one of the disadvantages of XRD, compared to electron diffraction, is the low intensity of diffracted X-rays, particularly for low-Z materials. Because of small-diffracted intensities, thin-film XRD generally requires large specimens (0.5 cm) and usually, XRD does not provide spatial resolution [6], and only gives averaged information whereas TEM is specific.

In the XRD experiment, the diffracted intensity is measured as a function of Bragg angle 2θ and the orientation of the specimen, which yields the diffraction pattern [7]. The experiment is done in a diffractometer, as shown in schematics in Figure A3, an electromechanical scanning system. The diffracted beam intensity is monitored electronically by a mechanically driven scanning radiation detector. After getting the diffraction pattern in the chart recorder, these patterns are compared against a large collection of known diffraction patterns. The unique relationship between such patterns and crystal structures provide a powerful tool for chemical identification of powders and polycrystalline materials [8]. Using this technique, polytypoid sialon powders were analyzed to identify the phases.

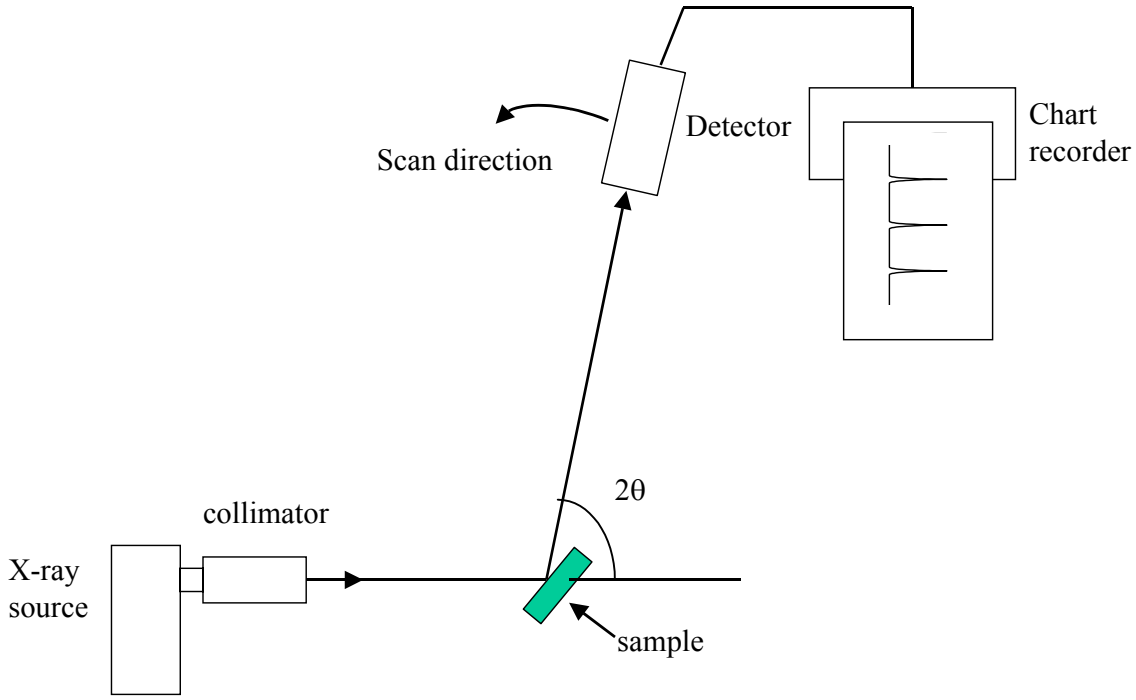

Figure A3. A schematic of X-ray diffractometer experiment (Ref. 7)

APPENDIX III. Electron Probe X-ray Microanalysis (EPMA)

EPMA is a spatially resolved, quantitative elemental analysis technique based on the generation of characteristic X-rays by a focused beam of energetic electrons. EPMA is used to measure the concentrations of elements at levels as low as 100 parts per million and to determine lateral distributions by mapping. The modern EPMA instrument has the following key components; an electron-optical column capable of forming a beam ranging in diameter from nm to μm and carrying a current ranging from pA to μA, An enery-dispersive X-ray spectrometer and at least one wavelength-dispersive X-ray spectrometer, An optical microscope for precise positioning of the specimen, a vacuum system with pressures ranging from 10^{-4} to 10^{-6} Pa, and a computer system to control the beam, spectrometers, specimen stage and quantitative date processing [9].

EPMA is based on the measurement of characteristic x-rays emitted from a microscopic part of a solid specimen bombarded by a beam of accelerated electrons. The electrons are focused into a beam of less than 1 μm in diameter, so that their action can be limited to the chosen microvolume at the surface of the specimen. The impinging electrons are decelerated and scattered; they lose energy and suffer directional changes through collision with the specimen atoms, which limits the maximum depth of penetration to about 1 μm. Most of the energy imparted to the specimen is in the form of heat. However, a small but important fraction of the interactions ionizes the inner shells of the target atoms. The ionized atoms emit x-rays and Auger electrons. The characteristic x-ray lines so formed, which are specific to the atomic number of the emitting atoms, are used in EPMA since their wavelengths

identify the emitting element (qualitative analysis). After some corrective calculations, the intensities of the emitted lines permit determination of the concentration of the emitters (quantitative analysis) [10].

In modern x-ray microanalysis, the analyst has two possible choices for the x-ray spectrometer: the energy-dispersive spectrometer or the wavelength-dispersive spectrometer. These two spectrometers are highly complementary. The energy-dispersive spectrometer (EDS) uses the photoelectric absorption of the X-ray in a semiconductor crystal, with proportional conversion of the X-ray energy into charge through inelastic scattering of the photoelectron, whereas the wavelength-dispersive spectrometer (WDS) is based upon the phenomenon of Bragg diffraction of X rays incident on a crystal. For survey work of major and minor constituents in unknowns, EDS has a significant advantage for rapid qualitative analysis compared to WDS, however, spectral resolution is better for WDS than for EDS. Peak-to-background ratio is higher for WDS than EDS, and limits of detection are much lower for WDS than for EDS. Therefore, a well-equipped electron probe instrument will have both spectrometers so that strengths of each compensate for the weaknesses of the other [10].

A powerful aspect of EPMA is the preparation of elemental distribution maps, which can provide qualitative and quantitative information on the spatial distribution of the constituents of a sample. By obtaining a series of maps for different elemental constituents, the spatial distribution of the composition of the sample can be directly visualized, at least on a qualitative basis. Using this feature, crack free FGM sample was analyzed to study the compositional gradient along the length of the sample.

References

1. K.E. Sickafus "Transmission Electron Microscopy" in Encyclopedia of Materials Characterization: Surfaces, Interfaces, Thin Films, Eds. C.R.Brundle, C.A. Evans, Jr., and S. Wilson, Butterworth-Heinemann & Manning, Boston, 99-115 (1992)

2. D.B. Williams and C.B. Carter, Transmission Electron Microscopy, Plenum Press, New York (1996)

3. M. Ohring, The Materials science of Thin Films, Academic press, New York, 269-273 (1992)

4. M. Von Heimendahl, Electron Microscopy of Materials: An Introduction. Materials science and Technology series, Eds. A.S. Nowick, Academic, New York (1980)

5. G. Thomas and M.J. Goringe, Transmission Electron Microscopy of Materials, Wiley, New York (1979)

6. M.F. Toney, "X-ray Diffraction", in Encyclopedia of Materials Characterization: Surfaces, Interfaces, Thin Films, Eds. C.R.Brundle, C.A. Evans, Jr., and S. Wilson, Butterworth-Heinemann & Manning, Boston, 198-213 (1992)

7. J.F. Shackelford, Introduction to Materials Science for Engineers, Macmilllian and collier Macmillan publishers, New York (1988)

8. R.P. Goehner, "X-ray powder Diffraction" in Metal Handbook Ninth Edition: Materials Characterization, Vol.**10**, American Society for metals, Ohio, 333-343 (1986)

9. D.E. Newbury, "Electron Probe X-ray Microanalysis" in Encyclopedia of Materials Characterization: Surfaces, Interfaces, Thin Films, Eds. C.R.Brundle, C.A. Evans, Jr., and S. Wilson, Butterworth-Heinemann & Manning, Boston, 175-191 (1992)

10. K.F. Heinrich and D.E. Newbury, "Electron Probe X-ray Microanalysis" in Metal Handbook Ninth Edition: Materials Characterization, Vol.**10**, American Society for metals, Ohio, 516-535 (1986)